Unconventional secretion of α-synuclein mediated by palmitoylated DNAJC5 oligomers

Shenjie Wu[1], Nancy C. Hernandez Villegas[2], Daniel W. Sirkis[3], Iona Thomas-Wright[4], Richard Wade-Martins[4], Randy Schekman[1*]

[1]Department of Molecular and Cell Biology, Howard Hughes Medical Institute, University of California, Berkeley, Berkeley, United States; [2]Helen Wills Neuroscience Institute, University of California, Berkeley, Berkeley, United States; [3]Memory and Aging Center, Department of Neurology, University of California San Francisco, San Francisco, United States; [4]Oxford Parkinson's Disease Centre, Department of Physiology, Anatomy and Genetics and Kavli Institute for Nanoscience Discovery, University of Oxford, Oxford, United Kingdom.

*For correspondence:

schekman@berkeley.edu

Abstract

Alpha-synuclein (α-syn), a major component of Lewy bodies found in Parkinson's disease (PD) patients, has been found exported outside of cells and may mediate its toxicity via cell-to-cell transmission. Here, we reconstituted soluble, monomeric α-syn secretion by the expression of DnaJ homolog subfamily C member 5 (DNAJC5) in HEK293T cells. DNAJC5 undergoes palmitoylation and anchors on the membrane. Palmitoylation is essential for DNAJC5-induced α-syn secretion, and the secretion is not limited by substrate size or unfolding. Cytosolic α-syn is actively translocated and sequestered in an endosomal membrane compartment in a DNAJC5-dependent manner. Reduction of α-syn secretion caused by a palmitoylation-deficient mutation in DNAJC5 can be reversed by a membrane-targeting peptide fusion-induced oligomerization of DNAJC5. The secretion of endogenous α-syn mediated by DNAJC5 is also found in a human neuroblastoma cell line, SH-SY5Y, differentiated into neurons in the presence of retinoic acid, and in human induced pluripotent stem cell-derived midbrain dopamine neurons. We propose that DNAJC5 forms a palmitoylated oligomer to accommodate and export α-syn.

35 # Introduction

36 Parkinson's disease, the second most common neurodegenerative disease, is
37 characterized by the deposit of clumps of protein aggregate, lipid and damaged
38 organelles known as Lewy bodies (LBs) (Dauer and Przedborski, 2003;
39 Shahmoradian et al., 2019). One of the main constituents of LB is the presynaptic
40 protein α-syn (Stefanis, 2012). α-syn is encoded by the *SNCA* gene and is highly
41 abundant in neurons. As a small, intrinsically disordered protein containing 140
42 amino acids (AA), α-syn can be divided into three domains, an amphipathic N-
43 terminal domain where most PD-related mutations are located, including A30P,
44 E46K and A53T, a central hydrophobic region known as the non-amyloid-β
45 component (NAC) which is essential for aggregation, and an acidic C-terminal
46 domain (**Fig 1A**) (Alderson and Markley, 2013). α-syn can undergo a
47 conformational change from a disordered monomer to an oligomer (Burre et al.,
48 2014; Lashuel et al., 2002), which can further polymerize to form insoluble fibrils
49 (Guerrero-Ferreira et al., 2019; Guerrero-Ferreira et al., 2018; Strohaker et al.,
50 2019).

51 In recent years, studies have suggested that α-syn deposits are not static, but rather
52 actively spread during disease progression. Grafted neurons in PD patients
53 developed α-syn positive LBs years after surgery, suggesting host-to-graft
54 pathology propagation (Kordower et al., 2008; Li et al., 2008). Based on analysis
55 of human pathology, the Braak hypothesis posits that α-syn aggregates can spread
56 in a stereotyped manner from the gastrointestinal tract to the brain, causing neuron
57 loss beginning in the brainstem, extending to the midbrain, and finally to the cortex
58 (Braak et al., 2006; Braak et al., 2003). In more recent work, Braak-like
59 transmission of *in vitro* generated α-syn fibrils has been recapitulated in mice and

60 non-human primates (Chu et al., 2019; Chung et al., 2020; Kim et al., 2019; Luk et
61 al., 2012).

62 Less-well understood is the molecular and cellular basis for the transfer of α-syn
63 between cells. Several mechanisms have been proposed for both monomeric and
64 aggregated α-syn export and transfer, including unconventional exocytosis (Jang et
65 al., 2010; Lee et al., 2005), exosomes (Danzer et al., 2012; Emmanouilidou et al.,
66 2010; Stykel et al., 2021) and membrane nanotubes (Abounit et al., 2016;
67 Scheiblich et al., 2021). The extracellular existence of both monomeric and
68 oligomeric α-syn was confirmed in blood and cerebrospinal fluid (CSF) (Borghi et
69 al., 2000; El-Agnaf et al., 2003). Packaging of different conformational forms of α-
70 syn inside extracellular vesicles (EVs) has been reported but requires further
71 vigorous scrutiny to differentiate membrane vesicles from secreted sedimentable
72 aggregates (Brahic et al., 2016).

73 DNAJC5, also known as cysteine string protein α (CSPα), is a co-chaperone of
74 HSC70 and has been shown to control the extracellular release of many
75 neurodegenerative disease proteins (Fontaine et al., 2016). This process of
76 unconventional traffic has been termed misfolding-associated protein secretion
77 (MAPS) (Fontaine et al., 2016; Lee et al., 2016) as opposed to conventional
78 secretion initiated by an amino-terminal signal peptide required for secretory and
79 membrane protein translocation into the endoplasmic reticulum (Zhang and
80 Schekman, 2013). DNAJC5 contains three domains – a common N-terminal J-
81 domain conserved among DnaJ proteins, the cysteine-string (CS) central domain
82 which is heavily palmitoylated and anchors the protein to late endosomes, and an
83 overall disordered C-terminal domain (**Fig 1A**). Deletion of DNAJC5 in

84 Drosophila and mice leads to a neurodegenerative phenotype and premature death,
85 indicating that DNAJC5 plays a neuroprotective role in the brain (Zinsmaier,
86 2010). Transgenic expression of α-syn appears to rescue the neurodegeneration
87 seen on depletion of DNAJC5 (Chandra et al., 2005). A previous study also
88 reported that neuron-derived EVs contain DNAJC5 (Deng et al., 2017). However,
89 the mechanism by which DNAJC5 recognizes and translocates soluble α-syn into a
90 membrane compartment for secretion remains elusive.

91 In this study, we characterized the mechanism of DNAJC5-induced α-syn
92 secretion in a cell-based secretion assay. Using biochemical characterization and
93 imaging of internalized α-syn in enlarged endosomes as a secretory intermediate,
94 we found previously underappreciated roles of palmitoylation and oligomerization
95 of DNAJC5 in the regulation of α-syn secretion.

96

97 # Results

98 ## Reconstitution of DNAJC5-induced α-syn secretion

99 Previous studies have shown that α-syn secretion can be stimulated by over-
100 expressing DNAJC5 (Fontaine et al., 2016). The CS domain of DNAJC5 plays a
101 role in promoting stable membrane attachment based on its overall hydrophobicity
102 and by enabling post-translational palmitoylation catalyzed by membrane-bound
103 Asp-His-His-Cys (DHHC) family palmitoyltransferases (Greaves and
104 Chamberlain, 2006). Using a common human cell line, HEK293T, we first tested
105 the expression and subcellular localization of DNAJC5 (**Fig 1B**). Further
106 subcellular enrichment of DNAJC5 was characterized using a C-terminal FLAG

107 tag. Coomassie blue staining revealed two bands of low and high mobility on SDS-
108 PAGE in the membrane and cytosolic fractions, respectively (**Fig 1C**). Similar
109 migration profiles of pamitoylated (P-) and non-palmitoylated (NP-) DNAJC5
110 have been reported (Greaves et al., 2012). We also transfected and fractionated
111 DNAJC5 in other common cell lines including MDA-MB-231 and Hela cells.
112 Compared to DNAJC5 in HEK293T cells, DNAJC5 in MDA-MB-231 and Hela
113 cells appeared predominantly to be in a palmitoylated and membrane-associated
114 form (**Fig 1 supplement 1A**). The mobility of P-DNAJC5 in the membrane
115 fraction shifted to that of NP-DNAJC5 after an overnight depalmitoylation reaction
116 with hydroxylamine (HA) (**Fig 1 supplement 1B**). Thus, we confirm that
117 membrane anchoring of DNAJC5 requires palmitoylation in our assay.

118 We next co-expressed DNAJC5 together with α-syn to examine their secretion
119 over time. At 16 h after transfection, we detected similar basal-levels secretion of
120 α-syn in both DNAJC5-negative and -positive conditions. Two bands of DNAJC5
121 corresponding to P-DNAJC5 and NP-DNAJC5 were seen in the lysate, but only
122 the P-DNAJC5 was secreted into the medium (**Fig 1D**). The stimulation of α-syn
123 secretion by DNAJC5 became obvious at a longer incubation time (36 h), and at
124 this time point NP-DNAJC5 was also enriched in the medium (**Fig 1E**). The
125 release of α-syn was not caused by cell death as little to undetected levels of
126 cytoplasmic tubulin found in the culture medium fraction (**Fig 1D&1E**). Cell
127 viability was not affected by transfection of different constructs, as shown by
128 trypan blue staining (**Fig 1 supplement 2A**). In addition to wild-type (WT) α-syn,
129 secretion of several PD-causing α-syn mutant proteins (A30P, E46K and A53T)
130 was also induced to differing levels by expression of DNAJC5 (**Fig 1 supplement
131 2B-2D**).

132 In addition to the stimulated secretion of α-syn produced by the expression of
133 exogenous DNAJC5, we examined the dependence of a basal secretion of α-syn on
134 endogenous DNAJC5. We fused α-syn with an N-terminal nanoluciferase (Nluc)
135 (England et al., 2016) for sensitive, quantitative detection (**Fig 1 supplement 3A**).
136 Stimulated secretion of Nluc-α-syn by overexpression of DNAJC5 was confirmed
137 by immunoblot, indicating that Nluc-fusion did not impede α-syn secretion (**Fig 1**
138 **supplement 3B**). Without over-expression of DNAJC5, we observed accumulation
139 of Nluc-α-syn signal in the medium over time (**Fig 1 supplement 3C**).

140 Quercetin is a plant-derived flavonoid that has previously been shown to inhibit
141 DNAJC5-mediated trafficking of a bacterial toxin (**Fig 1 supplement 3D**) (Deruelle
142 et al., 2021). We found that quercetin also inhibited Nluc-α-syn secretion in a dose-
143 dependent manner (**Fig 1 supplement 3E**), implying a role for endogenous DNAJC5
144 in α-syn secretion. To exclude the off-target effect of quercetin, we created a
145 DNAJC5 CRISPR knockout (KO) cell line (**Fig 1 supplement 3F**). Balfilomycin
146 A1 (BaFA1), a lysosomal ATPase inhibitor, has been shown to stimulate α-syn
147 secretion (**Fig 1 supplement 3G**) (Buratta et al., 2020; Fernandes et al., 2016).
148 BafA1 is also known to stimulate the fusion of lysosomes at the cell surface with the
149 secretion of lysosomal content (Tapper and Sundler, 1995). BaFA1-stimulated α-
150 syn secretion was confirmed in WT HEK293T cells but not observed in DNAJC5
151 KO cells (**Fig 1 supplement 3H**). Our results suggest that α-syn secretion depends
152 on the basal level of DNAJC5 and is enhanced by overexpression of DNAJC5.

153 **Characterization of extracellular DNAJC5 and α-syn**

154 In our established assay, DNAJC5 and α-syn co-secrete into the medium (**Fig 1E**).
155 Secreted α-syn has been reported to be encapsulated inside EVs (Danzer et al., 2012).
156 We sought to assess the EV association of secreted α-syn using a medium
157 fractionation protocol based on EV preparations developed by our lab (**Fig 2A**)
158 (Shurtleff et al., 2016). After serial differential centrifugation, α-syn and NP-
159 DNAJC5 remained soluble. In comparison, P-DNAJC5 co-sedimented with other
160 EV markers after 100k xg centrifugation (**Fig 2B**). In addition to WT α-syn, we
161 conducted medium fractionation with several PD-causing α-syn mutants and found
162 they all remained soluble in culture supernatant fractions (**Fig 2 supplement 1A**).
163 To test the EV association of P-DNAJC5, we performed a further sucrose step
164 gradient flotation (**Fig 2 supplement 2A**) with the 100k high-speed pellet fraction
165 (**Fig 2 supplement 2B**). P-DNAJC5 equilibrated with other EV markers to the
166 10%/40% interface expected for buoyant EVs (**Fig 2 supplement 2B**). We conclude
167 that the secreted α-syn induced by DNAJC5 is neither membrane bound nor in a
168 sedimentable fibrillar form.

169 Next we sought to characterize the conformation of secreted soluble α-syn. The
170 medium containing secreted α-syn was pooled, concentrated and applied to a gel
171 filtration column. Extracellular α-syn eluted from the column at around 60% of the
172 column volume (**Fig 2C**), similar to the elution volume of purified monomeric α-
173 syn (**Fig 2D and Fig 2 supplement 3E&F**). By an orthogonal assay, we examined
174 the interaction between tagged and untagged forms of secreted α-syn as an indicator
175 of oligomerization. In this assay, equal amounts of plasmids expressing FLAG-
176 tagged α-syn and non-tagged α-syn were co-transfected in HEK293T cells and the
177 medium was collected and incubated with anti-FLAG M2 beads for to detect co-

178 immunoprecipitation of the two forms (IP) (**Fig 2E**). FLAG-tagged α-syn migrated
179 more slowly than non-tagged α-syn as detected in samples of the culture medium
180 (**Fig 2F**). We found that only the FLAG-tagged α-syn was immuno-precipitated (**Fig**
181 **2F**), suggesting no stable interaction between the two species. The gel filtration and
182 IP assays reinforced our conclusion that α-syn is secreted as a monomer.

183 **Secretion of α-syn requires palmitoylation of DNAJC5**

184 Membrane targeting of DNAJC5 is dependent upon palmitoylation (Greaves et al.,
185 2008). Two specific mutations, L115R and L116Δ in the CS domain, cause adult-
186 onset neuronal ceroid lipofuscinosis (NCL), a type of neurodegenerative disorder
187 (Benitez et al., 2011). NCL mutations reduce the level of DNAJC5 palmitoylation
188 and promote aggregation of the protein (Diez-Ardanuy et al., 2017). We perturbed
189 DNAJC5 palmitoylation by either introducing the palmitoylation-deficient mutation
190 L115R or treating cells with the competitive palmitoyl transferase inhibitor, 2-
191 bromopalmitic acid (2-BA) (Resh, 2006), and subsequently examined the influence
192 on DNAJC5 membrane association. DNAJC5 palmitoylation largely decreased in
193 the L115R mutant or upon 2-BA treatment. Correspondingly, NP-DNAJC5
194 accumulated in the cytosol (**Fig 3A&3B**).

195 Having confirmed palmitoylation inhibition by 2-BA and the L115R mutation, we
196 next examined their effect on α-syn secretion. Upon 10 μM 2-BA treatment, α-syn
197 and DNAJC5 secretion were abolished (**Fig 3C, 3E&3F**). The efficacy of the
198 inhibitor was validated by the disappearance of the low-mobility band corresponding
199 to P-DNAJC5 in the cell lysate (**Fig 3D**). Furthermore, 2-BA inhibited DNAJC5
200 palmitoylation (**Fig 3 supplement 1C&1E**) and α-syn secretion in a concentration-
201 dependent manner (**Fig 3 supplement 1B&1D**). Likewise, α-syn secretion was

202 reduced by the palmitoylation-deficient DNAJC5 (L115R) compared with DNAJC5
203 (WT) (**Fig 3G-3J**). DNAJC5 has been proposed to function downstream of the
204 deubiquitinase USP19 in the MAPS pathway (Xu et al., 2018). In agreement with
205 the model, DNAJC5 carrying either NCL mutation L115R or L116Δ had no
206 palmitoylated protein band detected in the lysate (**Fig 3 supplement 2B**) and
207 blocked USP19-stimulated α-syn secretion (**Fig 3 supplement 2A&2C**). These
208 results establish that palmitoylation is essential for DNAJC5 membrane association
209 and function in stimulating α-syn secretion.

210 A previous study reported an altered distribution of DNAJC5 mutant protein to the
211 Golgi apparatus and cytosol (Noskova et al., 2011). In confocal immunofluorescence
212 (IF) images, we confirmed that WT DNAJC5 did not colocalize with the Golgi
213 marker GM130 whereas both the L115R mutant and 2-BA treated WT cells partially
214 retained DNAJC5 in puncta coincident with the Golgi marker GM130 (**Fig 3**
215 **supplement 3A,B&C**). We conclude that α-syn secretion depends upon an
216 appropriate subcellular organelle localization of DNAJC5.

217 **DNAJC5-dependent internalization of α-syn into enlarged endosomes**

218 DNAJC5 has been reported under normal conditions to be associated with late
219 endosomes (Lee et al., 2018). Using confocal IF, we found colocalization between
220 endogenous DNAJC5 and the late-endosomal marker CD63 (**Fig 4 supplement 1A**).
221 To visualize the topological localization of DNAJC5 and α-syn inside or outside
222 endosomes, we turned to a U2OS cell line expressing a fluorescent protein-fused,
223 constitutively active form of Rab5 ($Rab5^{Q79L}$) (Bohdanowicz et al., 2012). As a
224 positive control, CD63 localized to the lumen of enlarged endosomes labeled by
225 mCherry-$Rab5^{Q79L}$(**Fig 4 supplement 1B**). We labeled DNAJC5 with the self-labeling

226 HaloTag for multiple choices of color in live cell imaging (Los et al., 2008). Both
227 diffuse and punctate DNAJC5 localized to the lumen of enlarged endosomes (**Fig**
228 **4A**). Unlike WT DNAJC5, the DNAJC5 L115R mutant became disperse in the
229 cytosol, rather than being internalized into enlarged endosomes (**Fig 4 supplement**
230 **2A**). In contrast, mNeonGreen (mNG)-fused α-syn showed diffuse localization in
231 both the cytosol and nucleus but was completely excluded from enlarged endosomes
232 in L115R mutant cells (**Fig 4B**). Notably, we observed the entry of α-syn into
233 enlarged endosomes containing internalized DNAJC5, implying the translocation of
234 α-syn into the membrane compartment required DNAJC5 (**Fig 4C**). The ratio of α-
235 syn-containing endosomes in cells increased significantly with DNAJC5
236 overexpression (**Fig 4H)**. With no luminal localization inside enlarged endosomes,
237 the DNAJC5 L115R mutants also failed to induce entry of α-syn into the same
238 compartments (**Fig 4 supplement 2B**). As an independent test of the localization
239 suggested by the imaging results, we applied cell fractionation to separate
240 membranes of DNAJC5- and α-syn-expressing cells (**Fig 4D**). Both DNAJC5 and
241 α-syn were enriched in a 25k membrane pellet fraction (**Fig 4E**). In a protease
242 protection assay with 25k sedimented membranes, we found that α-syn and
243 DNAJC5 were partially resistant to digestion by proteinase K in the absence but not
244 in the presence of Triton X-100 consistent with the conclusion that about half of the
245 proteins were sequestered within membrane compartments (**Fig 4F&4G)**. Our visual
246 inspection and quantification results are consistent with a membrane translocation
247 role for DNAJC5 prior to α-syn secretion.

248 **Size and unfolding are dispensable for α-syn secretion**

249 In our medium fractionation assay, secreted α-syn in the extracellular space was
250 characterized as a soluble monomer (**Fig 2**). We generated a series of tandem repeats
251 of α-syn to mimic its oligomeric states (**Fig 5A**) (Dong et al., 2018). On SDS-PAGE,
252 α-syn tandem repeats showed a larger apparent size than their predicted molecular
253 weights, possibly caused by their extended conformation as intrinsically disordered
254 proteins (**Fig 2 supplement 2**). We first determined that these α-syn tandem repeats
255 could also be secreted upon overexpression of DNAJC5 (**Fig 5B**), indicating that
256 DNAJC5 can accommodate α-syn of different sizes. Fractionation of the growth
257 medium showed that secreted tandem repeats were also soluble (**Fig 5 supplement**
258 **1**).

259 In conventional and many unconventional secretion processes, the secreted proteins
260 undergo unfolding prior to translocation through a narrow channel across the
261 hydrophobic membrane barrier (Rapoport et al., 2017). Recent progress in protein
262 design has allowed the synthesis of super-folded protein constructs (Kuhlman and
263 Bradley, 2019). For example, a three helix-bundle protein (3H) designed in the
264 lowest-energy arrangements displayed extreme thermodynamic stability and
265 remained folded even in non-physiological denaturing conditions (Huang et al.,
266 2014). Given that mitochondrial protein import is dependent on protein unfolding
267 (Neupert, 1997), we tested the effect of 3H insertion on the import of mitochondrial
268 matrix enzyme ornithine transcarbamylase (OTC) (Horwich et al., 1985; Yano et al.,
269 1997). As a control, we created a pOTC leader peptide fused to GFP (**Fig 5**
270 **supplement 2A**). pOTC-GFP was enriched in a mitochondria-containing particulate
271 (P) fraction compared to non-tagged GFP. However, a construct in which 3H was
272 inserted between the leader sequence and GFP resulted in 80% of the fusion protein
273 retained in the soluble fraction (**Fig 5 supplement 2B&2C**). We then used

274 proteinase K protection to assess the topology of pOTC-3H-GFP associated with
275 crude mitochondria (**Fig 5 supplement 2D**). About 80% of citrate synthase (CS), a
276 known mitochondria matrix protein, was protected from proteinase K. In contrast,
277 neither the mitochondrial outer membrane protein Tom20 nor pOTC-3H-GFP was
278 protected, suggesting 3H prevented the translocation of GFP into mitochondria (**Fig**
279 **5 supplement 2E&2F**). Using a similar approach, we fused 3H to either the N- or
280 C-terminus of α-syn to impede the unfolding process (**Fig 5D**). These α-syn fusion
281 proteins were expressed and secreted normally into the growth medium (**Fig 5E&F**).
282 These data suggest that protein unfolding is dispensable for α-syn secretion.

283 **XPACK fusion rescues DNAJC5 L115R secretion deficiency by induced**
284 **oligomerization**

285 DNAJC5 has been reported to have an intrinsic propensity to form SDS-resistant
286 oligomers (Zhang and Chandra, 2014). In a whole gel immunoblot of extracellular
287 DNAJC5, we noticed many diffuse, ladder-like bands that migrated more slowly
288 than the two corresponding to P-DNAJC5 and NP-DNAJC5 (**Fig 6A**), possibly
289 higher molecular weight (HMW) oligomers. This apparent oligomerization of
290 DNAJC5 became more obvious when the J domain was deleted (**Fig 6 supplement**
291 **1A**). The migration of HMW-DNAJC5 was not altered in samples heated in the
292 presence of a reducing agent (**Fig 6 supplement 1B**). To assess the size of these
293 HMW species of DNAJC5, we evaluated a cell lysate by gel filtration
294 chromatography. HMW-DNAJC5 fractionated according to its apparent size,
295 forming a stair-like pattern on the DNAJC5 immunoblot (**Fig 6B**). HMW-DNAJC5
296 chromatographed within the gel filtration column volume, consistent with discrete
297 protein species rather than aggregates (**Fig 6B**). These results suggest the presence

298 of higher-order, SDS-resistant, non-disulfide-bonded DNAJC5 oligomers both in
299 intracellular and extracellular fractions.

300 XPACK (XP) is a membrane-targeting peptide sequence used widely in studies of
301 cargo loading into exosomes and delivery to target cells of choice (Yim et al., 2016).
302 The exosome loading process by XP is also dependent on two lipidation reactions –
303 myristoylation on the first glycine and palmitoylation on the second cysteine (**Fig 6**
304 **supplement 1C**) (Zacharias et al., 2002). Given the similarity of membrane
305 localization and lipidation between XP and the CS domain of DNAJC5, we
306 examined α-syn secretion in cells expressing an XP-DNAJC5 fusion. An N-terminal
307 XP fusion (XP-WT) resulted in the expression of a species that migrated at the
308 position of P-DNAJC5, in contrast to the two species representing P- and NP-
309 DNAJC5 in the WT DNAJC5 sample (**Fig 6 supplement 1D**). Again in contrast to
310 WT DNAJC5, XP-DNAJC5 was exclusively associated with the sedimentable
311 membrane fraction (**Fig 6 supplement 1E**). This suggested that XP-mediated
312 lipidation was highly efficient and possibly irreversible. Formation of the lower
313 electrophoretic mobility and membrane associated form of XP-DNAJC5 was
314 blocked by 2-BA treatment, indicating XP lipidation included palmitoylation (**Fig 6**
315 **supplement 1E**). XP fusion to the palmitoylation-deficient mutant of DNAJC5
316 (L115R) did not produce a species that migrated at the position of P-DNAJC5 but
317 resulted in several less abundant species that migrated between the positions of NP-
318 and P-DNAJC5 (**Fig 6 supplement 1D**). We introduced a serine to leucine point
319 mutation in the XPACK sequence which was predicted to block lipidation (dead
320 XPACK, DXP) (**Fig 6 supplement 1C**). The DXP-DNAJC5 L115R species had the
321 same mobility as NP-DNAJC5 (**Fig 6 supplement 1D**).

322 We conducted cellular fractionation on lysates of cells expressing DNAJC5 XP-
323 L115R. XP-L115R was highly enriched in the membrane fraction, likely as a result
324 of XPACK-mediated lipidation (**Fig 6C**). SDS-PAGE of XP-L115R released by
325 detergent solubilization migrated slowly and remained near the top of the gel,
326 suggesting XPACK induced high-order oligomerization or aggregation (**Fig 6C**). In
327 spite of the apparent difference between DNAJC5 XP-L115R and WT DNAJC5, α-
328 syn secretion was stimulated by the expression of both species (**Fig 6D**). Treatment
329 with the palmitoylation inhibitor 2-BA resulted in the formation of XP-L115R that
330 migrated to a position similar to that of monomeric DNAJC5 (**Fig 6E**).
331 Correspondingly, secretion of α-syn was no longer stimulated by the palmitoylation
332 deficient DNAJC5 XP-L115R monomer (**Fig 6D**).

333 In order to expand on the fractionation results, we employed confocal microscopy
334 to examine the subcellular localization of DNAJC5 XP-L115R fused with a C-
335 terminal HaloTag. In contrast to the diffuse distribution of the DNAJC5 L115R
336 mutant, which was excluded from the interior of enlarged endosomes (**Fig 4**
337 **supplement 2A**), punctate DNAJC5 XP-L115R was widely associated with
338 enlarged endosomes (**Fig 6 supplement 2A**). Internalization events were found in
339 several enlarged endosomes (**Fig 6 supplement 2A, magnified insets**). mNG-α-syn
340 was also incorporated into endosomal compartments in cells co-expressing DNAJC5
341 XP-L115R (**Fig 6 supplement 2B**). The level of α-syn containing endosomes in
342 cells expressing DNAJC5 XP-L115R was ~2-fold higher than in cells expressing the
343 DNAJC5 L115R mutant (**Fig 6 supplement 2C**). Our imaging data corroborate the
344 biochemical similarity between WT DNAJC5 and DNAJC5 XP-L115R.

345 **Secretion of endogenous α-syn from neurons is mediated by DNAJC5**

346 To evaluate the function of DNAJC5 in α-syn secretion at physiological levels of
347 expression in a neuronal cell line, we employed SH-SY5Y, a neuroblastoma line that
348 differentiates in the presence of retinoic acid (RA) into nerve cells that express
349 dopamine neuron (DA) markers including tyrosine hydroxylase (TH) (Lopes et al.,
350 2010). We observed elevated levels of expression of α-syn and dopamine transporter
351 (DAT) in SH-SY5Y cells after six days of RA-induced differentiation (**Fig 7**
352 **supplement 1A**). Fractionation of SH-SY5Y cell lysates resolved DNAJC5 into the
353 low electrophoretic mobility P form associated with sedimentable membranes (M)
354 and the non-sedimentable cytosolic NP form (**Fig 7A**). Hydroxylamine treatment of
355 the membrane associated form converted DNAJC5 to the electrophoretic mobility
356 position of the NP form, as before (**Fig 7 supplement 1B; Fig. 1 supplement 1B**).

357 We employed a sensitive α-syn enzyme-linked immunosorbent assay (ELISA) and
358 detected about 300 pg/ml α-syn secreted into the supernatant of RA-differentiated
359 SH-SY5Y cells (Forland et al., 2018) (**Fig 7B**). Differential centrifugation of the
360 medium fraction demonstrated that the bulk of the secreted α-syn remained soluble
361 (**Fig 7B**). A 100k pellet fraction was probed by protease protection for the
362 localization of Flot-2, an exosome marker and DNAJC5. Both were resistant to
363 degradation by proteinase K in the absence but not in the presence of TX-100,
364 suggesting that both were protected within the lumen of EVs (**Fig 7 supplement**
365 **1C**). In contrast, residual full-length (FL) α-syn in the pellet fraction was cleaved
366 by proteinase K without or with detergent (**Fig 7 supplement 1C**). As an

367 additional test, sucrose gradient flotation of the high-speed pellet fraction as used
368 in **Fig 2 supplement 2A,** revealed that α-syn secreted by differentiated SH-SY5Y
369 cells was not buoyant whereas DNAJC5 appeared associated with membranes
370 fractionating at the position of EVs (**Fig 7 supplement 1D**). Thus, as with
371 HEK293T cells, α-syn secreted by differentiated SH-SY5Y cells appears not to be
372 enclosed within EVs.
373 Midbrain dopamine (mDA) neurons (**Fig 7 supplement 2A**) differentiated from
374 human induced pluripotent stem cells (hiPSCs) from Parkinson's patients with the
375 *GBA-N370S* mutation, a genetic lesion which causes ER stress and dysfunctional
376 lysosomes, release about twice the level of α-syn compared to control WT
377 neurons(Fernandes et al., 2016; Lang et al., 2019) Treatment of *GBA-N370S*
378 hiPSC-derived dopamine neurons with the DNAJC5 inhibitor quercetin led to a
379 significant dose-dependent reduction in the secretion of endogenous α-syn (**Fig**
380 **7C**). Immunnoblotting of hiPSC-derived dopamine neuron lysate revealed that the
381 endogenous DNAJC5 is natively palmitoylated which can be partially reduced by
382 treatment with 2-BA (10 μM) to induce the formation of the lower, non-
383 palmitoylated band (**Fig 7 supplement 2B**). However, this partial de-
384 palmitoylation of DNAJC5 was insufficient to inhibit α-syn release by iPSC-

385 derived *GBA-N370S* dopamine neurons at the concentration of 2-BA used (**Fig 7**
386 **supplement 2C**).
387 To examine the role of DNAJC5 in differentiated SH-SY5Y cells, we silenced the
388 expression of the chromosomal locus by small hairpin RNAs (shRNAs) transduced
389 by lentivirus. The efficiency of shRNA targeting DNAJC5 was confirmed by
390 knockdown (KD) of endogenous DNAJC5 in HEK293T cells (**Fig 7 supplement**
391 **3A**). Similarly, DNAJC5 was successfully depleted in differentiated SH-SY5Y cells
392 (**Fig 7 supplement 3B**). As a result, secretion of α-syn was reduced 5-fold compared
393 with a control transduced with shRNA targeting GFP (**Fig 7D**).

394 In HEK293T cells, overexpression of DNAJC5 increased α-syn secretion (**Fig 1E**).
395 We were unable to observe enhanced secretion of α-syn in SH-SY5Y
396 overexpressing DNAJC5, possibly because of a high level of expression of
397 endogenous DNAJC5 in the differentiated cells (**data not shown**). To test the effect
398 of DNAJC5 on the basal level of α-syn secretion in neurons, we stably transduced
399 mouse embryonic stem cells (mESCs) with lentivirus containing human DNAJC5
400 WT or L115R and differentiated them into mDA neurons (**Fig 7 supplement 4A**).
401 After differentiation, DNAJC5 WT was expressed in mDA, but we were unable to
402 detect the expression of DNAJC5 L115R (**Fig 7 supplement 4B**). Analysis of
403 conditioned media by ELISA revealed a two-fold elevated α-syn secretion in
404 DNAJC5 WT overexpressing mDA compared to control with an empty vector in the
405 presence of BaFA1 (**Fig 7E**). With both BaFA1 treatment and DNAJC5
406 overexpression, α-syn secretion was increased three fold (**Fig 7E**). We examined the

407 cell lysate of mDA by immunoblot. The effect of BaFA1 inhibition was indicated
408 by the appearance of a lipidated form of LC3 (LC3-II) (**Fig 7F**). BaFA1 treatment
409 also induced more DNAJC5 oligomer formation (**Fig 7F**). We conclude that
410 DNAJC5 stimulates α-syn secretion in differentiated DA neurons as it does in
411 HEK293T cells.

412 **The J domain and C-terminal tail (C tail) of DNAJC5 are dispensable for α-syn**
413 **secretion**

414 The secretion deficiency caused by the L115R mutation highlights the importance
415 of the CS domain of DNAJC5 in regulating α-syn secretion. The structure of the J
416 domain of DNAJC5 has been solved by nuclear magnetic resonance (NMR) (Patel
417 et al., 2016). Recent progress in deep learning algorithms, exemplified by AlphaFold,
418 enables atomic accuracy in protein structure prediction (Jumper et al., 2021). We
419 searched the public AlphaFold database to examine the predicted structure of full-
420 length DNAJC5. In the predicted structure, the J domain showed a conserved overall
421 globular J protein fold within the N-terminus, linked by the helical CS domain to the
422 flexible C-terminal tail. Only a short helix was predicted to reside within the C-tail
423 (**Fig 8A**). We refined the boundary of each domain in DNAJC5 based on the
424 predicted structure.

425 Using this information, we showed that oligomerization of DNAJC5 increased when
426 the J domain was deleted (**Fig 6 supplement 1A and Fig 8C**). As recently reported
427 by Lee et al. (2022), deletion of the J domain increased the level of α-syn secretion
428 induced by DNAJC5 (**Fig 8B&8D**). Next, we examined the function of the C-tail by
429 truncating about ten amino acids at a time, resulting in a series of C-terminal
430 truncated DNAJC5 constructs, i.e., DNAJC5 ΔC10, ΔC20, ΔC30, ΔC40. All four

431 DNAJC5 C-terminal truncations were expressed and formed oligomers in cells (**Fig**
432 **8F**). C-terminal truncated oligomers were co-secreted with α-syn into the medium
433 (**Fig 8E&8G**). This result demonstrates that neither the J domain nor the C-tail is
434 required for DNAJC5 to induce α-syn secretion.

435

436 ## Discussion

437 Transmission of protein aggregates and subsequent self-amplification is emerging
438 as a common theme across various neurodegenerative diseases. DNAJC5 has been
439 shown to control the release of neurodegenerative disease proteins but the
440 mechanism of action of this protein in unconventional secretion remains elusive. In
441 this study, we reconstituted DNAJC5-regulated α-syn secretion in cultured
442 HEK293T cells, in RA neuronally differentiated human cells and in hiPSC-derived
443 midbrain DA neurons. By combining this assay with medium and cellular
444 fractionation, we demonstrated that membrane-anchoring of DNAJC5 through
445 palmitoylation is crucial for its secretion and the secretion of α-syn as a soluble
446 monomer. In addition, we observed the topological locations of DNAJC5 and α-
447 syn within enlarged endosomes, presumably at an intermediate stage prior to
448 secretion. Furthermore, DNAJC5 was found to form oligomers and the importance
449 of the oligomerzation was highlighted by the use of a lipidated XPACK fusion
450 peptide. Our findings on the role of DNAJC5 extend to differentiated DA neurons
451 of human and mouse origin. Finally, we provide evidence that both palmitoylation
452 and oligomerization are solely dependent on the CS domain, which is required for
453 α-syn secretion. Based on our biochemical assays and imaging observations, we
454 propose that palmitoylated DNAJC5 oligomers function at a step involving

455 membrane translocation of cytosolic α-syn, enabling it to become competent for
456 secretion (**Fig 8F**).

457

458 The in vivo toxicity of α-syn aggregates remains elusive (Lashuel et al., 2013) but
459 its propagation accompanies the progression of PD (Braak et al., 2006; Braak et al.,
460 2003). Recently, (Calo et al., 2021) found that DNAJC5 expression decreases in α-
461 syn transgenic mice. Overexpression of DNAJC5 in vivo is reported to rescue α-
462 syn aggregation-dependent pathology and increase the accumulation of monomeric
463 α-syn (Calo et al., 2021). As we find and others have reported, iPSC-derived
464 neurons also secrete α-syn in a largely soluble form (Fernandes et al., 2016). Using
465 the criteria of differential sedimentation and gel filtration chromatography, we
466 conclude that α-syn is secreted in cultures cells as a soluble monomeric species not
467 enclosed within extracellular vesicles, regardless of mutations modeled on PD (**Fig
468 2 supplement 1A**) or as expressed in tandem arrays or in gene fusions to tightly
469 folded proteins (**Fig 5 supplement 1**). Consistent with our results, other MAPS
470 substrates are also reported to be secreted in a soluble form (Lee et al., 2016).
471 Although α-syn oligomers have also been found in EVs (Danzer et al., 2012;
472 Emmanouilidou et al., 2010; Guo et al., 2020) we see no evidence for this in our
473 culture medium fractionation and immunoblot experiments (**Fig 2B**). With a more
474 sensitive and quantitative Nluc assay, 85% of secreted α-syn was found to be
475 soluble (**Fig 2 supplement 1B**). Similarly, the basal level of α-syn secreted by
476 differentiated neuroblastoma cells is mainly soluble and not detected within EVs
477 (**Fig 7 supplement 1A**).

478

479 The release of soluble α-syn may be an early event in pathogenesis of PD, prior to
480 the deposition of aggregates. Inhibition of the lysosomal ATPase with bafilomycin
481 A (BaFA1) is known to induce lysosome fusion to the cell surface and secretion of
482 lysosomal content including both soluble and aggregate forms of α-syn (Xie et al.,
483 2022) (**Fig 1 supplement 3H, Fig 7E**). Such secretion may be part of a cell
484 protective mechanism but it may also promote the interneuronal spread of
485 monomer and oligomer.

486 Numerous neuronal proteins are palmitoylated, including synaptic scaffolding
487 proteins, signaling proteins and synaptic vesicle proteins (Linder and Deschenes,
488 2007). Protein palmitoylation has been implicated in the pathogenesis of
489 neurodegenerative diseases (Cho and Park, 2016). In PD particularly, a recent
490 study reported that upregulation of cellular palmitoylation decreased α-syn
491 cytoplasmic inclusions (Ho et al., 2021). The neuropathology and behavior
492 deficiency of Huntington disease (HD) mice can be reversed by boosting brain
493 palmitoylation (Virlogeux et al., 2021). In the case of DNAJC5, L115R and
494 L116Δ, the two adjacent mutations causing decreased palmitoylation of DNAJC5
495 monomers, lead to a familial form of NCL (Benitez et al., 2011; Diez-Ardanuy et
496 al., 2017). Our results suggested that the secretion of neurodegenerative disease
497 proteins is also dependent on palmitoylation, possibly alleviating the cellular
498 burden of protein aggregate accumulation. Notably, the general inhibition of
499 cellular palmitoylation by 2-BA led to a complete block of α-syn secretion,
500 whereas the specific palmitoylation deficient DNAJC5 mutant L115R only
501 partially decreased α-syn secretion (**Fig 3**). The difference implies the existence of
502 palmitoylation-dependent factors other than DNAJC5.

503 Although DNAJC5 co-expressed with α-syn and palmitoylation are required for
504 secretion, EV-associated P-DNAJC5 clearly separated from soluble α-syn in the
505 culture medium (**Fig 2B and Fig 2 supplement 2B**). At which step do the two
506 separate? In our live cell imaging experiments, the internalized DNAJC5 inside
507 enlarged endosomes had both punctate and diffuse distributions (**Fig 4A**). This
508 may represent the soluble NP-DNAJC5 and membrane-attached P-DNAJC5,
509 respectively. In the time-lapse imaging of internalized α-syn induced by DNAJC5,
510 both DNAJC5 and α-syn moved dynamically inside the compartment, without
511 significant co-localization (**Fig4 supplementary video**). This observation suggests
512 that the separation of DNAJC5 and α-syn may occur prior to their secretion when
513 the late endosome and plasma membrane fuse.

514 Zhang et al. (2020) have reported a novel membrane channel, TMED10, for the
515 unconventional secretion of IL-1β. These authors speculate an activation-on-
516 demand oligomerization of TMED10 membrane subunits to form a conducting
517 channel for substrate translocation, a process they refer to as THU (Zhang et al.,
518 2020). α-syn was reported to not depend on TMED10 for unconventional secretion
519 (Zhang et al., 2020). Similarly, in chaperone-mediated autophagy (CMA),
520 cytosolic substrates are proposed to be translocated into lysosomes through a
521 channel formed by the oligomerization of a single-transmembrane protein,
522 LAMP2A (Bandyopadhyay et al., 2008). The secretion of α-syn has been shown to
523 be independent of CMA (Lee et al., 2018). Without a transmembrane domain,
524 membrane-tethered P-DNAJC5 oligomer is unlikely to be a channel for
525 translocation. A recent report identified CD98hc, an amino acid transporter
526 subunit, to be a DNAJC5 interactor that is required for α-syn secretion (Lee et al.,

527 2022). It remains to be determined whether CD98hc or other as yet uncharacterized
528 membrane proteins are directly involved in α-syn membrane translocation.

529 In SEC61-mediated co-translational translocation, substrates enter the SEC61
530 translocon in an unfolded state (Rapoport et al., 2017). In THU and CMA,
531 substrate unfolding is also required for translocation across the membrane
532 (Kaushik and Cuervo, 2018; Zhang et al., 2020). In striking contrast, unfolding and
533 size is not a limiting factor for α-syn secretion (**Fig 5**). As a precedent of
534 translocation without unfolding, studies have shown the import of folded proteins
535 into the matrix of peroxisomes and obviously through the nuclear pore (Kim and
536 Hettema, 2015; Lin and Hoelz, 2019). DNAJC5 forms a series of extremely stable
537 oligomers, which may provide versatile adaptors to accommodate diverse
538 misfolded or folded substrates with different dimensions. The structure of
539 DNAJC5 oligomers may shed light on the principle of this folding-independent
540 translocation pathway.

541

542

543 # Materials and methods

544

545 **Key Resources table**

REAGENT or RESOURCE	SOURCE	IDENTIFIER
Antibodies		
Mouse monoclonal anti-α-synuclein	BD Biosciences	Cat# 610787
Rabbit polyclonal anti-α-synuclein	Proteintech	Cat# 10842-1-AP

Rabbit polyclonal anti-DNAJC5	RayBiotech	Cat# 144-10489-200
Mouse monoclonal anti-alpha Tubulin	Abcam	Cat# ab7291
Mouse monoclonal anti-Alix	Santa Cruz Biotechnology	Cat# Sc-53540
Rabbit monoclonal anti-CD9	Cell Signaling Technology	Cat# 13174S
Mouse monoclonal anti-PDI	Enzo Life Sciences	Cat# ADI-SPA-891-D
Mouse monoclonal anti-CD63	Fisher Scientific	Cat# BDB556019
Mouse monoclonal anti-Flotillin-2	BD Biosciences	Cat# 610383
Mouse monoclonal anti-Transferrin Receptor	Thermo Fisher SCIENTIFIC	Cat# 13-6800
Mouse monoclonal anti-GM130	BD Biosciences	Cat# 610823
Rabbit monoclonal anti-Tom20	Cell Signaling Technology	Cat# 42406S
Rabbit polyclonal anti-GFP	Fisher Scientific	Cat# NC9589665
Rabbit polyclonal anti-LC3B	Novus Biologicals	Cat# NB100-2220
Rabbit monoclonal anti-Citrate Synthase	Cell Signaling Technology	Cat# 14309S
Rabbit polyclonal anti-Dopamine transporter	Bioss Antibodies	Cat# BS-1714R
Rabbit monoclonal anti-beta III Tubulin	Abcam	Cat# ab215037
Rabbit polyclonal anti-Tyrosine hydroxylase	Millipore	Cat# AB152
Chicken polyclonal Microtubule-associated protein 2	Abcam	Cat# ab92434
Mouse monoclonal anti-FLAG	Sigma-Aldrich	Cat# F9291

Bacterial and virus strains		
XL1-Blue competent cells	MacroLab Berkeley	N/A
Rossetta (DE3) pLysS competent cells	MacroLab Berkeley	N/A
Chemicals, peptides, and recombinant proteins		
Anti-FLAG M2 Affinity Gel	Sigma-Aldrich	Cat# A2220-5ML
Dimethyl sulfoxide (DMSO)	Fisher Scientific	Cat# BP231-100
Quercetin	Sigma-Aldrich	Cat# Q4951-10G
2-Bromopalmitic acid	Millipore Sigma	Cat# 21604-1G
Balfilomycin A1	Cayman Chemical	Cat# 11038
Retinoic acid	Sigma-Aldrich	Cat# R2625-100MG
HaloTag® Oregon Green® Ligand	Promega	Cat# G2802
HaloTag® TMR® Ligand	Promega	Cat# G8251
Prolong Gold with DAPI	Fisher Scientific	Cat# P36931
Proteinase K	Sigma-Aldrich	Cat# P2308
α-syn tandem repeats protein	This paper	N/A
Critical Commercial Assays		
Nano-Glo® Luciferase Assay System	Promega	Cat# N1150
LEGEND MAX™ Human α-synuclein (Colorimetric) ELISA Kit	BioLegend	Cat# 448607
Mouse α-synulcein ELISA Kit	Abcam	Cat# ab282865
Experimental Models: Cell Lines		
HEK293T Cells	Cell culture facility, UC Berkeley	N/A

HEK293-lenti-X Cells	Cell culture facility, UC Berkeley	N/A
MDA-MB-231 Cells	Cell culture facility, UC Berkeley	N/A
Hela Cells	Cell culture facility, UC Berkeley	N/A
SH-SY5Y Cells	Cell culture facility, UC Berkeley	N/A
U2OS Cells	Cell culture facility, UC Berkeley	N/A
HEK293T-DNAJC5-CRISPR KO cells	This study	N/A
SH-SY5Y-DNAJC5-shRNA KD cells	This study	N/A
Mouse Embryonic Stem Cells		
Mouse Embryonic Stem Cells-hDNAJC5-OE cells	This study	N/A
Human Induced Pluripotent Stem Cells	University of Oxford; EBiSC repository	N/A
Recombinant DNA plasmids		
mCherry-Rab5CA(Q79L)	Addgene	Cat# 35138
BFP-Rab5CA(Q79L)	This study	N/A
SNCA (Myc-DDK-tagged)-Human synuclein, alpha	OriGene Technoogy	Cat# RC221446
CSP (DNAJC5) (NM_025219) Human Tagged ORF Clone	OriGene Technology	Cat# RC208826

TCH1003-MGC premier cDNA clone for USP19	transOMIC	Cat# TCH1003
pCMV-α-synuclein-A30P	Gift of Dr. Thomas Südhof lab	N/A
pCMV-α-synuclein-E46K	Gift of Dr. Thomas Südhof lab	N/A
pCMV-α-synuclein-A53T	Gift of Dr. Thomas Südhof lab	N/A
αS-2 (α-syn-α-syn) tandem dimer	Gift of Michael Woodside lab	N/A
αS-4 (α-syn-α-syn-α-syn-α-syn) tandem Tetramer	Gift of Michael Woodside lab	N/A
pCMV-αS-2	This study	N/A
pCMV-αS-4	This study	N/A
pCMV-DNAJC5-L115R	This study	N/A
pCMV-DNAJC5-L116Δ	This study	N/A
pCMV-DNAJC5 (WT)-HaloTag	This study	N/A
pCMV-DNAJC5 (L115R)-HaloTag	This study	N/A
pCMV-XPACK-DNAJC5 (L115R)-HaloTag	This study	N/A
mNeonGreen-α-synuclein	This study	N/A
3H-α-synuclein	This study	N/A
α-synuclein-3H	This study	N/A
pCMV-XPACK-DNAJC5 (WT)	This study	N/A

pCMV-XPACK-DNAJC5 (L115R)	This study	N/A
pCMV-DEAD XPACK-DNAJC5 (L115R)	This study	N/A
pCMV-DNAJC5-ΔJ (Δ14-82)	This study	N/A
pCMV-DNAJC5-ΔC10 (D189-198)	This study	N/A
pCMV-DNAJC5-ΔC20 (D179-198)	This study	N/A
pCMV-DNAJC5-ΔC30 (D169-198)	This study	N/A
pCMV-DNAJC5-ΔC40 (D151-198)	This study	N/A
pCMV-pOTC-GFP	This study	N/A
pCMV-pOTC-3H-GFP	This study	N/A
pX330-Venus-DNAJC5-Exon 4-gRNA	This study	N/A
pLenti-CMV-DNAJC5	This study	N/A
pLenti-CMV-DNAJC5 (L115R)	This study	N/A
plKO.1-DNAJC5-ShRNA	This study	N/A
Software and algorithms		
Fiji (ImageJ)	NIH	https://imagej.nih.gov/ij/
PyMOL	Schrödinger	https//pymol.org/2/
Prism 8	Graphpad	https://www.graphpad.com/scientific-software/prism/
AlphaFold Protein Structure Database	DeepMind	https://alphafold.ebi.ac.uk/

546

547

548

549 **Cell culture and transfection**

550 Cells were grown at 37°C in 5% CO2 and maintained in Dulbecco's modified
551 Eagle's medium (DMEM) supplemented with 10% fetal bovine serum (FBS). For
552 secretion assays, the FBS concentration was reduced to 1% for up to 36 h during
553 which time the growth rate of cells slowed but cells remained viable. For EV
554 preparation and medium fractionation, we grew cells in DMEM supplemented with
555 exosome-depleted FBS. Exosome-depleted FBS was prepared by overnight
556 centrifugation of 30% diluted FBS in DMEM at 100,000xg. Transfection of
557 plasmids into cells was performed using Lipofectamine 2000 (Thermo Fisher
558 Scientific, Waltham, MA) according to the manufacturer's protocols.

559 **Reconstitution of α-syn secretion in HEK293T cells**

560 HEK293T cells (cultured in 6-well plates) were cultured to 60% confluence and
561 co-transfected with plasmids encoding different constructs of α-syn and DNAJC5.
562 pCMV-GFP was used as a transfection control in all secretion experiments. At 4 h
563 after transfection, we replaced cell culture medium with DMEM supplemented
564 with 1% FBS containing indicated drugs for treatment. At indicated time points,
565 we collected media fractions which were centrifuged at 1,000xg for 10 min to
566 remove floating cells and cell debris. The media were mixed with
567 methanol/chloroform to precipitate proteins which were collected by centrifugation
568 (10,000 g x 10 min) and resuspended in SDS-PAGE sample loading buffer to
569 achieve concentration (20-fold). Cells were lysed in lysis buffer (10 mM Tris, pH
570 7.4, 100 mM NaCl, 1% Triton X-100). Both the concentrated media and cell lysate
571 fractions were analyzed by immunoblot.

572 To exclude the release of cytoplasmic proteins from cell death, we monitored the
573 viability of cells after transfection with a Countess™ II Automated Cell Counter
574 (Thermo Scientific) using trypan blue staining.

575 For a nanoluciferase-based assay, media fractions were collected and centrifuged at
576 1,000xg for 10 min. The supernatant fractions were harvested and further diluted
577 with PBS buffer (1000-fold). The nanoluciferase activity was assayed using a
578 Nano-Glo® Luciferase Assay System (Promega, Madison, WI) according to the
579 manufacturer's protocol.

580 **Membrane and Cytosol fractionation**

581 Cells (one 10cm dish) were cultured to 70% confluence and transfected with
582 different constructs of DNAJC5. One day after transfection, we harvested the
583 transfected cells by scraping in 1 ml B88 (20 mM HEPES-KOH, pH 7.2, 250 mM
584 sorbitol, 150 mM potassium acetate and 5 mM magnesium acetate) plus a cocktail
585 of protease inhibitors (Sigma-Aldrich, St. Louis, MO). Cells were homogenized by
586 10 passages through a 22G needle. Homogenates were centrifuged at 500xg for 10
587 min and the resulting post-nuclear supernatant (PNS) fractions were centrifuged at
588 100,000xg for 1.5 h. High-speed supernatant fractions were then subjected to a
589 repeat centrifugation to achieve a clarified cytosol fraction. The pellet fraction was
590 washed and resuspended in the same volume of B88. Resuspended material was
591 also centrifuged again to collect a washed membrane fraction. Membranes were
592 lysed in lysis buffer.

593 For membrane fractionation, the PNS was subjected to differential centrifugation at
594 3,000xg (10 min), 25,000xg (20 min) and 100,000xg (30min). Membrane fractions

595 were normalized to phosphatidylcholine content and analyzed by immunoblot (Ge
596 et al., 2013).

597 For proteinase K protection assays, the 25,000xg membrane fraction was aliquoted
598 into three tubes: one without proteinase K, one with proteinase K (10 μg/ml), and
599 one with proteinase K plus TritonX-100 (0.5%). The incubation was conducted on
600 ice for 20 min and stopped by sequential addition of PMSF (1mM) and sample
601 buffer and samples were then heated on metal block at 95°C for 5 min and
602 analyzed by SDS-PAGE and immunoblot.

603 **In vitro depalmitoylation assay**

604 Cells (HEK293T, MDA-MB-231 or Hela) were transfected with DNAJC5.
605 Cellular membranes were prepared as described above. For chemical
606 deplamitoylation, the membranes were resuspended and incubated with 0.5 M
607 hydroxylamine (pH 7.2) or 0.5 M Tris (pH 7.2, control) at room temperature
608 overnight in the presence of a cocktail of protease inhibitors (Sigma-Aldrich, St.
609 Louis, MO). The mobility of DNAJC5 was examined by SDS-PAGE followed by
610 immunoblot.

611 **CRISPR/Cas9 genome editing**

612 gRNA targeting exon 4 of DNAJC5 (CACCGGAGGCCGCAGAAGACAAACA)
613 was inserted into a pX330-based plasmid expressing Venus fluorescent protein
614 (Shurtleff et al., 2016). HEK293T cells were transfected with pX330-pX330-
615 Venus-DNAJC5-Exon 4-gRNA by Lipofectamine 2000 (Thermo Fisher Scientific,
616 Waltham, MA). After 48 h, we diluted the cells and single colonies were isolated,
617 expanded and determined for DNAJC5 KO by immunoblot.

618 **Medium fractionation and extracellular vesicle preparation**

619 Conditioned medium was harvested and centrifuged first at 1,500xg for 20 min
620 followed by 10,000xg for 30 min and 100,000xg for 1.5 h. The supernatant
621 fractions at each step were collected and treated with methanol/chloroform to
622 precipitate proteins which were then collected by centrifugation. Pellet fractions
623 were resuspended in sample buffer to achieve a 20-fold concentration. The
624 sedimented fractions at each step were also collected and resuspended in sample
625 buffer. All the fractions were analyzed by immunoblot.

626 EVs were isolated by buoyant density flotation on a sucrose step gradient. The
627 pellet fraction from a 100,000xg centrifugation was resuspended in PBS and mixed
628 with 60% sucrose buffer (10mM Tris-HCl pH 7.4, 100 mM NaCl) to achieve a
629 final sucrose concentration >50% as measured with a refractometer. Aliquots of
630 40% (5 ml) and 10% (2 ml) sucrose buffer were sequentially overlaid above the
631 sample. The tubes were then centrifuged at 150,000xg for 16 h in an SW41 Ti
632 swinging-bucket rotor (Beckman Coulter). After centrifugation, 0.5 ml fractions
633 were collected from top to bottom and samples analyzed by SDS-PAGE and
634 immunoblot.

635 **Co-immunoprecipitation**

636 Media fractions were collected and centrifuged at 1,000xg for 10min. The
637 supernatant fractions were collected and concentrated (20-fold) using a 10 kDa
638 Amicon filter (Millipore, Billerica, MA). Concentrated media fractions (1 ml)
639 were incubated with 20 μl of anti-FLAG M2 affinity gel (Sigma-Aldrich, St.
640 Louis, MO) for 1h at 4°C. After washing 5x with lysis buffer, SDS-PAGE sample

641 loading buffer was added to the beads and samples were processed for SDS-PAGE
642 and immunoblot.

643 **Protein purification**

644 The purification of different α-syn tandem-oligomer constructs was performed as
645 previously described (Dong et al., 2018). Briefly, an osmotic shock protocol was
646 adapted to enrich proteins released from the periplasm of transfected *E. coli*. The
647 supernatant fraction containing released proteins was subjected to ammonium
648 sulfate (AS) precipitation, with 50%, 45% and 40% saturated concentration of AS
649 for monomer, dimer and tetramer, respectively. After overnight precipitation, the
650 precipitated proteins were collected by centrifugation at 100,000xg for 30 min. The
651 pellet fractions were dissolved in Buffer A (20mM Tris-HCl pH 8.0) and clarified
652 by repeated centrifugation at 100,000xg for 30 min.

653 Clarified supernatants were applied to an equilibrated HiPrep Q Fast Flow 16/10
654 column (GE Healthcare, Chicago, IL). Eluted proteins were collected, concentrated
655 by 10 kDa Amicon filter (Millipore, Billerica, MA) and further purified by gel
656 filtration (Superdex-200, GE Healthcare) with PBS used as gel filtration buffer.
657 Purified proteins were assessed by SDS-PAGE followed by coomassie-blue
658 staining.

659 **Immunofluorescence and live-cell Imaging**

660 For immunofluorescence, U2OS cells were washed once with PBS and
661 immediately fixed by 4% EM-grade paraformaldehyde (Electron Microscopy
662 Science, Hatfield, PA) for 10 min at room temperature. Cells were washed three
663 times with PBS and blocked and permeabilized for 30 min in permeabilization
664 buffer (5% FBS and 0.1% saponin in PBS). hiPSC dopamine neurons were fixed

665 with 4% paraformaldehyde in PBS and 0.1% Triton-X was used for permablization
666 (10 mins) followed by blocking in 10% normal donkey serum for 1 h. Cells were
667 then incubated with 1:100 dilution of primary antibodies overnight at 4°C. After
668 three washes with PBS, cells were incubated with 1:500 dilution of fluorophore-
669 conjugated secondary antibodies for 30 min at room temperature. Prolong Gold
670 with DAPI (Thermo Fisher) was used as mounting solution. Images were acquired
671 with a Zeiss LSM900 confocal microscope and analyzed with Fiji/ImageJ software
672 (https://imagej.nih.gov/ij/).

673 For live-cell imaging, cells were cultured in 35mm glass bottom dishes (MatTek).
674 The addition of HaloTag fluorescent ligands were added according to the
675 manufacturer's protocol (Promega). After incubation, the medium was replaced
676 with Opti-MEM supplemented with 10% FBS. Imaging was performed using a
677 Zeiss LSM900 confocal microscope in a temperature-controlled (37°C and 5%
678 CO2) environment.

679 **Mitochondria purification**

680 HEK293T cells were trypsinized and collected by centrifugation. Cells were
681 washed twice with NKM buffer (1 mM Tris HCl, pH7.3, 0.13 M NaCl, 5mM KCl,
682 7.5 mM $MgCl_2$), and resuspended in 6 packed cell volumes of homogenization
683 buffer (10 mM Tris pH 7.4, 10 mM KCl, 0.15 mM $MgCl_2$). Cells were
684 homogenized by 10 passages through a 22G needle. Cell homogenates were mixed
685 gently with the same volume of 2.3M sucrose solution and centrifuged at 1,200xg
686 for 5 min to remove unbroken cells and large cell debris. The recovered
687 supernatant fractions were centrifuged at 7,000xg for 10min. Mitochondria
688 enriched in the pellet fraction were resuspended in 3 packed cell volumes of

689 Mitochondria Suspension Buffer (10 mM Tris, pH 7.3, 0.15 mM MgCl2, 0.25mM
690 sucrose).

691

692 **Differentiation of SH-SY5Y cells**

693 SH-SY5Y neuroblastoma cells were maintained in Dulbecco's modified Eagle's
694 medium (DMEM) supplemented with 1x non-essential amino acid (NEAA), 1x
695 sodium pyruvate and 10% fetal bovine serum (FBS). Differentiation was induced
696 by lowering the FBS in culture medium to 1% plus 10 μM retinoic acid (RA). Cell
697 medium was replaced each 3 d to replenish RA. Cell morphology was monitored
698 by microscopy and experiments on SH-SY5Y cells were performed from D6 of
699 differentiation.

700 **shRNA knockdown**

701 plKO.1-Hygro plasmids containing shRNA targeting DNAJC5
702 (ccggGCAACCTCAGATGACATTAAACTCGAGTTTAATGTCATCTGAGGTT
703 GCTTTTTG) together with pMD2.G and PsPAX2 were transfected into HEK293T
704 cells to produce lentiviral particles for 72 h. Lentivirus particles were concentrated
705 with Lenti-X™ Concentrator (Takara Bio). SH-SY5Y was transduced by lentivirus
706 before differentiation. Three days post transduction, cells were selected with 250
707 μg/ml hygromycin for 10 d. The selected cells were differentiated, and the
708 knockdown was verified with immunoblot.

709 **Culture and differentiation of mouse embryonic stem cells**

710 Mouse ESCs (R1) were maintained and differentiated into dopaminergic neurons
711 following a modified protocol from (Ni et al., 2013). Briefly, R1 cells were

712 maintained in a feeder-independent system, plated in 0.1% gelatin (StemCell
713 technologies) and cultured in KSR medium consisting of KnockOut DMEM, 20%
714 KnockOut serum replacement, 2mM L-glutamine, 0.1mM nonessential amino
715 acids, 0.1 mM β-mercaptoethanol, and 1000 U/ml leukemia inhibitory factor (LIF,
716 Chemicon International) with a media change every day. Cells were then grown in
717 aggregate cultures to form EBs in DMEM/F12 media supplemented with 10%
718 knock-out serum replacement, 2.4% N2, 4500 mg/l Glucose, 2mM L-glutamine,
719 and 0.1mM β-mercaptoethanol. EBs were formed for 4 d and then plated on
720 10ug/ml laminin-coated plates. After 24h of culture, the media was replaced by
721 DMEM/F12, 3% Knockout serum, N2, Glucose, 1X Glutamine, 2-BME
722 supplemented with 1% Insulin/Transferrin/Selenium with a media change every
723 day. After 7 d, cells were dissociated by Accutase StemPro and plated on laminin-
724 coated plates using a 1:1 ratio of Neurobasal media and DMEM/F12, N2, B27,
725 2mM L-glutamine, 0.1mM nonessential amino acids, 0.1 mM β-mercaptoethanol
726 supplemented with 20 ng/ml bFGF (R&D Systems), 200 ng/ml SHH (R&D
727 Systems) and 25ng/ml FGF8b (R&D Systems) with a media change every day.
728 After 8 d, the culture medium was changed to Neurobasal/B27 medium
729 supplemented with 0.5mM dbcAMP (Santa cruz), 0.2 mM ascorbic acid (Stem cell
730 technologies), 20ng/ml BDNF (Petrotech) and 20ng/ml GDNF (Petrotech) with a
731 media change every other day.

732

733 **Differentiation and culture of dopaminergic neurons from human induced-**
734 **pluripotent stem cells (hiPSCs)**

735 Primary fibroblasts derived from PD patients carrying the *GBA-N370S* mutation and
736 a healthy control (below) were reprogrammed to pluripotency as described
737 previously (Fernandes et al., 2016) and clones were selected, tested for mycoplasma

738 and QCed according to established protocols (Lang et al., 2019). hiPSCs were
739 differentiated toward dopaminergic fate as described by (Kriks et al., 2011) with
740 small modifications (Beevers et al., 2017). Briefly, hiPSCs were patterned for 21
741 days with a growth factor cocktail to promote differentiation toward ventral
742 midbrain neuronal progenitor cells for 11 days (10 mM SB431542, Tocris; 100 nM
743 LDN193189, Sigma-Aldrich; 2 mM puromorphamine, Milipore; 100 ng/ml sonic
744 hedgehog, Bio-Techne; 100 ng/ml fibroblast growth factor-8a, Bio-Techne and 3
745 mM CHIR99021), followed by 10 d of differentiation to dopaminergic neurons (20
746 ng/ml brain-derived neurotrophic factor, Peprotech; 20 ng/ml glial cell line-derived
747 neurotrophic factor, Peprotech; 1 ng/ml transforming growth factor type β3,
748 Peprotech; 0.5 mM dibutyryl cAMP, Sigma-Aldrich; 0.2 mM Ascorbic acid, Sigma-
749 Aldrich and 10 mM DAPT, Abcam). Neurons were matured for a further 2 weeks
750 (to day 35) for $\boldsymbol{\alpha}$-synuclein secretion, or for a further 5 weeks (to day 65) for analysis
751 by SDS-PAGE and immunoblot. Neurons were then treated with DMSO, quercetin
752 or 2-bromoplamitic acid for 3 d.

Donor ID	Study ID	Genotype	Age / Gender	Characterisation
SFC156-03	Control	GBA wt /GBA wt	75 Male	(Lang et al., 2019)
MK071	PD 1	GBA N370S / GBA wt	81 Female	(Fernandes et al., 2016)
MK088	PD 2	GBA N370S / GBA wt	46 Male	(Fernandes et al., 2016)
SFC871-03-09	PD 3	GBA N370S / GBA wt	70 Female	(Helle Bogetofte, 2021)
MK082	PD 4	GBA N370S / GBA wt	51 Male	(Lang et al., 2019)

753

754

755 **Extracellular α-syn measurements**

756 Commercial ELISA Kits as listed in Key Resources Table were used to quantify
757 the extracellular α-syn in SH-SY5Y and mouse mDA neuronal culture.
758 Conditioned media were collected and centrifuged at 1,000 g for 10 min. α−Syn in
759 the recovered supernatant was measured using the protocol provided in the kit.

760 α-syn secretion by hiPSC-derived dopaminergic neurons was measured as
761 described previously (Fernandes et al., 2016) (Fernandes et al., 2016) using an
762 electro-chemiluminescent assay (Meso Scale Discovery, MD, USA, Cat#
763 K151TGD-2) and a MESO QuickPlex SQ 120 instrument (Meso Scale Discovery)
764 according to the manufacturer's instructions. Briefly, culture media was collected
765 3d after drug treatment (differentiation day 38) and quantified relative to a standard
766 curve. Data was normalized relative to the total protein content of the cells from
767 which the conditioned media had been collected, as determined by BCA assay.

768 **Immunoblots**

769 Cell lysate, cytosol or membrane samples, and extracellular vesicle samples were
770 mixed with SDS sample loading buffer. Samples were heated at 95 °C for 5 min
771 and separated on SDS-PAGE gels. Proteins were transferred to PVDF membranes
772 (EMD Millipore, Darmstadt, Germany), blocked with 5% bovine serum albumin in
773 TBST (20 mM Tris pH 7.4, 150 mM NaCl and 0.1% Tween-20) and incubated
774 overnight with primary antibodies. For immunoblots from hiPSC dopamine
775 neurons, samples in loading buffer were heated to 70°C for 10 minutes and
776 blocking was carried out with 5% skimmed milk. For immunoblots of endogenous
777 α-syn in SH-SY5Y cells, PVDF membranes were fixed with 0.4%
778 paraformaldehyde (Electron Microscopy Science, Hatfield, PA) in TBST at room
779 temperature for 30 min (Lee and Kamitani, 2011). Blots were then washed with

780 TBST, followed by incubation with anti-rabbit or anti-mouse secondary antibodies
781 (GE Healthcare Life Sciences, Pittsbugh, PA). Detection was performed with
782 Supersignal™ Chemiluminescent substrate (Thermo Fisher) and quantified with
783 Fiji/ImageJ. Primary antibodies used in this study were listed in Key Resources
784 Table. All antibodies used for immunoblots were diluted 1:1,000, except for
785 1:2,000 of mouse anti-Tubulin, 1:500 of rabbit anti-α-syn and of rabbit anti-
786 tyrosine hydroxylase.

787

788 **Acknowledgements**

789 We thank Dr. Michael Woodside and Dr. Thomas Südhof for sharing the plasmids,
790 and Dr. Kalina Naidoo, Dr. Mootaz Salman and William McGuinness for
791 preparation of iPSC samples. We also thank the staff at the UC Berkeley shared
792 facilities, the cell culture facility, the DNA sequencing facility and Biological
793 imaging facility. SW is supported as Associate of the HHMI. RS is an Investigator
794 of the HHMI, a Senior fellow of the UC Berkeley Miller Institute of Science and
795 the Scientific Director of Aligning Science Across Parkinson's Disease.

796 **Additional information**

797 **Competing Interests**

798 Randy Schekman: Reviewing Editor and Founding Editor-in-Chief, *eLife*. The
799 other authors declare that no competing interests exist.

800 **Funding**

801 **Funder** **Grant reference number** **Author**

802 Howard Hughes Medical Institute Investigator Randy Schekman

803 Aligning Science Across Parkinson's Disease Scientific Director Randy Schekman

804 NIH Biology and Biotechnology of Cell and Gene Therapy Training Program, NIH training
805 program T32GM139780, Nancy C. Hernandez Villegas

806 Aligning Science Across Parkinson's Disease [ASAP-020370] Richard Wade-Martins

807 The funders had no role in study design, data collection and interpretation, or the
808 decision to submit the work for publication.

809

810 Author Contributions

811 SW, Conception and design, Acquisition of data, Analysis and interpretation of
812 data, Drafting or revising the article; DS, Conception and design, Acquisition of
813 data, Analysis and interpretation of data, Drafting or revising the article; RS,
814 Conception and design, Analysis and interpretation of data, Drafting or revising the
815 article. NHV, Acquisition of data, analysis and interpretation of data, drafting or
816 revising the article. IT-W, Acquisition of data, analysis and interpretation of data,
817 drafting or revising the article. RW-M, Analysis and interpretation of data, drafting
818 or revising the article.

819 References

820 Abounit, S., Bousset, L., Loria, F., Zhu, S., de Chaumont, F., Pieri, L., Olivo-Marin, J.C., Melki, R., and
821 Zurzolo, C. (2016). Tunneling nanotubes spread fibrillar alpha-synuclein by intercellular trafficking of
822 lysosomes. EMBO J *35*, 2120-2138.
823 Alderson, T.R., and Markley, J.L. (2013). Biophysical characterization of alpha-synuclein and its
824 controversial structure. Intrinsically Disord Proteins *1*, 18-39.
825 Bandyopadhyay, U., Kaushik, S., Varticovski, L., and Cuervo, A.M. (2008). The chaperone-mediated
826 autophagy receptor organizes in dynamic protein complexes at the lysosomal membrane. Mol Cell Biol
827 *28*, 5747-5763.

828 Benitez, B.A., Alvarado, D., Cai, Y., Mayo, K., Chakraverty, S., Norton, J., Morris, J.C., Sands, M.S., Goate,
829 A., and Cruchaga, C. (2011). Exome-sequencing confirms DNAJC5 mutations as cause of adult neuronal
830 ceroid-lipofuscinosis. PLoS One *6*, e26741.
831 Bohdanowicz, M., Balkin, D.M., De Camilli, P., and Grinstein, S. (2012). Recruitment of OCRL and Inpp5B
832 to phagosomes by Rab5 and APPL1 depletes phosphoinositides and attenuates Akt signaling. Mol Biol
833 Cell *23*, 176-187.
834 Borghi, R., Marchese, R., Negro, A., Marinelli, L., Forloni, G., Zaccheo, D., Abbruzzese, G., and Tabaton,
835 M. (2000). Full length alpha-synuclein is present in cerebrospinal fluid from Parkinson's disease and
836 normal subjects. Neurosci Lett *287*, 65-67.
837 Braak, H., de Vos, R.A., Bohl, J., and Del Tredici, K. (2006). Gastric alpha-synuclein immunoreactive
838 inclusions in Meissner's and Auerbach's plexuses in cases staged for Parkinson's disease-related brain
839 pathology. Neurosci Lett *396*, 67-72.
840 Braak, H., Del Tredici, K., Rub, U., de Vos, R.A., Jansen Steur, E.N., and Braak, E. (2003). Staging of brain
841 pathology related to sporadic Parkinson's disease. Neurobiol Aging *24*, 197-211.
842 Brahic, M., Bousset, L., Bieri, G., Melki, R., and Gitler, A.D. (2016). Axonal transport and secretion of
843 fibrillar forms of alpha-synuclein, Abeta42 peptide and HTTExon 1. Acta Neuropathol *131*, 539-548.
844 Buratta, S., Tancini, B., Sagini, K., Delo, F., Chiaradia, E., Urbanelli, L., and Emiliani, C. (2020). Lysosomal
845 Exocytosis, Exosome Release and Secretory Autophagy: The Autophagic- and Endo-Lysosomal Systems
846 Go Extracellular. Int J Mol Sci *21*.
847 Burre, J., Sharma, M., and Sudhof, T.C. (2014). alpha-Synuclein assembles into higher-order multimers
848 upon membrane binding to promote SNARE complex formation. Proc Natl Acad Sci U S A *111*, E4274-
849 4283.
850 Calo, L., Hidari, E., Wegrzynowicz, M., Dalley, J.W., Schneider, B.L., Podgajna, M., Anichtchik, O., Carlson,
851 E., Klenerman, D., and Spillantini, M.G. (2021). CSPalpha reduces aggregates and rescues striatal
852 dopamine release in alpha-synuclein transgenic mice. Brain *144*, 1661-1669.
853 Chandra, S., Gallardo, G., Fernandez-Chacon, R., Schluter, O.M., and Sudhof, T.C. (2005). Alpha-synuclein
854 cooperates with CSPalpha in preventing neurodegeneration. Cell *123*, 383-396.
855 Cho, E., and Park, M. (2016). Palmitoylation in Alzheimer's disease and other neurodegenerative
856 diseases. Pharmacol Res *111*, 133-151.
857 Chu, Y., Muller, S., Tavares, A., Barret, O., Alagille, D., Seibyl, J., Tamagnan, G., Marek, K., Luk, K.C.,
858 Trojanowski, J.Q.*, et al.* (2019). Intrastriatal alpha-synuclein fibrils in monkeys: spreading, imaging and
859 neuropathological changes. Brain *142*, 3565-3579.
860 Chung, H.K., Ho, H.A., Perez-Acuna, D., and Lee, S.J. (2020). Modeling alpha-Synuclein Propagation with
861 Preformed Fibril Injections. J Mov Disord *13*, 77-79.
862 Danzer, K.M., Kranich, L.R., Ruf, W.P., Cagsal-Getkin, O., Winslow, A.R., Zhu, L., Vanderburg, C.R., and
863 McLean, P.J. (2012). Exosomal cell-to-cell transmission of alpha synuclein oligomers. Mol Neurodegener
864 *7*, 42.
865 Dauer, W., and Przedborski, S. (2003). Parkinson's disease: mechanisms and models. Neuron *39*, 889-
866 909.
867 Deng, J., Koutras, C., Donnelier, J., Alshehri, M., Fotouhi, M., Girard, M., Casha, S., McPherson, P.S.,
868 Robbins, S.M., and Braun, J.E.A. (2017). Neurons Export Extracellular Vesicles Enriched in Cysteine String
869 Protein and Misfolded Protein Cargo. Sci Rep *7*, 956.
870 Deruelle, V., Bouillot, S., Job, V., Taillebourg, E., Fauvarque, M.O., Attree, I., and Huber, P. (2021). The
871 bacterial toxin ExoU requires a host trafficking chaperone for transportation and to induce necrosis. Nat
872 Commun *12*, 4024.

873 Diez-Ardanuy, C., Greaves, J., Munro, K.R., Tomkinson, N.C., and Chamberlain, L.H. (2017). A cluster of
874 palmitoylated cysteines are essential for aggregation of cysteine-string protein mutants that cause
875 neuronal ceroid lipofuscinosis. Sci Rep *7*, 10.
876 Dong, C., Hoffmann, M., Li, X., Wang, M., Garen, C.R., Petersen, N.O., and Woodside, M.T. (2018).
877 Structural characteristics and membrane interactions of tandem alpha-synuclein oligomers. Sci Rep *8*,
878 6755.
879 El-Agnaf, O.M., Salem, S.A., Paleologou, K.E., Cooper, L.J., Fullwood, N.J., Gibson, M.J., Curran, M.D.,
880 Court, J.A., Mann, D.M., Ikeda, S.*, et al.* (2003). Alpha-synuclein implicated in Parkinson's disease is
881 present in extracellular biological fluids, including human plasma. FASEB J *17*, 1945-1947.
882 Emmanouilidou, E., Melachroinou, K., Roumeliotis, T., Garbis, S.D., Ntzouni, M., Margaritis, L.H.,
883 Stefanis, L., and Vekrellis, K. (2010). Cell-produced alpha-synuclein is secreted in a calcium-dependent
884 manner by exosomes and impacts neuronal survival. J Neurosci *30*, 6838-6851.
885 England, C.G., Ehlerding, E.B., and Cai, W. (2016). NanoLuc: A Small Luciferase Is Brightening Up the Field
886 of Bioluminescence. Bioconjug Chem *27*, 1175-1187.
887 Fernandes, H.J., Hartfield, E.M., Christian, H.C., Emmanoulidou, E., Zheng, Y., Booth, H., Bogetofte, H.,
888 Lang, C., Ryan, B.J., Sardi, S.P.*, et al.* (2016). ER Stress and Autophagic Perturbations Lead to Elevated
889 Extracellular alpha-Synuclein in GBA-N370S Parkinson's iPSC-Derived Dopamine Neurons. Stem Cell
890 Reports *6*, 342-356.
891 Fontaine, S.N., Zheng, D., Sabbagh, J.J., Martin, M.D., Chaput, D., Darling, A., Trotter, J.H., Stothert, A.R.,
892 Nordhues, B.A., Lussier, A.*, et al.* (2016). DnaJ/Hsc70 chaperone complexes control the extracellular
893 release of neurodegenerative-associated proteins. EMBO J *35*, 1537-1549.
894 Forland, M.G., Ohrfelt, A., Dalen, I., Tysnes, O.B., Blennow, K., Zetterberg, H., Pedersen, K.F., Alves, G.,
895 and Lange, J. (2018). Evolution of cerebrospinal fluid total alpha-synuclein in Parkinson's disease.
896 Parkinsonism Relat Disord *49*, 4-8.
897 Ge, L., Melville, D., Zhang, M., and Schekman, R. (2013). The ER-Golgi intermediate compartment is a key
898 membrane source for the LC3 lipidation step of autophagosome biogenesis. Elife *2*, e00947.
899 Greaves, J., and Chamberlain, L.H. (2006). Dual role of the cysteine-string domain in membrane binding
900 and palmitoylation-dependent sorting of the molecular chaperone cysteine-string protein. Mol Biol Cell
901 *17*, 4748-4759.
902 Greaves, J., Lemonidis, K., Gorleku, O.A., Cruchaga, C., Grefen, C., and Chamberlain, L.H. (2012).
903 Palmitoylation-induced aggregation of cysteine-string protein mutants that cause neuronal ceroid
904 lipofuscinosis. J Biol Chem *287*, 37330-37339.
905 Greaves, J., Salaun, C., Fukata, Y., Fukata, M., and Chamberlain, L.H. (2008). Palmitoylation and
906 membrane interactions of the neuroprotective chaperone cysteine-string protein. J Biol Chem *283*,
907 25014-25026.
908 Guerrero-Ferreira, R., Taylor, N.M., Arteni, A.A., Kumari, P., Mona, D., Ringler, P., Britschgi, M., Lauer,
909 M.E., Makky, A., Verasdonck, J.*, et al.* (2019). Two new polymorphic structures of human full-length
910 alpha-synuclein fibrils solved by cryo-electron microscopy. Elife *8*.
911 Guerrero-Ferreira, R., Taylor, N.M., Mona, D., Ringler, P., Lauer, M.E., Riek, R., Britschgi, M., and
912 Stahlberg, H. (2018). Cryo-EM structure of alpha-synuclein fibrils. Elife *7*.
913 Guo, M., Wang, J., Zhao, Y., Feng, Y., Han, S., Dong, Q., Cui, M., and Tieu, K. (2020). Microglial exosomes
914 facilitate alpha-synuclein transmission in Parkinson's disease. Brain *143*, 1476-1497.
915 Helle Bogetofte, B.J.R., Pia Jensen, Dana L.E. Vergoossen, Mike B. Barnkob, Lisa Kiani, Uroosa Chughtai,
916 Janine Brandes, Jane Vowles, Fiona Bunn, Peter Kilfeather, Hugo J.R. Fernandes, Tara Caffrey, Morten
917 Meyer,Sally A. Cowley,Martin R. Larsen, Richard Wade-Martins (2021). A novel post-translational

918 proteomics platform identifies neurite outgrowth impairments in Parkinson's disease GBA-N370S
919 dopamine neurons. BioRxiv.
920 Ho, G.P.H., Ramalingam, N., Imberdis, T., Wilkie, E.C., Dettmer, U., and Selkoe, D.J. (2021). Upregulation
921 of Cellular Palmitoylation Mitigates alpha-Synuclein Accumulation and Neurotoxicity. Mov Disord *36*,
922 348-359.
923 Horwich, A.L., Kalousek, F., Mellman, I., and Rosenberg, L.E. (1985). A leader peptide is sufficient to
924 direct mitochondrial import of a chimeric protein. EMBO J *4*, 1129-1135.
925 Huang, P.S., Oberdorfer, G., Xu, C., Pei, X.Y., Nannenga, B.L., Rogers, J.M., DiMaio, F., Gonen, T., Luisi, B.,
926 and Baker, D. (2014). High thermodynamic stability of parametrically designed helical bundles. Science
927 *346*, 481-485.
928 Jang, A., Lee, H.J., Suk, J.E., Jung, J.W., Kim, K.P., and Lee, S.J. (2010). Non-classical exocytosis of alpha-
929 synuclein is sensitive to folding states and promoted under stress conditions. J Neurochem *113*, 1263-
930 1274.
931 Jumper, J., Evans, R., Pritzel, A., Green, T., Figurnov, M., Ronneberger, O., Tunyasuvunakool, K., Bates, R.,
932 Zidek, A., Potapenko, A.*, et al.* (2021). Highly accurate protein structure prediction with AlphaFold.
933 Nature *596*, 583-589.
934 Kaushik, S., and Cuervo, A.M. (2018). The coming of age of chaperone-mediated autophagy. Nat Rev Mol
935 Cell Biol *19*, 365-381.
936 Kim, P.K., and Hettema, E.H. (2015). Multiple pathways for protein transport to peroxisomes. J Mol Biol
937 *427*, 1176-1190.
938 Kim, S., Kwon, S.H., Kam, T.I., Panicker, N., Karuppagounder, S.S., Lee, S., Lee, J.H., Kim, W.R., Kook, M.,
939 Foss, C.A.*, et al.* (2019). Transneuronal Propagation of Pathologic alpha-Synuclein from the Gut to the
940 Brain Models Parkinson's Disease. Neuron *103*, 627-641 e627.
941 Kordower, J.H., Chu, Y., Hauser, R.A., Freeman, T.B., and Olanow, C.W. (2008). Lewy body-like pathology
942 in long-term embryonic nigral transplants in Parkinson's disease. Nat Med *14*, 504-506.
943 Kriks, S., Shim, J.W., Piao, J., Ganat, Y.M., Wakeman, D.R., Xie, Z., Carrillo-Reid, L., Auyeung, G.,
944 Antonacci, C., Buch, A.*, et al.* (2011). Dopamine neurons derived from human ES cells efficiently engraft
945 in animal models of Parkinson's disease. Nature *480*, 547-551.
946 Kuhlman, B., and Bradley, P. (2019). Advances in protein structure prediction and design. Nat Rev Mol
947 Cell Biol *20*, 681-697.
948 Lang, C., Campbell, K.R., Ryan, B.J., Carling, P., Attar, M., Vowles, J., Perestenko, O.V., Bowden, R., Baig,
949 F., Kasten, M.*, et al.* (2019). Single-Cell Sequencing of iPSC-Dopamine Neurons Reconstructs Disease
950 Progression and Identifies HDAC4 as a Regulator of Parkinson Cell Phenotypes. Cell Stem Cell *24*, 93-106
951 e106.
952 Lashuel, H.A., Overk, C.R., Oueslati, A., and Masliah, E. (2013). The many faces of alpha-synuclein: from
953 structure and toxicity to therapeutic target. Nat Rev Neurosci *14*, 38-48.
954 Lashuel, H.A., Petre, B.M., Wall, J., Simon, M., Nowak, R.J., Walz, T., and Lansbury, P.T., Jr. (2002). Alpha-
955 synuclein, especially the Parkinson's disease-associated mutants, forms pore-like annular and tubular
956 protofibrils. J Mol Biol *322*, 1089-1102.
957 Lee, B.R., and Kamitani, T. (2011). Improved immunodetection of endogenous alpha-synuclein. PLoS One
958 *6*, e23939.
959 Lee, H.J., Patel, S., and Lee, S.J. (2005). Intravesicular localization and exocytosis of alpha-synuclein and
960 its aggregates. J Neurosci *25*, 6016-6024.
961 Lee, J., Xu, Y., Saidi, L., Xu, M., Zinsmaier, K., and Ye, Y. (2022). Abnormal triaging of misfolded proteins
962 by adult neuronal ceroid lipofuscinosis-associated DNAJC5/CSPalpha mutants causes lipofuscin
963 accumulation. Autophagy, 1-20.

964 Lee, J., Xu, Y., Zhang, T., Cui, L., Saidi, L., and Ye, Y. (2018). Secretion of misfolded cytosolic proteins from
965 mammalian cells is independent of chaperone-mediated autophagy. J Biol Chem *293*, 14359-14370.
966 Lee, J.G., Takahama, S., Zhang, G., Tomarev, S.I., and Ye, Y. (2016). Unconventional secretion of
967 misfolded proteins promotes adaptation to proteasome dysfunction in mammalian cells. Nat Cell Biol
968 *18*, 765-776.
969 Li, J.Y., Englund, E., Holton, J.L., Soulet, D., Hagell, P., Lees, A.J., Lashley, T., Quinn, N.P., Rehncrona, S.,
970 Bjorklund, A.*, et al.* (2008). Lewy bodies in grafted neurons in subjects with Parkinson's disease suggest
971 host-to-graft disease propagation. Nat Med *14*, 501-503.
972 Lin, D.H., and Hoelz, A. (2019). The Structure of the Nuclear Pore Complex (An Update). Annu Rev
973 Biochem *88*, 725-783.
974 Linder, M.E., and Deschenes, R.J. (2007). Palmitoylation: policing protein stability and traffic. Nat Rev
975 Mol Cell Biol *8*, 74-84.
976 Lopes, F.M., Schroder, R., da Frota, M.L., Jr., Zanotto-Filho, A., Muller, C.B., Pires, A.S., Meurer, R.T.,
977 Colpo, G.D., Gelain, D.P., Kapczinski, F.*, et al.* (2010). Comparison between proliferative and neuron-like
978 SH-SY5Y cells as an in vitro model for Parkinson disease studies. Brain Res *1337*, 85-94.
979 Los, G.V., Encell, L.P., McDougall, M.G., Hartzell, D.D., Karassina, N., Zimprich, C., Wood, M.G., Learish,
980 R., Ohana, R.F., Urh, M.*, et al.* (2008). HaloTag: a novel protein labeling technology for cell imaging and
981 protein analysis. ACS Chem Biol *3*, 373-382.
982 Luk, K.C., Kehm, V., Carroll, J., Zhang, B., O'Brien, P., Trojanowski, J.Q., and Lee, V.M. (2012). Pathological
983 alpha-synuclein transmission initiates Parkinson-like neurodegeneration in nontransgenic mice. Science
984 *338*, 949-953.
985 Neupert, W. (1997). Protein import into mitochondria. Annu Rev Biochem *66*, 863-917.
986 Ni, N., Hu, Y., Ren, H., Luo, C., Li, P., Wan, J.B., and Su, H. (2013). Self-assembling peptide nanofiber
987 scaffolds enhance dopaminergic differentiation of mouse pluripotent stem cells in 3-dimensional
988 culture. PLoS One *8*, e84504.
989 Noskova, L., Stranecky, V., Hartmannova, H., Pristoupilova, A., Baresova, V., Ivanek, R., Hulkova, H.,
990 Jahnova, H., van der Zee, J., Staropoli, J.F.*, et al.* (2011). Mutations in DNAJC5, encoding cysteine-string
991 protein alpha, cause autosomal-dominant adult-onset neuronal ceroid lipofuscinosis. Am J Hum Genet
992 *89*, 241-252.
993 Patel, P., Prescott, G.R., Burgoyne, R.D., Lian, L.Y., and Morgan, A. (2016). Phosphorylation of Cysteine
994 String Protein Triggers a Major Conformational Switch. Structure *24*, 1380-1386.
995 Rapoport, T.A., Li, L., and Park, E. (2017). Structural and Mechanistic Insights into Protein Translocation.
996 Annu Rev Cell Dev Biol *33*, 369-390.
997 Resh, M.D. (2006). Use of analogs and inhibitors to study the functional significance of protein
998 palmitoylation. Methods *40*, 191-197.
999 Scheiblich, H., Dansokho, C., Mercan, D., Schmidt, S.V., Bousset, L., Wischhof, L., Eikens, F., Odainic, A.,
1000 Spitzer, J., Griep, A.*, et al.* (2021). Microglia jointly degrade fibrillar alpha-synuclein cargo by distribution
1001 through tunneling nanotubes. Cell *184*, 5089-5106 e5021.
1002 Shahmoradian, S.H., Lewis, A.J., Genoud, C., Hench, J., Moors, T.E., Navarro, P.P., Castano-Diez, D.,
1003 Schweighauser, G., Graff-Meyer, A., Goldie, K.N.*, et al.* (2019). Lewy pathology in Parkinson's disease
1004 consists of crowded organelles and lipid membranes. Nat Neurosci *22*, 1099-1109.
1005 Shurtleff, M.J., Temoche-Diaz, M.M., Karfilis, K.V., Ri, S., and Schekman, R. (2016). Y-box protein 1 is
1006 required to sort microRNAs into exosomes in cells and in a cell-free reaction. Elife *5*.
1007 Stefanis, L. (2012). alpha-Synuclein in Parkinson's disease. Cold Spring Harb Perspect Med *2*, a009399.

1008 Strohaker, T., Jung, B.C., Liou, S.H., Fernandez, C.O., Riedel, D., Becker, S., Halliday, G.M., Bennati, M.,
1009 Kim, W.S., Lee, S.J., *et al.* (2019). Structural heterogeneity of alpha-synuclein fibrils amplified from
1010 patient brain extracts. Nat Commun *10*, 5535.
1011 Stykel, M.G., Humphries, K.M., Kamski-Hennekam, E., Buchner-Duby, B., Porte-Trachsel, N., Ryan, T.,
1012 Coackley, C.L., Bamm, V.V., Harauz, G., and Ryan, S.D. (2021). alpha-Synuclein mutation impairs
1013 processing of endomembrane compartments and promotes exocytosis and seeding of alpha-synuclein
1014 pathology. Cell Rep *35*, 109099.
1015 Tapper, H., and Sundler, R. (1995). Bafilomycin A1 inhibits lysosomal, phagosomal, and plasma
1016 membrane H(+)-ATPase and induces lysosomal enzyme secretion in macrophages. J Cell Physiol *163*,
1017 137-144.
1018 Virlogeux, A., Scaramuzzino, C., Lenoir, S., Carpentier, R., Louessard, M., Genoux, A., Lino, P.,
1019 Hinckelmann, M.V., Perrier, A.L., Humbert, S., *et al.* (2021). Increasing brain palmitoylation rescues
1020 behavior and neuropathology in Huntington disease mice. Sci Adv *7*.
1021 Xie, Y.X., Naseri, N.N., Fels, J., Kharel, P., Na, Y., Lane, D., Burre, J., and Sharma, M. (2022). Lysosomal
1022 exocytosis releases pathogenic alpha-synuclein species from neurons in synucleinopathy models. Nat
1023 Commun *13*, 4918.
1024 Xu, Y., Cui, L., Dibello, A., Wang, L., Lee, J., Saidi, L., Lee, J.G., and Ye, Y. (2018). DNAJC5 facilitates USP19-
1025 dependent unconventional secretion of misfolded cytosolic proteins. Cell Discov *4*, 11.
1026 Yano, M., Kanazawa, M., Terada, K., Namchai, C., Yamaizumi, M., Hanson, B., Hoogenraad, N., and Mori,
1027 M. (1997). Visualization of mitochondrial protein import in cultured mammalian cells with green
1028 fluorescent protein and effects of overexpression of the human import receptor Tom20. J Biol Chem
1029 *272*, 8459-8465.
1030 Yim, N., Ryu, S.W., Choi, K., Lee, K.R., Lee, S., Choi, H., Kim, J., Shaker, M.R., Sun, W., Park, J.H., *et al.*
1031 (2016). Exosome engineering for efficient intracellular delivery of soluble proteins using optically
1032 reversible protein-protein interaction module. Nat Commun *7*, 12277.
1033 Zacharias, D.A., Violin, J.D., Newton, A.C., and Tsien, R.Y. (2002). Partitioning of lipid-modified
1034 monomeric GFPs into membrane microdomains of live cells. Science *296*, 913-916.
1035 Zhang, M., Liu, L., Lin, X., Wang, Y., Li, Y., Guo, Q., Li, S., Sun, Y., Tao, X., Zhang, D., *et al.* (2020). A
1036 Translocation Pathway for Vesicle-Mediated Unconventional Protein Secretion. Cell *181*, 637-652 e615.
1037 Zhang, M., and Schekman, R. (2013). Cell biology. Unconventional secretion, unconventional solutions.
1038 Science *340*, 559-561.
1039 Zhang, Y.Q., and Chandra, S.S. (2014). Oligomerization of Cysteine String Protein alpha mutants causing
1040 adult neuronal ceroid lipofuscinosis. Biochim Biophys Acta *1842*, 2136-2146.
1041 Zinsmaier, K.E. (2010). Cysteine-string protein's neuroprotective role. J Neurogenet *24*, 120-132.

1042

1043 # Figure legends

1044 **Figure 1.** Reconstitution of α-syn secretion regulated by palmitoylated DNAJC5
1045 in HEK293T cells.

1046 (A) Schematic diagrams of α-syn and DNAJC5. Domains are highlighted in
1047 different colors. Red arrows indicate known disease-causing mutations on each
1048 protein.
1049 (B) Membrane and cytosol fractionation scheme. Briefly, homogenized
1050 HEK293T cells were centrifuged at low speed to prepare a post-nuclear
1051 supernatant (PNS). High-speed centrifugation was then performed to separate
1052 the sedimentable membrane (M) from cytosol (C).
1053 (C) Partition of palmitoylated DNAJC5 (P-DNAJC5) and non-palmitoylated
1054 DNAJC5 (NP-DNAJC5) between the membrane (M) and cytosol (C) fractions.
1055 DNAJC5 was immunoprecipitated from cytosol and membrane with anti-
1056 FLAG resin and evaluated by Coomassie-blue stained SDS-PAGE.
1057 (D) α-syn secretion 16 h after transfection. The secretion of P-DNAJC5 in the
1058 medium was detected.
1059 (E) α-syn secretion 36 h after transfection. NP-DNAJC5 was also secreted in
1060 the medium together with α-syn.
1061

1062 **Figure 1 – figure supplement 1**. Validation of palmitoylation of DNAJC5 in
1063 various cell lines.

1064 (A) Membrane and cytosol fractionation of various cell lines (HEK293T, MDA-
1065 MB-231 and Hela) transfected with DNAJC5. The fractionation was performed
1066 as depicted in Figure 1B. PNS, post-nuclear supernatant. C, cytosol. M,
1067 membrane. Transferrin receptor (TFR) was used as a membrane marker.
1068 Tubulin was used as a cytosol marker.
1069 (B) In vitro depalmitoylation assay. Sedimented membranes (M) from different
1070 DNAJC5-transfected cell lines were collected and resuspended in 0.25M Tris

1071 pH 7.2 buffer or 0.25M Hydroxylamine (HA) pH 7.2 buffer. After overnight
1072 incubation at room temperature, the samples were examined by SDS-PAGE
1073 followed by anti-DNAJC5 immunoblot. PNS and C were used to compare the
1074 mobility of P-DNAJC5 and NP-DNAJC5, respectively.

1075

1076 **Figure 1 – figure supplement 2**. Secretion of α-syn variants.

1077 (A) Trypan blue cell vital staining after transfection with various constructs
1078 used in Figure 1. Ratios of trypan blue positive cells indicate the toxicity caused
1079 by transfection. Error bars represent standard deviations of 3 samples.
1080 (B) Secretion of α-syn variants into conditioned medium. Medium was collected,
1081 concentrated and evaluated by SDS-PAGE and immunoblot.
1082 (C) Expression of α-syn variants in HEK293T cells. HEK293T cells were co-
1083 transfected with Parkinson's disease (PD)-causing α-syn mutant (A30P, E46K,
1084 A53T) and DNAJC5.
1085 (D) Quantification of normalized secretion (amount in medium divided by
1086 amount in lysate) of various α-syn variants and DNAJC5. The quantification
1087 was based on immunoblot in (B) and (C).

1088 **Figure 1 – figure supplement 3.** Secretion of α-syn is partially dependent on
1089 endogenous DNAJC5 in HEK293T cells.

1090 (A) Schematic diagram of nanoluciferase (Nluc)-fused α-syn.
1091 (B) Nluc-α-syn secretion was stimulated by DNAJC5 expression. Plasmids
1092 encoding Nluc-α-syn and DNAJC5 were co-transfected into HEK293T cells.

1093 Expression and secretion of proteins were detected with immunoblot 36 h after
1094 transfection.
1095 (C) Time-dependent of accumulation of Nluc-α-syn in the medium without
1096 DNAJC5 overexpression. After transfecting HEK293T cells with Nluc-α-syn
1097 alone, fractions of medium were collected at indicated time points.
1098 (D) Chemical structure of quercetin (QLT), a reported DNAJC5 inhibitor.
1099 (E) QLT inhibited endogenous Nluc-α-syn secretion in a concentration-
1100 dependent manner. AU, arbitrary unit. Secretion assay similar to (B) was
1101 performed with treatment of indicated concentration of QLT. Amounts of
1102 secreted proteins were quantified with nanoluciferase assay 36h after
1103 transfection. Immunoblot of α-syn and DNAJC5 in cell lysate after QLT
1104 treatment was shown on the right. Error bars represent standard deviations of
1105 three samples.
1106 (F) Validation of DNAJC5 knockout (KO) cell line generated by CRISPR.
1107 Wildtype (WT) HEK293T cell was used as a control. In all three single clones
1108 of DNAJC5 KO cell lines, DNAJC5 was not detectable by immunoblot.
1109 (G) Treatment of bafilomycin A1 (BaFA1) induced LC3 lipidation in cells. After
1110 24h of 100 nM BaFA1 treatment, media were collected, and cells were lysed
1111 for evaluation with SDS-PAGE followed by immunoblot. The accumulation of
1112 the lipidated form of LC3 (LC3-II) was used to indicate the inhibition of
1113 autophagy and lysosomal degradation in cells.
1114 (H) Quantification of α-syn secretion from WT and DNAJC5 KO HEK293T
1115 cells after 24h treatment of BaFA1. The normalized secretion was calculated as
1116 nanoluciferase reading from media divided by the reading from cell lysate.
1117 Error bars represent standard deviations of three samples.

1118 **Figure 2.** Characterization of secreted α-syn.

1119 (A) Medium fractionation scheme.

1120 (B) Secreted α-syn was soluble. Differential centrifugation was performed with
1121 conditioned medium from HEK293T cells transfected with DNAJC5 and α-
1122 syn. Alix and CD9, exosome markers. PDI, an endoplasmic reticulum (ER)
1123 marker, was used as exosome-negative control.

1124 (C) Gel filtration fractionation of medium. Conditioned medium was
1125 concentrated and subjected to gel filtration fractionation. Fractions were
1126 evaluated by anti-α-syn immunoblot.

1127 (D) Chromatograms of tandem α-syn monomer (blue curve), dimer (green
1128 curve) and tetramer (red curve) were overlaid. In comparison, the relative
1129 intensity of secreted α-syn in each fraction was plotted as blue bars.

1130 (E) Schematic diagram of co-immunoprecipitation (co-IP) of secreted α-syn and
1131 FLAG-α-syn. Shown here is possible interaction between α-syn (blue circle)
1132 and FLAG-α-syn (yellow circle) in a representative tetrameric conformation.

1133 (F) Anti-FLAG immunoprecipitation (FLAG-IP) of media from cells transfected
1134 with indicated plasmids. Both the medium input and FLAG-IP samples were
1135 evaluated with anti-α-syn immunoblot (anti-α-syn WB).

1136 **Figure 2 – figure supplement 1**. Solubility of secreted α-syn variants.

1137 (A) Medium fractionation of secreted α-syn PD mutants (A30P, E46K and
1138 A53T). After differential centrifugation of medium, supernatant (10ks and
1139 100ks) and pellet fractions (100kp) were evaluated by immunoblot.

1140 (B) Medium fractionation of basal secreted Nluc-α-syn without DNAJC5
1141 overexpression. Similar fractionation assay was performed in (A) with medium
1142 from HEK293T cells transfected with Nluc-α-syn alone. Secreted Nluc-α-syn
1143 was quantified with a nanoluciferase assay. AU, arbitrary unit.

1144 **Figure 2- figure supplement 2.** DNAJC5 enriched in buoyant EV fraction.

1145 (A) Schematic diagram of EV flotation protocol. Briefly, high-speed pellet
1146 fractions of growth medium were resuspended in 60% sucrose buffer and
1147 overlaid sequentially with 40% and 10% sucrose buffer. The tubes were
1148 centrifuged at 150,000 (150k)xg at 4°C for overnight. Buoyant EVs floated at
1149 the 10%/40% sucrose interface, separated from other insoluble materials.
1150 (B) Immunoblots across the sucrose step gradient. DNAJC5 as well as other
1151 classical exosome markers (Flot-2, CD63 and CD9) were highly enriched in
1152 fractions 4 to 6 at the 10%/40% interface.

1153 **Figure 2 – figure supplement 3**. Assessment of tandem α-syn oligomers by gel
1154 filtration chromatography.

1155 (A) Chromatogram of purified tetrameric α-syn tandem oligomer (α-syn-α-syn-
1156 α-syn-α-syn).
1157 (B) Coomassie-blue stained SDS-PAGE of fractions from gel filtration of
1158 tetrameric α-syn tandem oligomer (α-syn-α-syn-α-syn-α-syn).
1159 (C) Chromatogram of purified dimeric α-syn tandem oligomer (α-syn-α-syn).
1160 (D) Coomassie-blue stained SDS-PAGE of fractions from gel filtration of
1161 dimeric α-syn tandem oligomer (α-syn-α-syn).
1162 (E) Chromatogram of purified WT α-syn (α-syn).

1163 (F) Coomassie-blue stained SDS-PAGE of fractions from gel filtration of
1164 WT α-syn (α-syn).
1165
1166 **Figure 3**. Disruption of palmitoylation of DNAJC5 inhibited α-syn secretion.
1167 (A) Inhibition of DNAJC5 palmitoylation by 2-bromopalmitic acid (2-BA) or
1168 introduced mutation L115R. Cellular fractionation was performed with
1169 HEK293T cells transfected with WT DNAJC5 and treated with 10 μm 2-BA, or
1170 transfected with DNAJC5 L115R mutant. TFR, transferrin receptor. PNS, post-
1171 nuclear supernatant. C, cytosol. M, membrane.
1172 (B) Quantification of the percentage of P-DNAJC5 and NP-DNAJC5 in different
1173 conditions as shown in (A). Error bars represent standard deviations of 3
1174 experiments.
1175 (C) α-syn secretion was blocked with 2-BA treatment. HEK293T cells
1176 transfected with indicated plasmids were treated with DMSO or 10 μm 2-BA.
1177 Media fractions were collected and secretion was evaluated by SDS-PAGE and
1178 immunoblot.
1179 (D) Palmitoylation of DNAJC5 was blocked in HEK293T cells treated with 2-
1180 BA.
1181 (E) Quantification of normalized α-syn secretion in HEK293T cells after 2-BA
1182 treatment. The quantification was based on immunoblot in (C) and (D). The α-
1183 syn secretion was calculated as the amount of α-syn in media divided by the
1184 amount in lysate.
1185 (F) Quantification of normalized DNAJC5 secretion in HEK293T cells after 2-
1186 BA treatment. The quantification was based on immunoblot in (C) and (D). The

1187 DNAJC5 secretion was calculated as the amount of DNAJC5 in media divided
1188 by the amount in lysate.
1189 (G) DNAJC5 L115R mutant reduced α-syn secretion compared with WT
1190 DNAJC5. Secretion assay with HEK293T cells transfected with indicated
1191 plasmids encoding DNAJC5 variant was performed similar to (C).
1192 (H) DNAJC5 L115R was non-palmitoylated in HEK293T cells.
1193 (I) Quantification of normalized α-syn secretion in HEK293T cells transfected
1194 with DNAJC5 L115R mutant. The quantification was based on immunoblot in
1195 (G) and (H).
1196 (J) Quantification of normalized DNAJC5 secretion in HEK293T cells transfected
1197 with DNAJC5 L115R mutant. The quantification was based on immunoblot in
1198 (G) and (H).

1199 **Figure 3 – figure supplement 1**. Dose-dependent inhibition of α-syn secretion by
1200 2-bromopalmitic acid (2-BA).

1201 (A) Chemical structure of palmitoylation inhibitor 2-bromopalmitic acid
1202 (2-BA). The single bromo substituent at position 2 is highlighted by a red
1203 dashed square.
1204 (B) α-syn secretion in the medium was inhibited by 2-BA in a dose-
1205 dependent manner. Ten μm 2-BA was serially diluted by DMSO into 5 μm,
1206 2μm, 1μm solution. HEK293T cells were first transfected with DNAJC5
1207 and α-syn. After medium replacement, 2-BA of indicated concentration was
1208 added to cell culture. Media was collected after 36h and followed by sample
1209 preparation, SDS-PAGE and immunoblot.

1210 (C) With increasing concentration of 2-BA, P-DNAJC5 decreased and NP-
1211 DNAJC5 increased in HEK293T cells.
1212 (D) Quantification of normalized α-syn secretion upon increasing
1213 concentration of 2-BA. Quantification was based on immunoblot in (B) and
1214 (C). The α-syn secretion was calculated as the amount of α-syn in media
1215 divided by the amount in lysate.
1216 (E) Quantification of ratio of P-DNAJC5/NP-DNAJC5. The quantification
1217 was based on immunoblot in (C).

1218 **Figure 3 – figure supplement 2.** Blockage of USP19-induced α-syn secretion by
1219 DNAJC5 L115R or L116Δ mutant.

1220 (A) USP19 induced α-syn secretion in the medium, which was further enhanced
1221 by WT DNAJC5 and blocked by two DNAJC5 palmitoylation-deficient
1222 mutants (L115R and L116Δ).
1223 (B) Both mutations, L115R and L115Δ, inhibited DNAJC5 palmitoylation in
1224 HEK293T cells.
1225 (C) Quantification of normalized α-syn secretion in HEK293T cell transfected
1226 with indicated constructs. The quantification was based on immunoblot in (A)
1227 and (B). α-Syn secretion was calculated as the amount of α-syn in media
1228 divided by the amount in lysate.
1229

1230 **Figure 3 – figure supplement 3.** Golgi retention of DNAJC5 in secretion-
1231 deficient conditions.

1232 (A) Immunofluorescence (IF) images of U2OS cells transfected with wildtype
1233 (WT) DNAJC5-HaloTag. Before fixation, HaloTag TMR ligands were added to
1234 the cell culture to label DNAJC5. Golgi apparatus was visualized by IF using
1235 anti-GM130 antibody. Nuclei were stained with DAPI. Scale bar: 10 μm.
1236 (B) Immunofluorescence (IF) images of U2OS cells transfected with DNAJC5
1237 (L115R)-HaloTag. Same staining procedure was performed as in (A). Scale
1238 bar: 20 μm.
1239 (C) Immunofluorescence (IF) images of U2OS cells transfected with wildtype
1240 (WT) DNAJC5-HaloTag and treated with 5 μM 2-BA. After transfection with
1241 WT DNAJC5-HaloTag, cells were incubated with 5μM 2-BA for 1d to block
1242 palmitoylation of DNAJC5. Same staining procedure was performed as in (A).
1243 Scale bar: 10 μm.
1244

1245 **Figure 4**. Topological localization of α-syn and DNAJC5 in enlarged endosomes.

1246 (A) DNAJC5 was internalized inside enlarged endosomes. Live U2OS cells
1247 expressing mCherry-Rab5^{Q79L}(red) showed circular enlarged endosomes labeled
1248 by Rab5 mutant. DNAJC5-HaloTag (green) was visualized by addition of
1249 HaloTag® Oregon Green® Ligand. Representative enlarged endosomes show
1250 diffuse (1) or punctate (2 and 3) internalized DNAJC5. Scale bar: 15 μm in
1251 overviews and 1 μm in magnified insets.
1252 (B) α-syn was excluded from enlarged endosomes. In live U2OS cells,
1253 expression of BFP-Rab5^{Q79L} (blue) produced enlarged endosomes of similar
1254 morphology compared with mCherry-Rab5^{Q79L}. mNeonGreen-α-syn (mNG-α-
1255 syn, green) was expressed both in the nucleus and cytosol. No mNG-α-syn

1256 was found inside enlarged endosomes (1, 2, 3). Scale bar: 20 μm in overviews
1257 and 1 μm in magnified insets.
1258 (C) α-syn enters into enlarged endosomes in the presence of DNAJC5.
1259 DNAJC5-HaloTag (red) and mNG-α-syn (green) were co-expressed in U2OS
1260 cells carrying BFP-Rab5^{Q79L} (blue) mutant and imaged. No mNG-α-syn was
1261 internalized in endosome without DNAJC5-HaloTag inside (1). In contrast,
1262 mNG-α-syn was found inside endosomes with DNAJC5-HaloTag inside (2
1263 and 3). Scale bar: 10 μm in overviews and 1 μm in magnified insets.
1264 (D) α-syn and DNAJC5 co-sedimented in membrane fractionation. HEK293T
1265 cell homogenate was sequentially centrifuged at increasing velocity from
1266 3000g (3k), 25,000g (25k) and 100,000g (100k). The 25k membrane fraction
1267 had the highest amount of both α-syn and DNAJC5.
1268 (E) Quantification of the membrane fractionation results in (D).
1269 (F) Proteinase K protection assay of 25k membrane containing α-syn and
1270 DNAJC5.
1271 (G) Quantification of the proteinase K protection assay in (F).
1272 (H) Quantification of the ratio of α-syn containing endosomes in control cells
1273 (no-DNAJC5 transfection) or cells co-transfected with DNAJC5. More than
1274 100 enlarged endosomes were counted in each group. Error bars represent
1275 standard deviations. ****p value<0.0001, two-tailed t test.
1276

1277 **Figure 4 – figure supplement 1**. Immunofluorescence (IF) images of endogenous
1278 DNAJC5 and enlarged endosomes.

1279 (A) Co-localization between endogenous CD63 (red) and DNAJC5 (green).
1280 U2OS cells were cultured and fixed, incubated with corresponding antibodies
1281 for IF detection of endogenous CD63 and DNAJC5. Representative co-
1282 localized region is shown in magnified insets. Scale bar, 20 μm.
1283 (B) CD63 (green) was inside the enlarged endosomes labeled by peripheral
1284 mCherry-Rab5^{Q79L} (red). U2OS expressing mCherry-Rab5^{Q79L} were fixed, followed
1285 by IF using anti-CD63 antibody. Scale bar, 25 μm.

1286 **Figure 4 – figure supplement 2**. Live-cell images of U2OS cells expressing
1287 DNAJC5 L115R mutant and α-syn.

1288 (A) Live cell imaging of U2OS cells transfected with DNAJC5 (L115R)-
1289 HaloTag and mCherry-Rab5^{Q79L}. DNAJC5 (L115R)-HaloTag (green) is diffuse in
1290 cytosol and outside of the enlarged endosomes labeled by peripheral mCherry-
1291 Rab5^{Q79L} (red). Scale bar, 10 μm in overviews and 1 μm in magnified insets.
1292 (B) Live cell imaging of U2OS cells transfected with mNeonGreen (mNG)-α-
1293 syn, DNAJC5 (L115R)-HaloTag and mCherry-Rab5^{Q79L}. In the condition of co-
1294 expression with DNAJC5 (L115R)-HaloTag (red), no mNG-α-syn (green) was
1295 found inside of enlarged endosomes labeled by peripheral BFP-Rab5^{Q79L}(blue).
1296 Scale bar, 10 μm in overviews and 1 μm in magnified insets.

1297 **Figure 4 - supplement video**. Time lapse of movement of internalized α-syn and
1298 DNAJC5 in the enlarged endosomes. DNAJC5-HaloTag (red) and mNG-α-syn
1299 (green) were co-expressed in U2OS cells carrying BFP-Rab5^{Q79L} (blue) mutant and
1300 imaged. Scale bar: 10 μm.

1301 **Figure 5**. Secretion of tandem α-syn oligomers and α-syn fused with thermostable
1302 helix bundle protein.
1303 (A) Schematic diagrams of tandem α-syn oligomers. α-syn protomers (yellow)
1304 were linked head to tail by flexible linker (green) to mimic increased size of α-
1305 syn oligomers.
1306 (B) Secretion of tandem α-syn oligomers in medium. Secretion assay was
1307 performed with media from HEK293T cells transfected with indicated tandem
1308 α-syn oligomers. Tandem α-syn oligomers are more sensitively detected by
1309 immunoblot which were exposed for shorter time compared with WT α-syn.
1310 (C) Expression of tandem α-syn oligomers in HEK293T cells. *a non-specific
1311 band.
1312 (D) Schematic diagrams of N-terminal fused and C-terminal fused thermostable
1313 three helix bundle (3H-) α-syn. 3H shown as three blue dashes, α-syn shown as
1314 orange circle.
1315 (E) Secretion of 3H-α-syn and α-syn-3H in medium. Secretion assay was
1316 performed with media from HEK293T cells transfected with indicated 3H-
1317 fused α-syn constructs. *a non-specific band.
1318 (F) Expression of 3H-α-syn and α-syn-3H in HEK293T cells. *a non-specific
1319 band.
1320 **Figure 5 – figure supplement 1**. Medium fractionation of secreted tandem α-syn
1321 oligomers. Medium fractionation of secreted tandem α-syn oligomers. P-DNAJC5
1322 was depleted in the supernatant after centrifugation at 100,000 (100k) xg.
1323 However, no significant decrease of tandem α-syn oligomers in the supernatant
1324 was observed.

1325 **Figure 5 – figure supplement 2**. Thermostable three helix bundle blocked pOTC-
1326 mediated mitochondrial import of GFP.

1327 (A) Schematic diagrams of constructs used in mitochondrial import assay. GFP,
1328 GFP alone. pOTC-GFP, GFP with leader peptide from ornithine
1329 ranscarbamylase (OTC) fused at amino-terminus. pOTC-3H-GFP, the
1330 thermostable three helix bundle was inserted between the leader peptide pOTC
1331 and GFP.
1332 (B) Immunoblot analysis of proteins in crude mitochondria fraction. Whole cell
1333 lysate (W) was prepared by mixing homogenized cells with equal volume of
1334 2.3M sucrose buffer and centrifugation at 1,200 g to remove large debris.
1335 Soluble fraction (S) and particulate fraction (P) were separated by centrifuging
1336 W fraction at 7,000 g for 10 min. Mitochondria were enriched in P fraction.
1337 Tom20, mitochondrial marker. Tubulin, soluble marker.
1338 (C) The mitochondrial localization efficiency was calculated by quantifying the
1339 protein amount in P fraction divided by the amount in S fraction.
1340 (D) Cartoon depicting relative localization of proteins inside or outside of
1341 mitochondria. Tom20, a mitochondrial outer membrane protein. Citrate
1342 synthase (CS), a mitochondrial matrix protein. The import of pOTC-3H-GFP is
1343 blocked by 3H.
1344 (E) Proteinase K protection assay of crude mitochondria. SDS (0.5%) was added
1345 in addition to 1% TX-100 to sensitize protease treatment of well-folded protein,
1346 e.g. CS. The protease accessibility of pOTC-3H-GFP was revealed by the
1347 production of GFP fragment and disappearance of the full-length (FL) band.
1348 (F) Quantification of percentage of protection of proteins in (E).

1349 **Figure 6.** XPACK (XP)-induced DNAJC5 L115R oligomerization rescued α-syn
1350 secretion.

1351 (A) Ladder pattern of higher molecular weight (HMW) DNAJC5 oligomers in
1352 the medium. Medium from HEK293T cell culture transfected with DNAJC5
1353 was centrifuged at 1000 (1k) g, 10,000 (10k) g and 100,000 (100k) g, followed
1354 by SDS-PAGE and immunoblot of supernatant (s) fractions at each
1355 centrifugation step.
1356 (B) Fractionation of HMW-DNAJC5 with gel filtration. HEK293T cells
1357 transfected with DNAJC5 were lysed, clarified and subjected to gel filtration.
1358 HMW-DNAJC5 of different sizes were separated based on their corresponding
1359 molecular weight.
1360 (C) XP-DNAJC5 L115R mutant forms a membrane-bound oligomer. Cellular
1361 fractionation was performed with HEK293T cells transfected with indicated
1362 DNAJC5 variants. Note the substantial change of electrophoretic mobility of
1363 XP-DNAJC5 L115R on SDS-PAGE.
1364 (D) α-syn secretion induced by XP-DNAJC5 L115R. Secretion assay was
1365 performed with HEK293T cells transfected with indicated plasmids. Ten μm 2-
1366 BA was used to block induced α-syn.
1367 (E) Expression of α-syn and DNAJC5 variants in HEK293T cells. Note the
1368 substantial change in electrophoretic mobility of 2-BA-treated XP-DNAJC5
1369 L115R on SDS-PAGE.

1370 **Figure 6 – figure supplement 1**. Characterization of HMW-DNAJC5 and
1371 XPACK fusion.

1372 (A) DNAJC5 (ΔJ) forms a series of SDS-resistant oligomers. HEK293T cells
1373 transfected with WT DNAJC5 or DNAJC5 (ΔJ) were lysed and evaluated by
1374 immunoblot using anti-DNAJC5 antibody.
1375 (B) HMW-DNAJC5 is not formed by non-specific disulfide bonds. HEK293T
1376 cells transfected with DNAJC5 were lysed for SDS-PAGE followed by
1377 immunoblot. The loading samples for SDS-PAGE were prepared with
1378 increasing amount of DTT up to 40 mM.
1379 (C) Schematic diagram of XPACK. XPACK is myristoylated on the first glycine
1380 (G) and palmitoylated on the second cystine (C). Replacement of Serine (S) at
1381 position 5 with a hydrophobic isoleucine (I) abolishes normal lipidation of
1382 XPACK.
1383 (D) Assessment of different XPACK fusion constructs. Cell lysate containing
1384 different DNAJC5 constructs were evaluated by anti-DNAJC5 immunoblot.
1385 (E) Membrane-association of XP-DNAJC5 dependent on palmitoylation.
1386 HEK293T cells transfected with XP-DNAJC5 were treated with DMSO or 10
1387 μM 2-BA. After cell culture for 24 h, cellular fractionation was performed with
1388 homogenized cells. Distribution of XP-DNAJC5 in cytosol (C) and membrane
1389 (M) fractions were evaluated with immunoblot.

1390 **Figure 6 – figure supplement 2**. Live-cell images of U2OS cells expressing XP-
1391 DNAJC5 L115R mutant and α-syn.

1392 (A) Internalization of punctate XP-DNAJC5 (green) into enlarged endosomes
1393 labeled by mCherry-Rab5^{Q79L} (red). U2OS cells were transfected with XP-
1394 DNAJC5 and mCherry-Rab5^{Q79L}. Live cell imaging was performed 24 h after
1395 transfection. Representative enlarged endosomes with XP-DNAJC5 are shown

1396 in magnified inset. Scale bar: 10 μm in overviews and 1 μm in magnified
1397 insets.
1398 (B) α-syn enters into enlarged endosomes in the presence of XP-DNAJC5. XP-
1399 DNAJC5-HaloTag (red) and mNG-α-syn (green) were co-expressed in U2OS
1400 cells carrying BFP-Rab5^{Q79L} (blue) mutant and imaged. Representative enlarged
1401 endosome with both XP-DNAJC5-HaloTag and mNG-α-syn inside is shown in
1402 magnified inset. Scale bar: 10 μm in overviews and 1 μm in magnified insets.
1403 (C) Quantification of the ratio of α-syn containing endosomes in cells co-
1404 transfect with DNAJC5 L115R or cells co-transfected with DNAJC5 XP-
1405 L115R. More than 100 enlarged endosomes were counted in each group. Error
1406 bars represent standard deviations. ****p value<0.0001, two-tailed t test.
1407

1408 **Figure 7**. Recapitulation of endogenous DNAJC5-mediated α-syn secretion in
1409 various neuronal cell cultures.

1410 (A) Membrane and cytosol fractionation of differentiated SH-SY5Y
1411 neuroblastoma cells. The fractionation was performed as depicted in Figure 1B.
1412 C, cytosol. M, membrane. The distribution of endogenous DNAJC5 and α-syn
1413 was evaluated by immunoblot. Transferrin receptor (TFR) was used as a
1414 membrane marker. Tubulin was used as a cytosol marker.
1415 (B) Quantification of α-syn level in the supernatant of centrifuged media with
1416 ELISA. Conditioned media were collected and sequentially centrifuged at 1,000
1417 (1k) g, 10,000 (10k) g, and 100,000 (100k) g. The supernatant from each
1418 centrifugation step (1ks, 10ks and 100ks) was collected and measured by
1419 LEGEND MAX™ Human α-synuclein (Colorimetric) ELISA Kit. One-way

1420 ANOVA showed no significant (ns) difference of α-syn level between
1421 fractions.
1422 (C) Quercetin inhibited endogenous α-syn secretion in hiPSC-derived midbrain
1423 dopamine neurons. hiPSC-dopamine neurons carrying the *GBA-N370S*
1424 mutation were treated with quercetin (5 μM or 10 μM) at Day 35. Culture
1425 media samples were harvested after 3d treatment at Day 38 and α-syn levels in
1426 the media were analyzed by electro-chemiluminescent immunoassay. Data
1427 points represent individual cell lines derived from different donors and are
1428 normalised to total protein in the corresponding cell lysates. One-way ANOVA
1429 followed by Tukey's post-hoc test shows a significant reduction in α-syn
1430 secretion with increasing quercetin concentration (*$p<0.05$, **$p<0.01$).
1431 (D) Depletion of endogenous DNAJC5 in SH-SY5Y cells decreased basal α-syn
1432 secretion. After 3d of culture, the media from differentiated SH-SY5Y cells
1433 transduced with shRNA targeting GFP (shRNA-GFP) or shRNA targeting
1434 DNAJC5 (shRNA-DNAJC5) were collected and the extracellular α-syn was
1435 quantified with ELISA. ***p value<0.0002, two-tailed t test.
1436 (E) Expression of exogenous human DNAJC5 in mouse mDA stimulated basal
1437 α-syn secretion. WT mDA and mDA expressing hDNAJC5 were treated with
1438 DMSO or 100 nM BaFA1. Quantification of α-syn in conditioned media was
1439 performed with Mouse α-synuclein ELISA Kit (Abcam). α-syn secretion was
1440 normalized by dividing the α-syn in media (pg/mL) by the α-syn in cell lysates
1441 (ng/mL). **p value<0.01, one-way ANOVA.
1442 (F) BaFA1 increased DNAJC5 oligomerization in mouse mDA neurons.

1443 **Figure 7 – figure supplement 1**. Basal α-syn secreted as a soluble form from
1444 differentiated SH-SY5Y.

1445 (A) Differentiation of SH-SY5Y was initiated by lowering the serum
1446 concentration to 1% FBS and addition of 10uM retinoic acid (RA). Media were
1447 replaced every three days and the cells were harvested at indicated time to
1448 examine the expression of neuronal marker. DAT, dopamine transporter. Tuj1,
1449 neuron-specific class III β-tubulin.
1450 (B) In vitro depalmitoylation assay of endogenous DNAJC5 in differentiated SH-
1451 SY5Y cells. The depalmitoylation assay was performed as in **Fig 1 supplement**
1452 **1B** using membrane (M) fraction from SH-SY5Y cells. HA, hydroxylamine.
1453 (C) Proteinase K protection assay of 100,000 (100k) pellet fraction from the
1454 centrifuged media of differentiated SH-SY5Y culture. Flot-2 and CD63 were
1455 used as exosome markers.
1456 (D) Sedimented α-syn was not buoyant. 100k pellet from (C) was mixed with
1457 60% sucrose in PBS and layered with 40% and 20% sucrose in PBS
1458 sequentially. After centrifuged at 150,000xg for 16 h, fractions were collected
1459 from top to bottom.

1460 **Figure 7 – figure supplement 2**.

1461 (A) Schematic of the differentiation protocol used to generate hiPSC-derived
1462 dopamine neurons, including a patterning phase to generate neural progenitor
1463 cells followed by differentiation into mature neurons. Green arrows represent
1464 points of replating when cells are supplemented with ROCK inhibitor (Ri) to
1465 increase survival. Puro = puromorphamine, SHH = sonic hedgehog, FGF8a =
1466 fibroblast growth factor 8a, BDNF = brain-derived neurotrophic factor, GDNF

1467 = glial cell line-derived neurotrophic factor, TGF-β3 = transforming growth
1468 factor beta 3. (see Kriks et al, 2011; Beevers et al 2017; Lang et al 2019 for full
1469 details). Neurons are mature and harvested between 35-68 d for analysis.
1470 Immunocytochemical fluorescent images of mature neurons at Day 50 stained
1471 for neuronal marker microtubule-associated protein (MAP2), the dopaminergic
1472 marker tyrosine hydroxylase (TH), and DAPI. Scale bar = 20 μm.

1473 (B) DNAJC5 is palmitoylated in iPSC-derived dopamine neurons. Immunoblot
1474 analysis of DNAJC5 palmitoylation in hiPSC-derived dopamine neurons
1475 treated with DMSO, 7.5 μM Quercetin or 10 μM 2-BA on Day 65 and
1476 harvested on Day 68. Tyrosine hydroxylase was used as a marker of
1477 dopaminergic identity.

1478 (C) Partial depalmitoylation of DNAJC5 by 2-BA in iPSC-derived dopamine
1479 neurons does not reduce α-syn secretion. hiPSC-derived dopamine neurons
1480 carrying the *GBA-N370S* mutation were treated with palmitoylation inhibitor
1481 2-BA (5 μM or 10 μM) at Day 35. Culture media samples were harvested
1482 after 3d treatment at Day 38 and α-syn levels in the media were analyzed by
1483 electro-chemiluminescent immunoassay. Data points represent individual cell
1484 lines derived from different donors and are normalized to total protein in the
1485 corresponding cell lysates. One-way ANOVA shows no effect of 2-BA on α-
1486 syn secretion.

1487 **Figure 7 – figure supplement 3**. shRNA-mediated DNAJC5 knockdown in
1488 differentiated SH-SY5Y cells.

1489 (A) Examination of knockdown efficiency by shRNA targeting DNAJC5 in
1490 HEK293T cells.

1491 (B) Endogenous DNAJC5 expression decreased in SH-SY5Y cells transduced
1492 with shRNA targeting DNAJC5.

1493 **Figure 7 – figure supplement 4**. Differentiation of mouse embryonic stem cells
1494 (mESCs) and expression of human DNAJC5.

1495 (A) Schematic overview of protocol used for differentiation of mESCs into
1496 middle-brain dopaminergic (mDA) neuronal cultures. Immunocytochemical
1497 staining using stem cell markers (Nanog, Sox2), neuronal precursor marker
1498 (Nestin), mDA markers [FoxA2, Nurr1, Lmx1a, Sox6 (selective marker of
1499 substantia nigra pars compacta lineage), TH (tyrosine hydroxylase), Girk2 (G-
1500 protein-regulated inward-rectifier potassium channel 2, expressed in DA
1501 neurons)], neuronal marker (Tuj1) and nuclear marker (dapi).
1502 (B) Expression of human DNAJC5 with C-terminal FLAG tag in mDA neurons.
1503

1504

1505 **Figure 8**. Domain mapping of secretion-competent DNAJC5.

1506 (A) Predicted structure of DNAJC5 by AlphaFold. Color scheme: J domain
1507 (magenta), Cys string domain (yellow) and C-terminal helix (green).
1508 (B) DNAJC5 (ΔJ) was competent to induce α-syn secretion into the medium.
1509 HEK293T cells were transfected with indicated plasmids. Media were collected
1510 after 36 h and evaluated with immunoblot.
1511 (C) DNAJC5 (ΔJ) formed oligomers in HEK293T cells.
1512 (D) Quantification of normalized α-syn secretion in HEK293T cells transfected
1513 with WT DNAJC5 or DNAJC5 (ΔJ). Quantification was based on immunoblot

1514 in (B) and (C). The α-syn secretion was calculated as the amount of α-syn in
1515 media divided by the amount in lysate. α-syn secretion in cells transfected with
1516 WT DNAJC5 was normalized as 1.
1517 (E) C-terminal truncated DNAJC5 constructs were competent to induce α-syn
1518 secretion in the medium. HEK293T cells were transfected with C-terminal
1519 truncated DNAJC5 and α-syn. DNAJC5 antibodies cannot recognize DNAJC5
1520 (ΔC30) and DNAJC5 (ΔC40) because of a missing epitope in the C-terminus.
1521 Instead, DNAJC5 (ΔC30) and DNAJC5 (ΔC40) were detected by C-terminal
1522 FLAG tags. All the C-terminal truncated DNAJC5 constructs showed smear-
1523 like oligomers.
1524 (F) Expression of C-terminal truncated DNAJC5 constructs in HEK293T cells.
1525 Immunoblot of anti-FLAG antibody and anti-DNAJC5 antibody cross-validated
1526 the existence of oligomers.
1527 (G) Quantification of normalized α-syn secretion in HEK293T cells transfected
1528 with WT DNAJC5 or different C-terminal truncated DNAJC5 constructs
1529 (ΔC10, ΔC20, ΔC30 and ΔC40). Quantification was based on immunoblot in
1530 (E) and (F). The α-syn secretion was calculated as the amount of α-syn in
1531 media divided by the amount in lysate. α-syn secretion in cells without
1532 DNAJC5 transfection was normalized as 1.
1533 (H) A model for palmitoylated DNAJC5 oligomer-mediated α-syn secretion.

1534

1535

Figure 1 – source data. Uncropped immunoblot and gel images corresponding to Figure 1.

Figure 1 – figure supplement 1 – source data. Uncropped immunoblot images corresponding to Figure 1 supplement 1.

Figure 1 – figure supplement 2 – source data. Uncropped immunoblot images corresponding to Figure 1 supplement 2.

Figure 1 – figure supplement 3 – source data. Uncropped immunoblot images corresponding to Figure 1 supplement 3.

Figure 2 – source data. Uncropped immunoblot corresponding to Figure 2.

Figure 2 – figure supplement 1 – source data. Uncropped immunoblot images corresponding to Figure 2 supplement 1.

Figure 2 – figure supplement 2 – source data. Uncropped immunoblot images corresponding to Figure 2 supplement 2.

Figure 2 – figure supplement 3 – source data. Uncropped gel images corresponding to Figure 2 supplement 3.

Figure 3 – source data. Uncropped immunoblot corresponding to Figure 3.

Figure 3 – figure supplement 1 – source data. Uncropped immunoblot corresponding to Figure 3 supplement 1.

Figure 3 – figure supplement 2 – source data. Uncropped immunoblot corresponding to Figure 3 supplement 2.

Figure 4 – source data. Uncropped immunoblot corresponding to Figure 4.

Figure 5 – source data. Uncropped immunoblot corresponding to Figure 5.

Figure 5 – figure supplement 1– source data. Uncropped immunoblot corresponding to Figure 5 supplement 1.

Figure 5 – figure supplement 2– source data. Uncropped immunoblot corresponding to Figure 5 supplement 2.

Figure 6 – source data. Uncropped immunoblot corresponding to Figure 6.

Figure 6 – figure supplement 1 – source data. Uncropped immunoblot corresponding to Figure 6 supplement 1.

Figure 7 – source data. Uncropped immunoblot corresponding to Figure 7.

Figure 7 – figure supplement 1 – source data. Uncropped immunoblot corresponding to Figure 7 supplement 1.

Figure 7 – figure supplement 2 – source data. Uncropped immunoblot corresponding to Figure 7 supplement 2.

Figure 7 – figure supplement 3 – source data. Uncropped immunoblot corresponding to Figure 7 supplement 3.

Figure 7 – figure supplement 4 – source data. Uncropped immunoblot corresponding to Figure 7 supplement 4.

Figure 8 – source data. Uncropped immunoblot corresponding to Figure 8.

1590 **Figure 1.** Reconstitution of α-syn secretion regulated by palmitoylated DNAJC5

1591 in HEK293T cells.

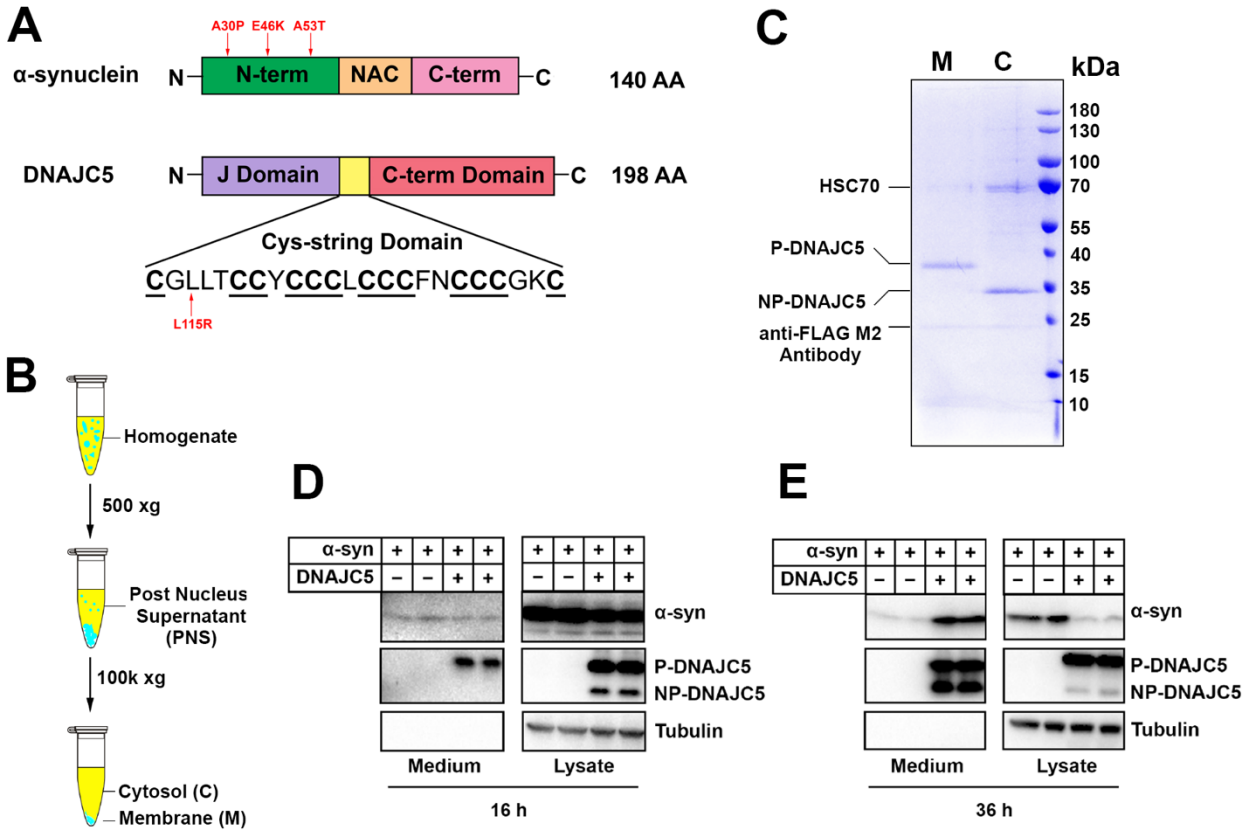

1592

1593

1594 **Figure 1 – figure supplement 1**. Validation of palmitoylation of DNAJC5 in
1595 various cell lines.

1596

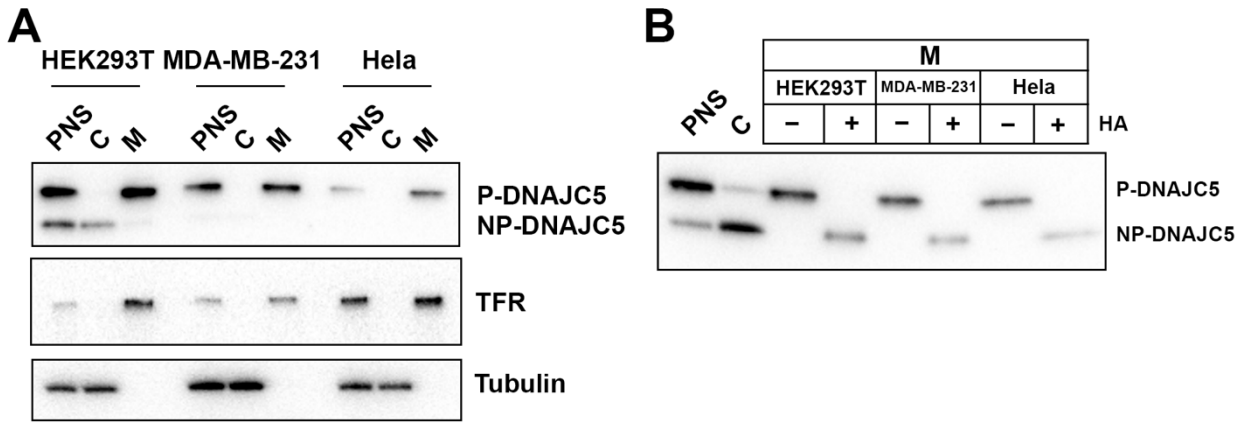

1597

1598

1599 **Figure 1 – figure supplement 2.** Secretion of α-syn variants.

1600

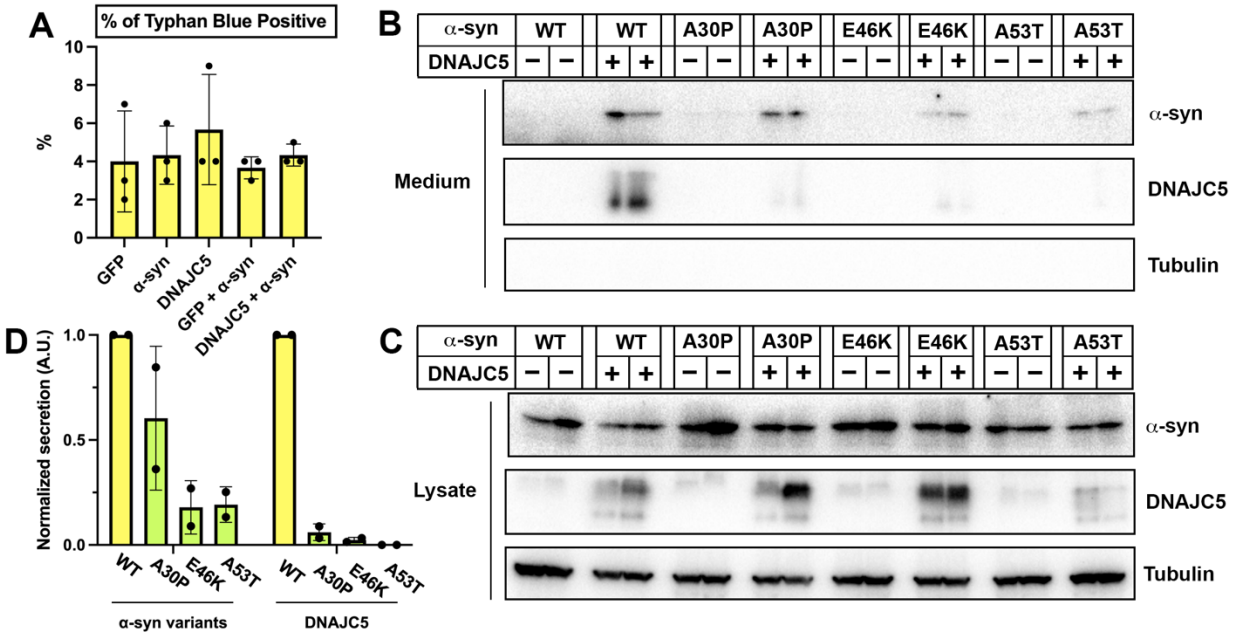

1601

1602

1603

1604

1605 **Figure 1 – figure supplement 3.** Secretion of α-syn is partially dependent on

1606 endogenous DNAJC5 in HEK293T cells.

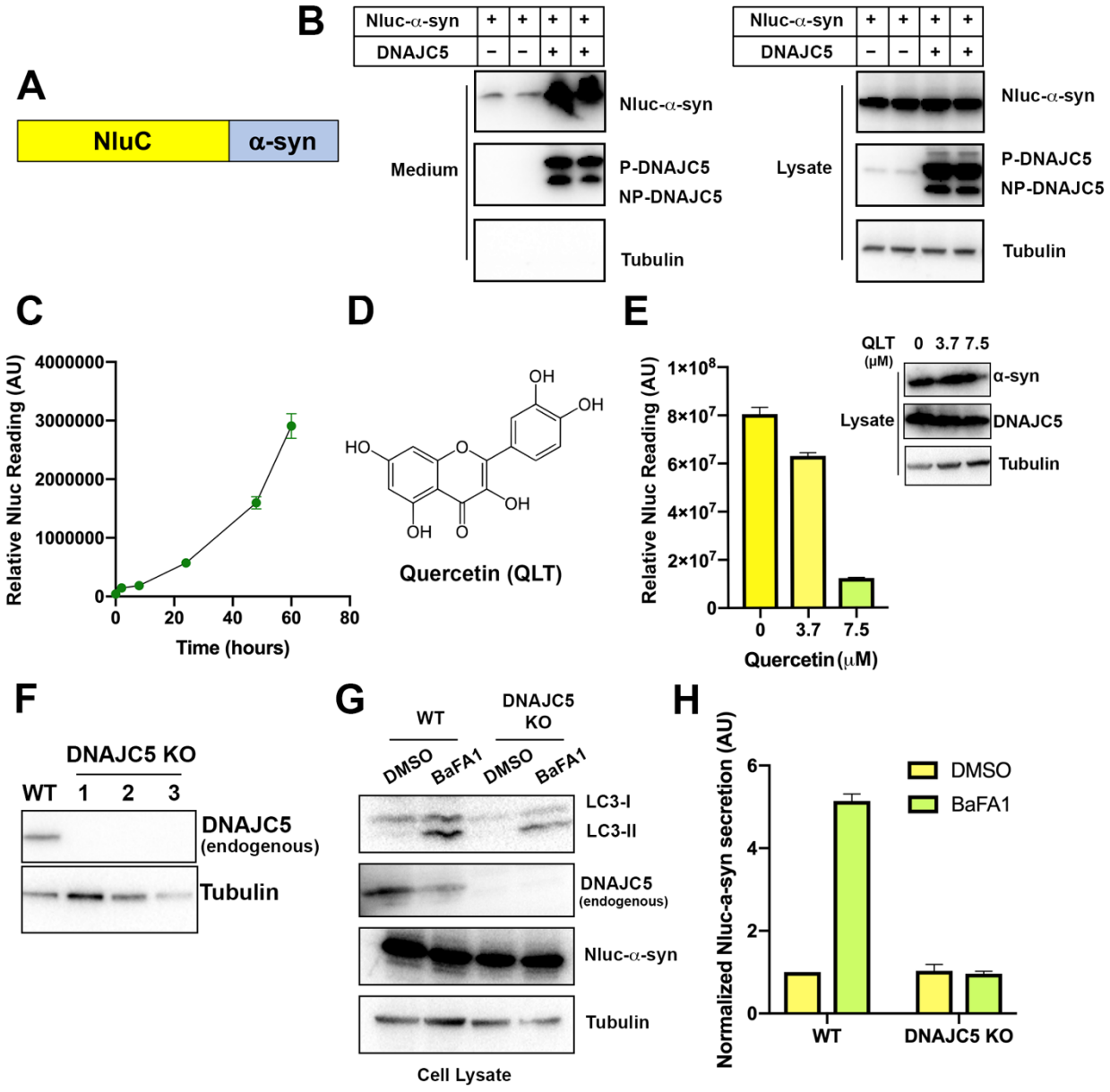

1607

1608

1609

1610

1611

1612

1613

1614 **Figure 2.** Characterization of secreted α-syn.

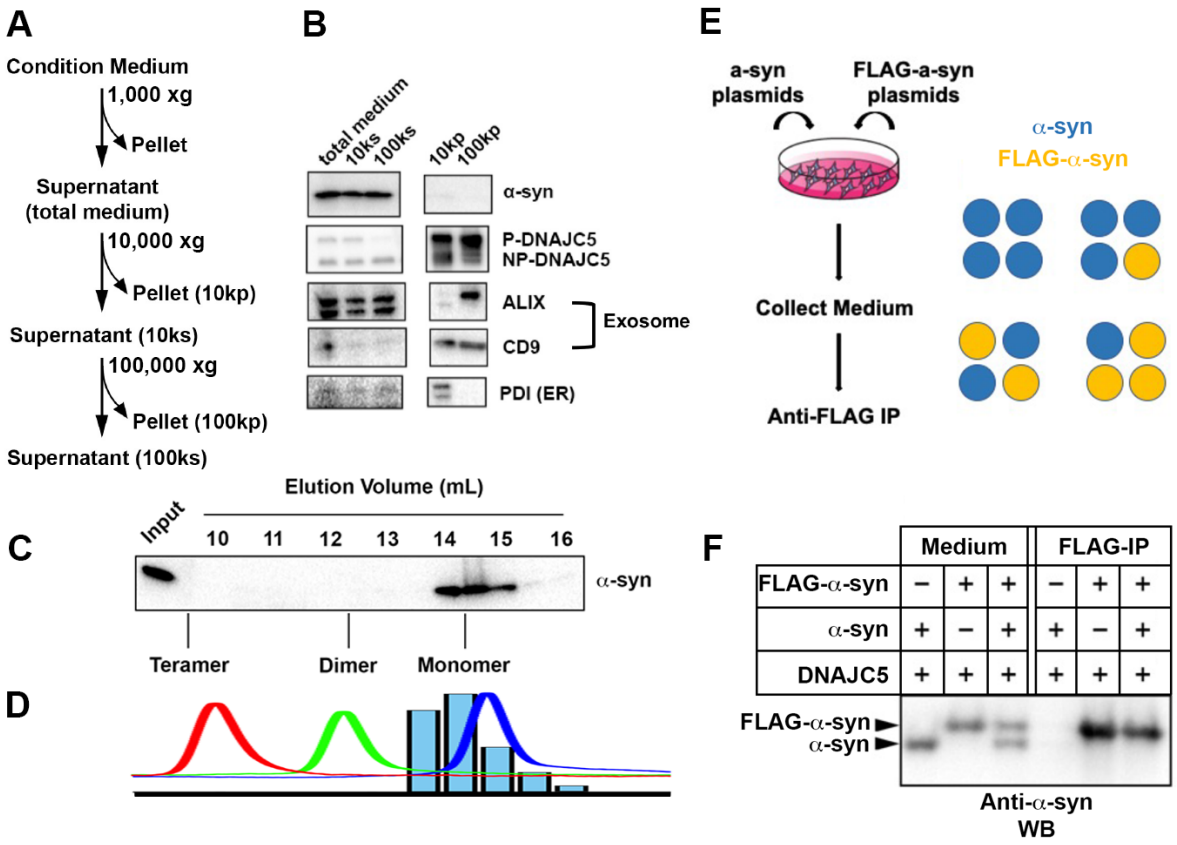

1615

1616

1617

1618 **Figure 2 – figure supplement 1**. Solubility of secreted α-syn variants.

1619

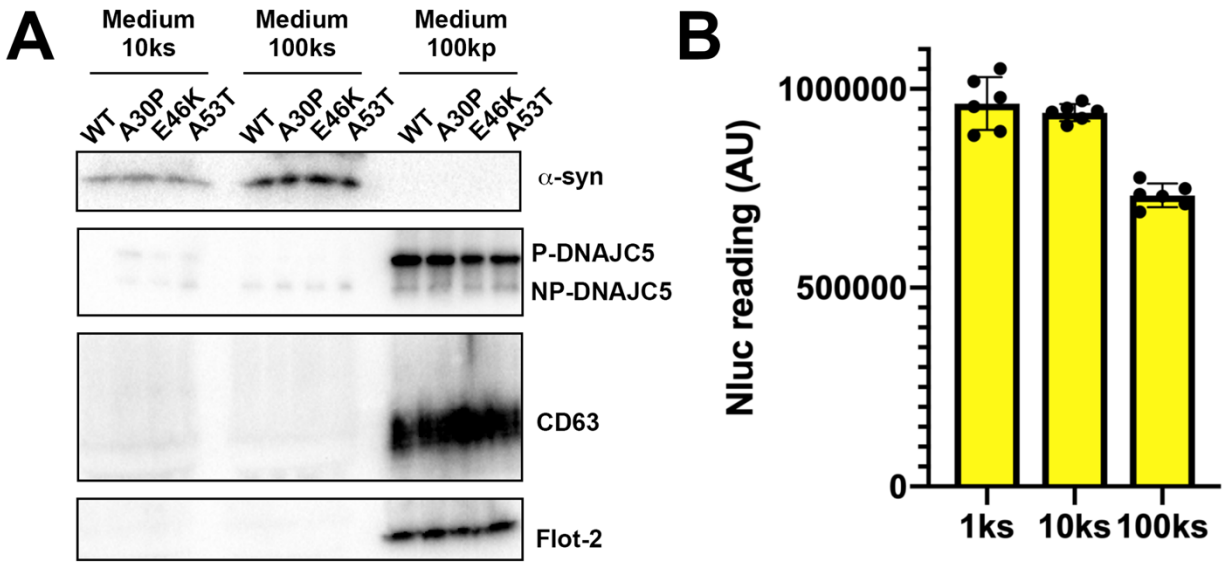

1620

1621

1622

1623 **Figure 2- figure supplement 2.** DNAJC5 enriched in floated EV fraction.

1624

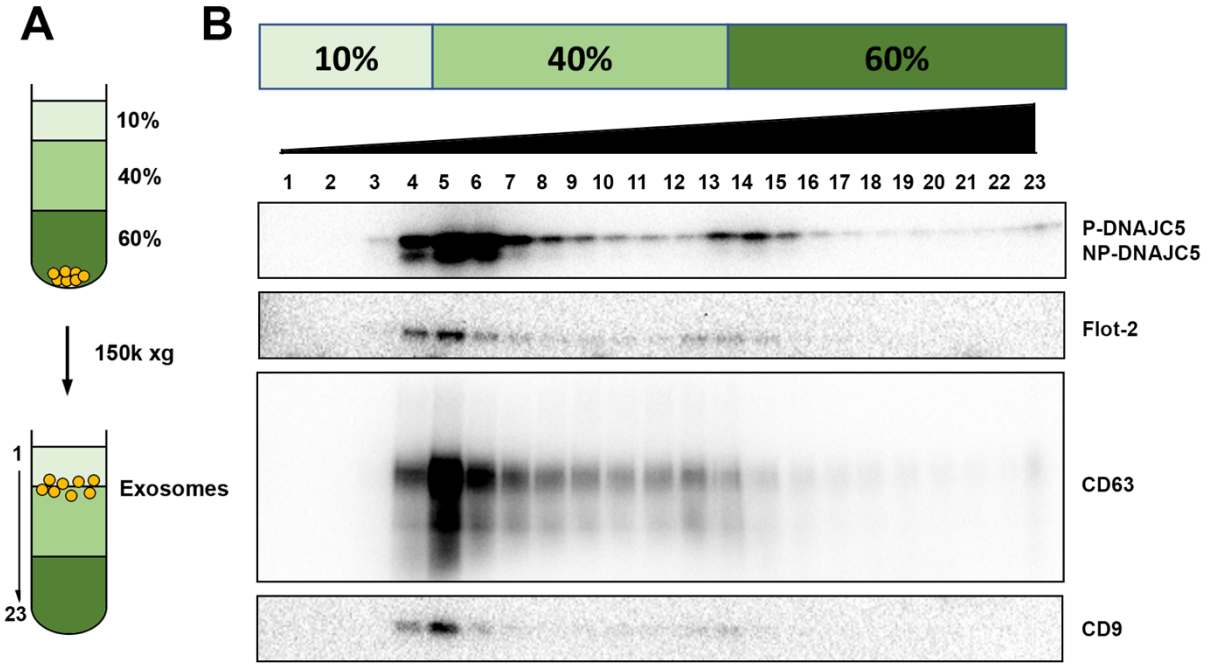

1625

1626

1627

1628 **Figure 2 – figure supplement 3**. Assessment of tandem α-syn oligomers with gel

1629 filtration chromatography.

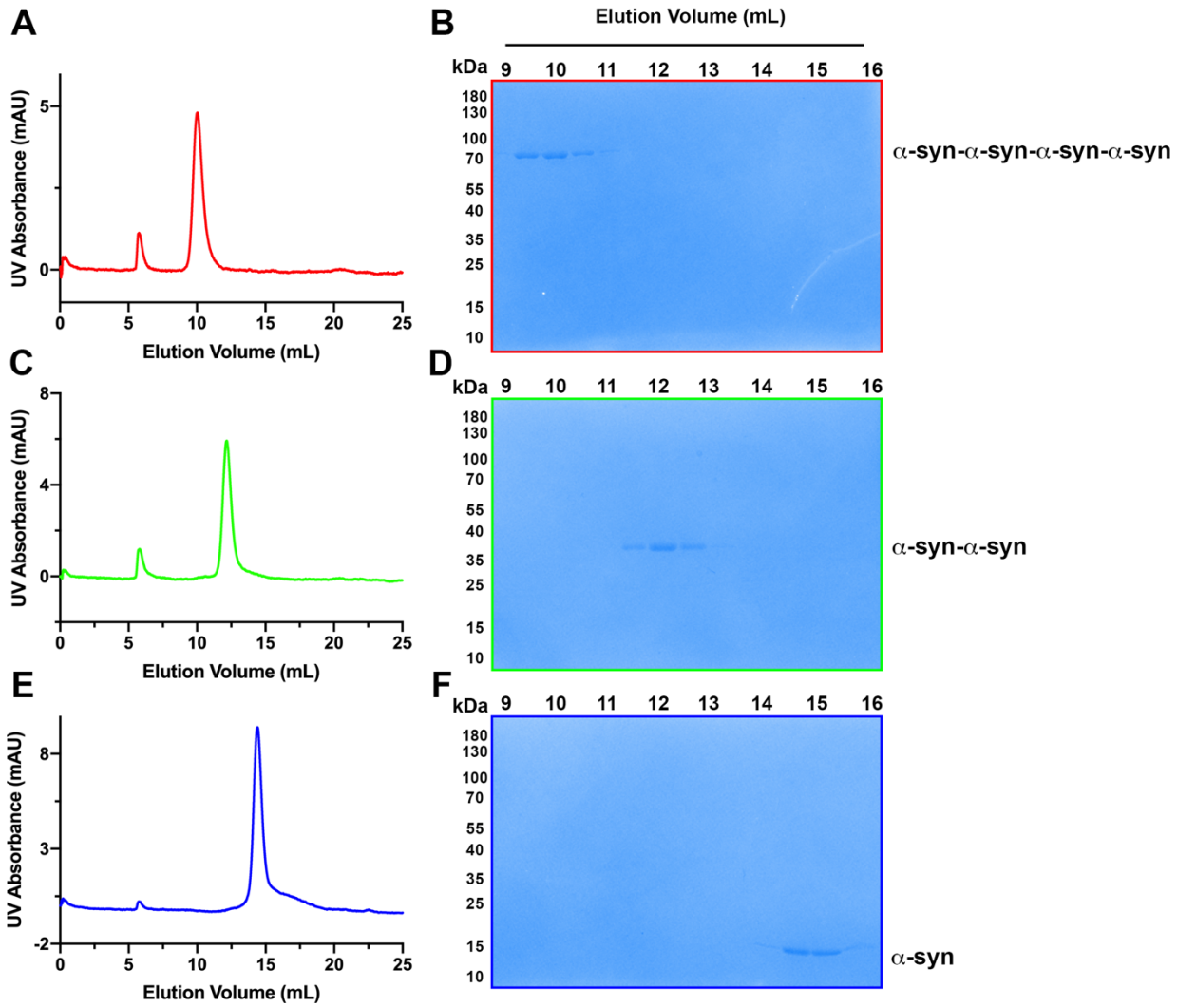

1630

1631

1632

1633 **Figure 3**. Disruption of palmitoylation of DNAJC5 inhibited α-syn secretion.

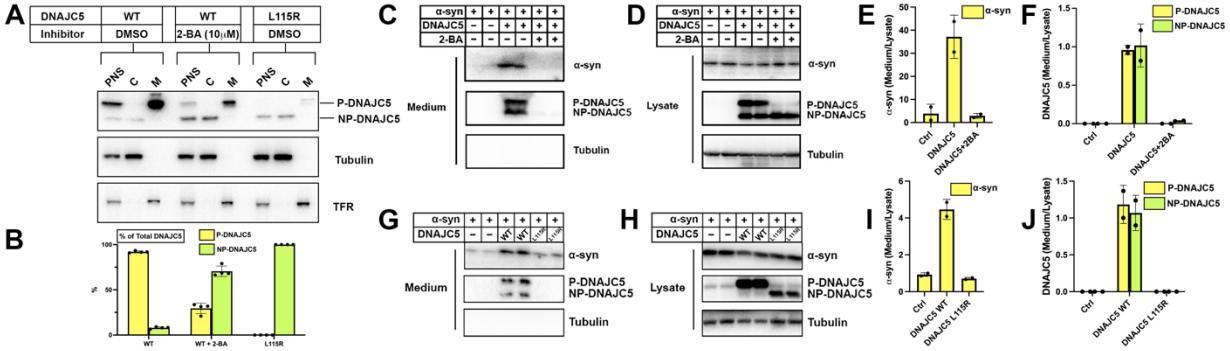

1634

1635

1636

1637 **Figure 3 – figure supplement 1**. Dose-dependent inhibition of α-syn secretion by

1638 2-bromopalmitic acid (2-BA).

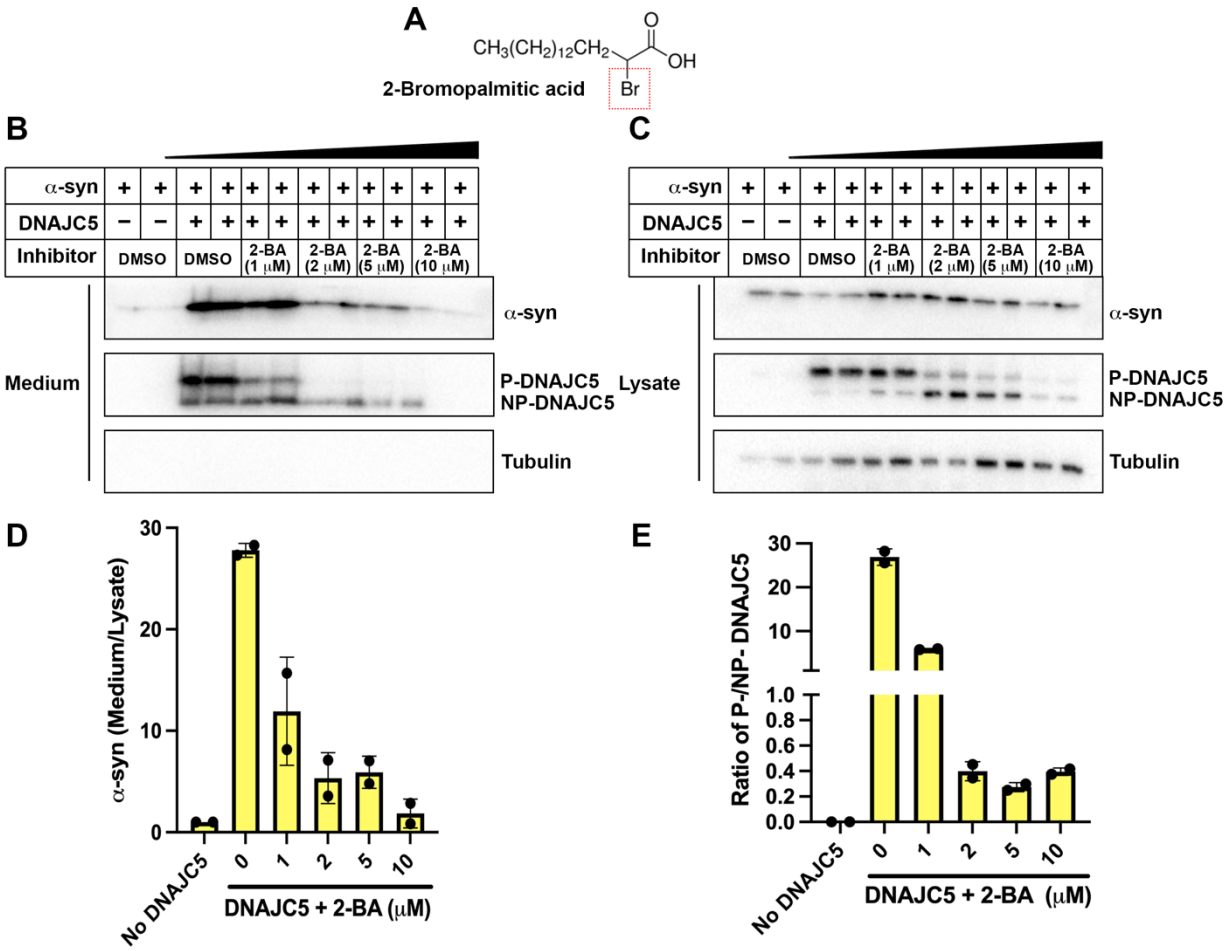

1639

1640

1641

1642 **Figure 3 – figure supplement 2.** Blockage of USP19-induced α-syn secretion by

1643 DNAJC5 L115R or L116Δ mutant.

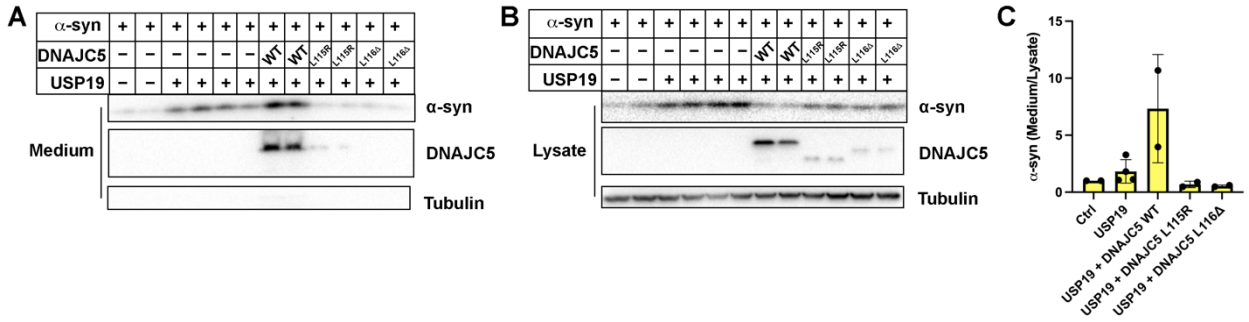

1644

1645

1646

1647 **Figure 3 – figure supplement 3.** Golgi retention of DNAJC5 in α-syn secretion-

1648 deficient conditions.

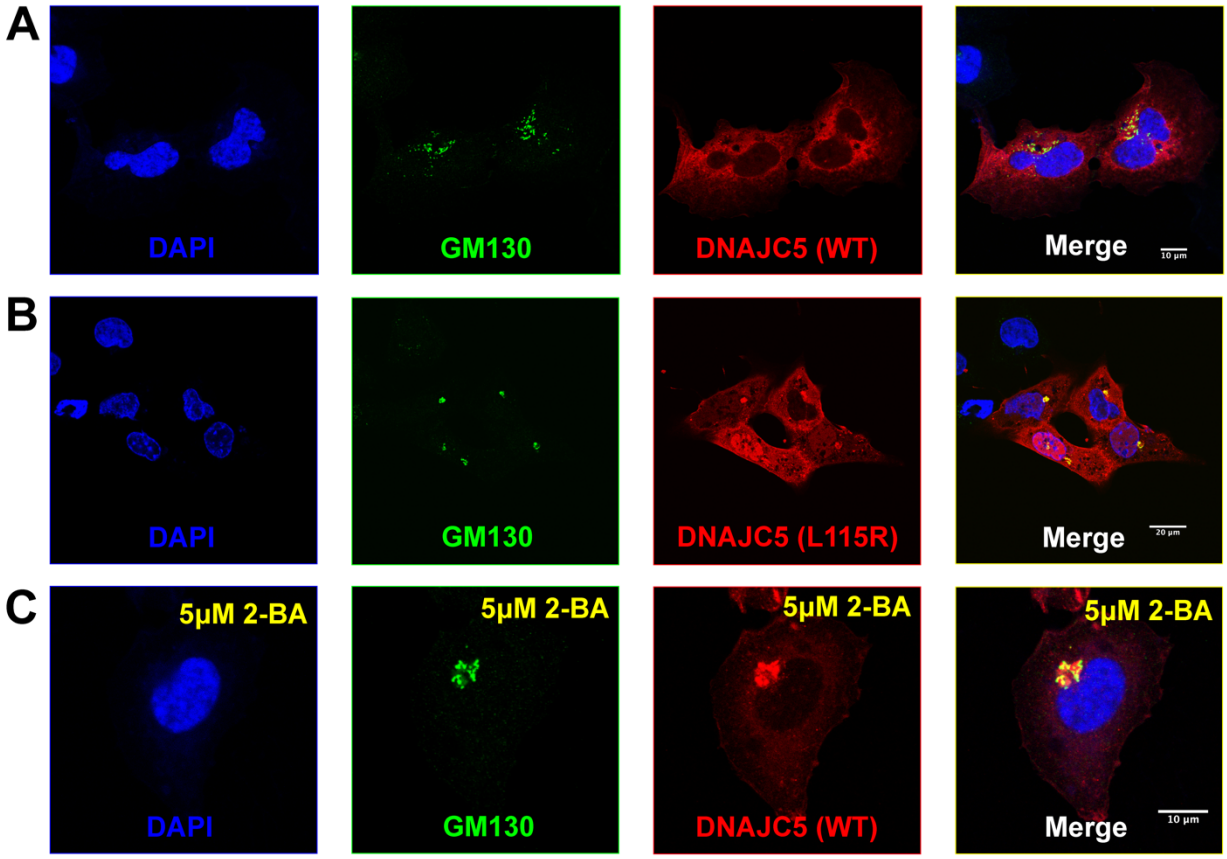

1649

1650

1651

1652 **Figure 4**. Topological localization of α-syn and DNAJC5 in enlarged endosomes.

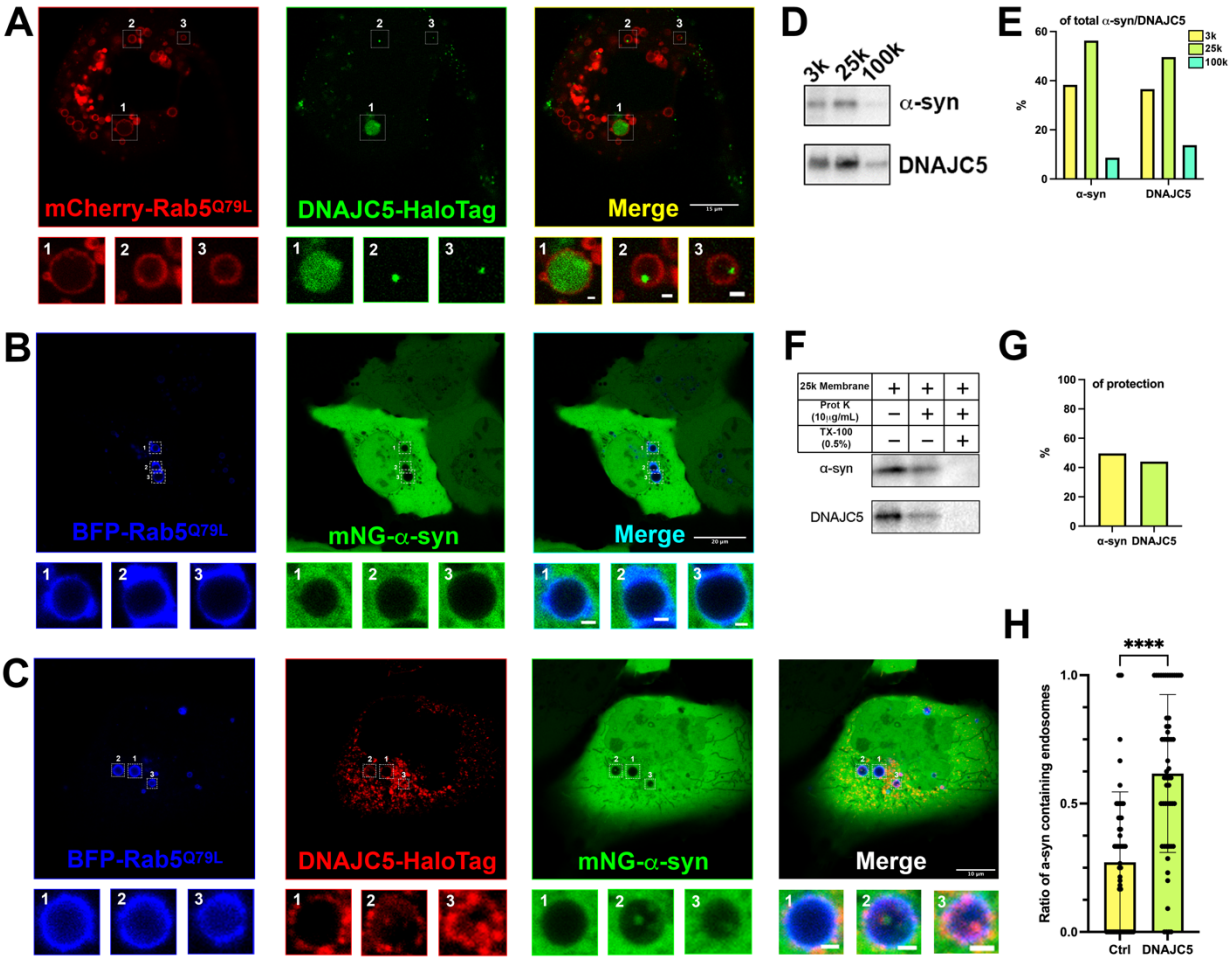

1653

1654

1655

1656 **Figure 4 – figure supplement 1**. Immunofluorescence (IF) images of endogenous

1657 DNAJC5 and enlarged endosomes.

1658

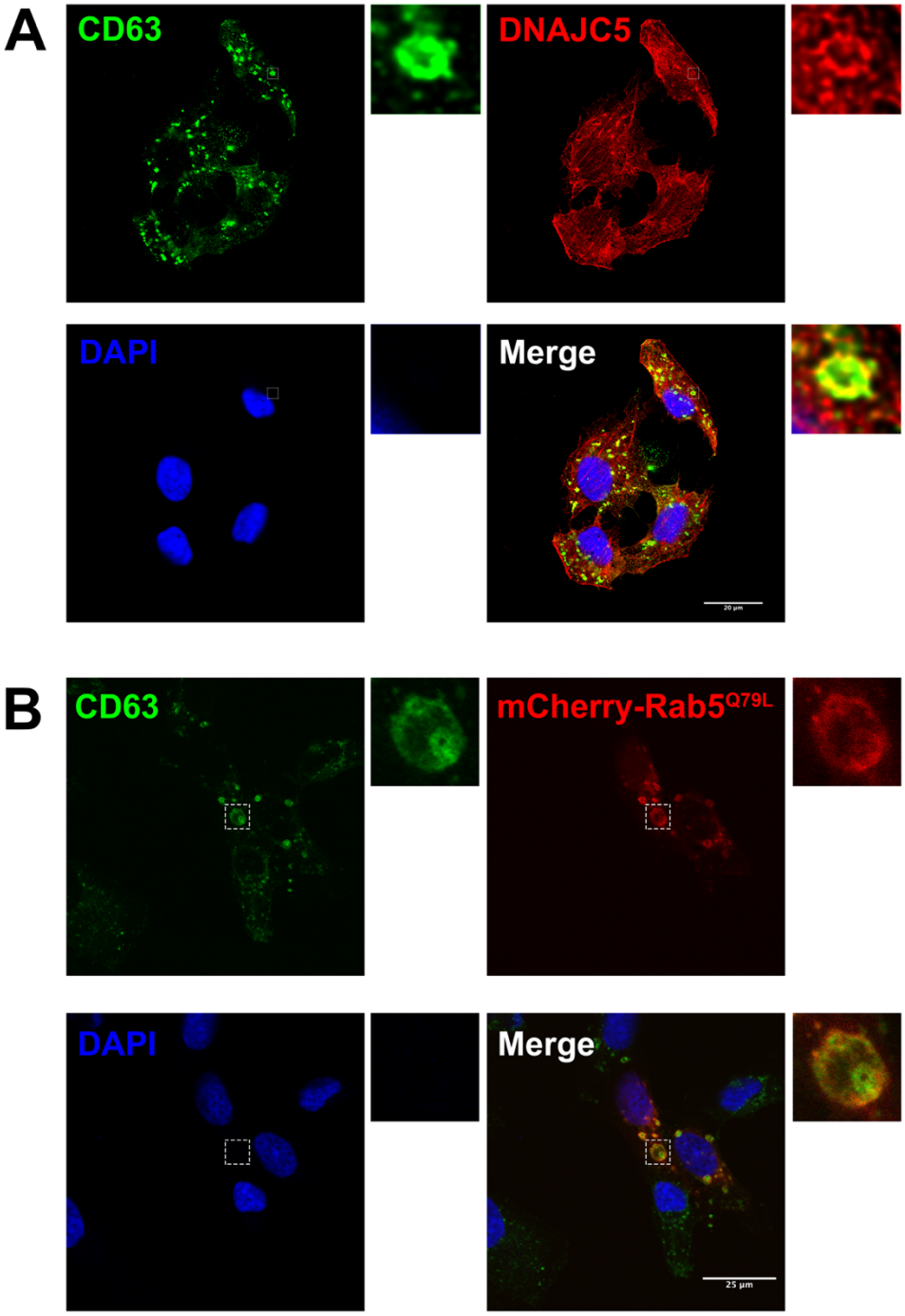

1659

1660 **Figure 4 – figure supplement 2**. Live-cell images of DNAJC5 L115R mutant and

1661 α-syn.

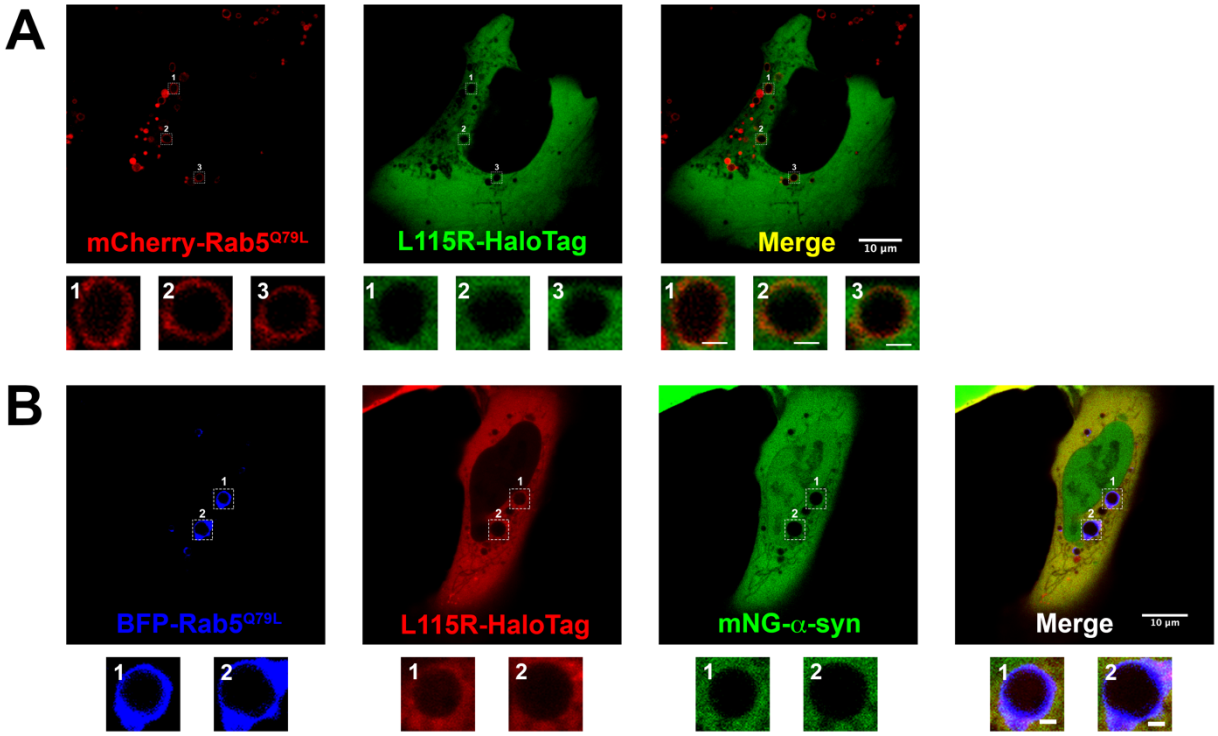

1662

1663

1664

1665 **Figure 4 - supplement video**. Time lapse of movement of internalized α-syn and
1666 DNAJC5 in the enlarged endosomes. Blue, Rab5^{Q79L}; Green, α-syn; Red, DNAJC5.
1667 Scale bar: 10 μm.

1668

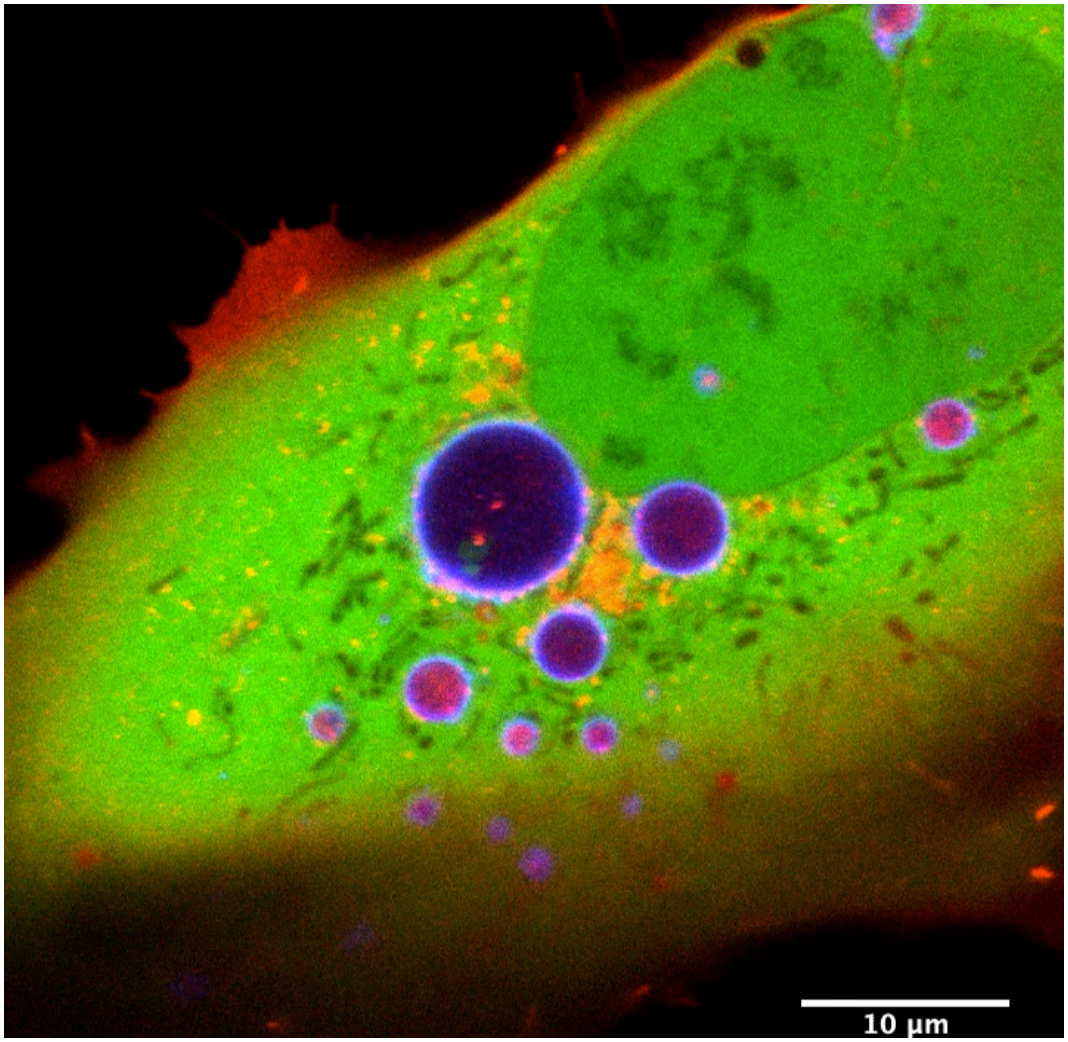

1669 **Figure 5**. Secretion of tandem α-syn oligomers and α-syn fused with thermostable

1670 helix bundles.

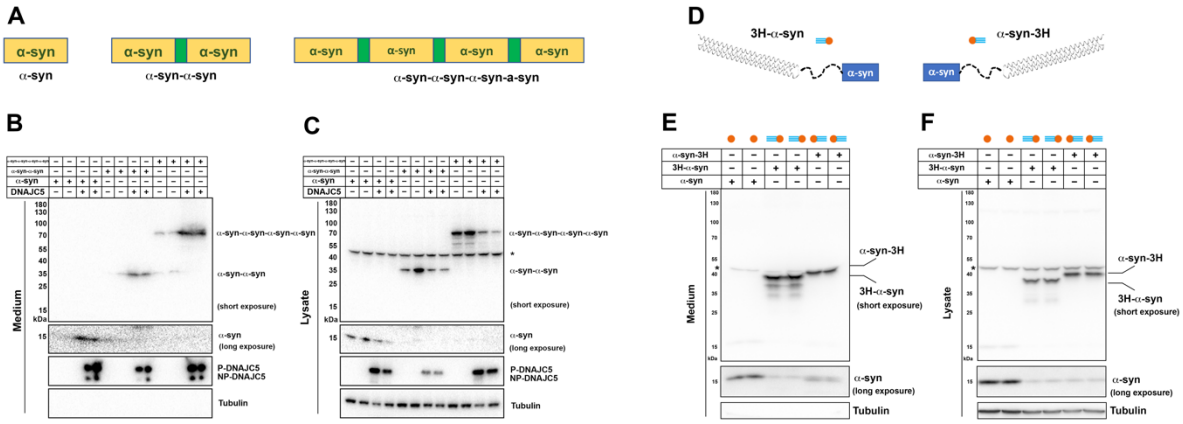

1671

1672

1673

1674 **Figure 5 – figure supplement 1**.

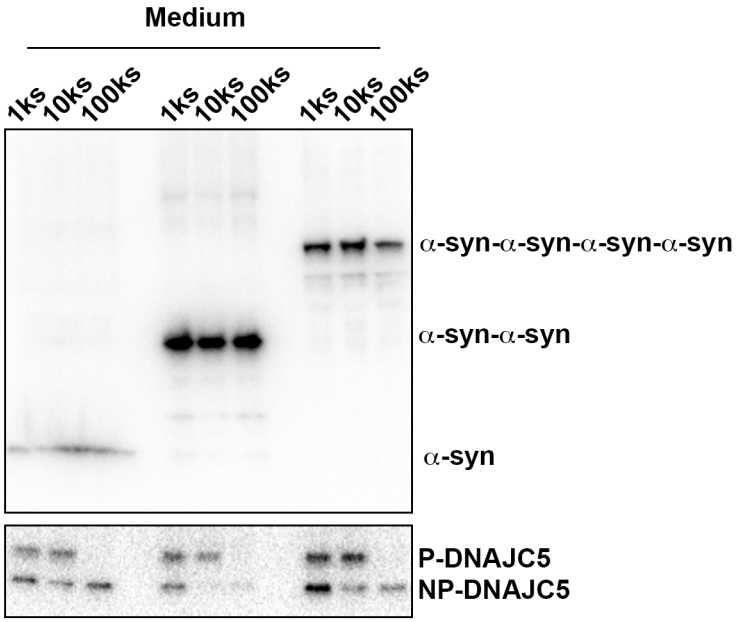

1675

1676

1677

1678 **Figure 5 – figure supplement 2**. Thermostable three helix bundle blocked pOTC-
1679 mediated mitochondrial import of GFP.

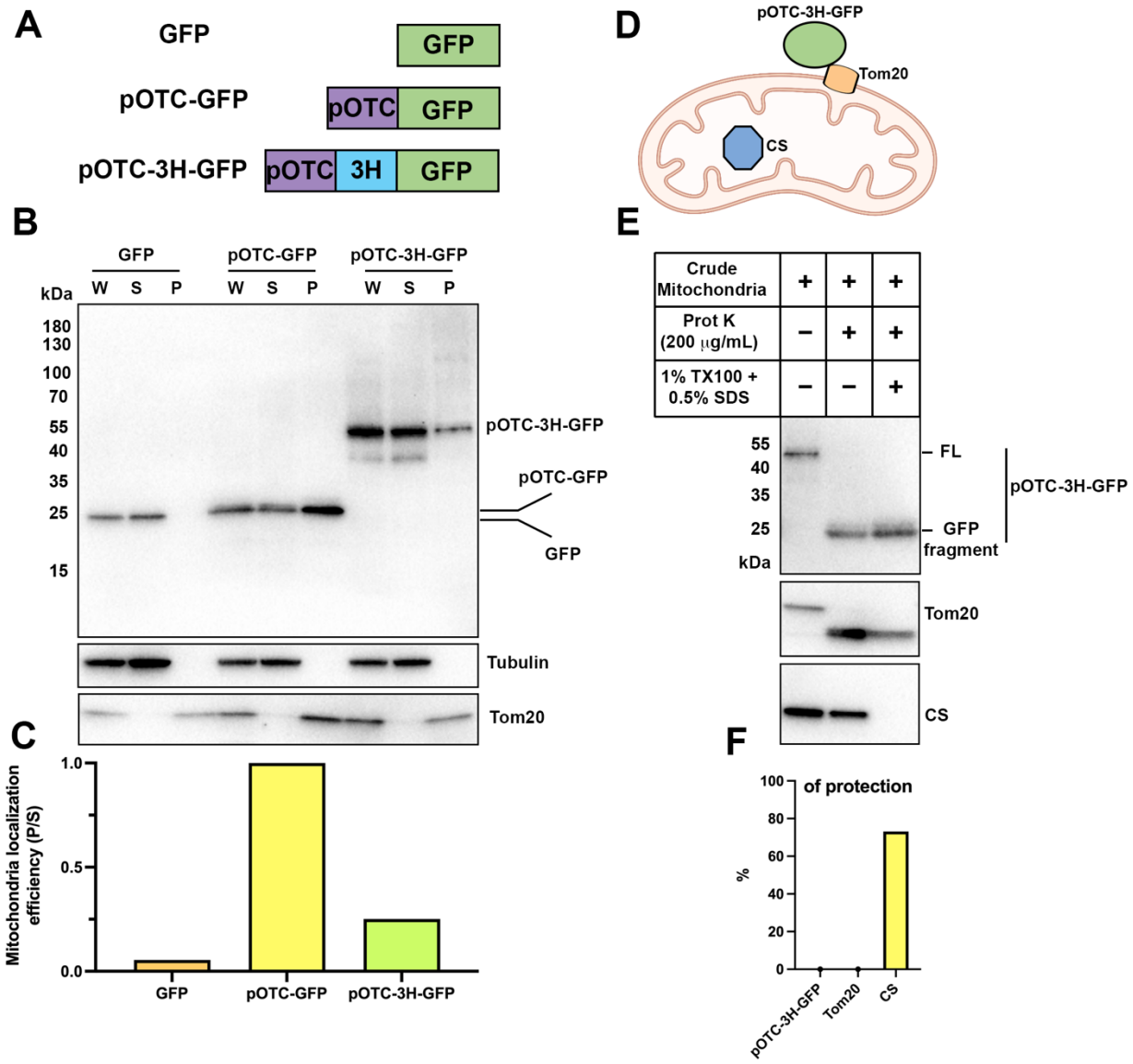

1680

1681

1682 **Figure 6.** XPACK (XP)-induced DNAJC5 L115R oligomerization rescued α-syn

1683 secretion.

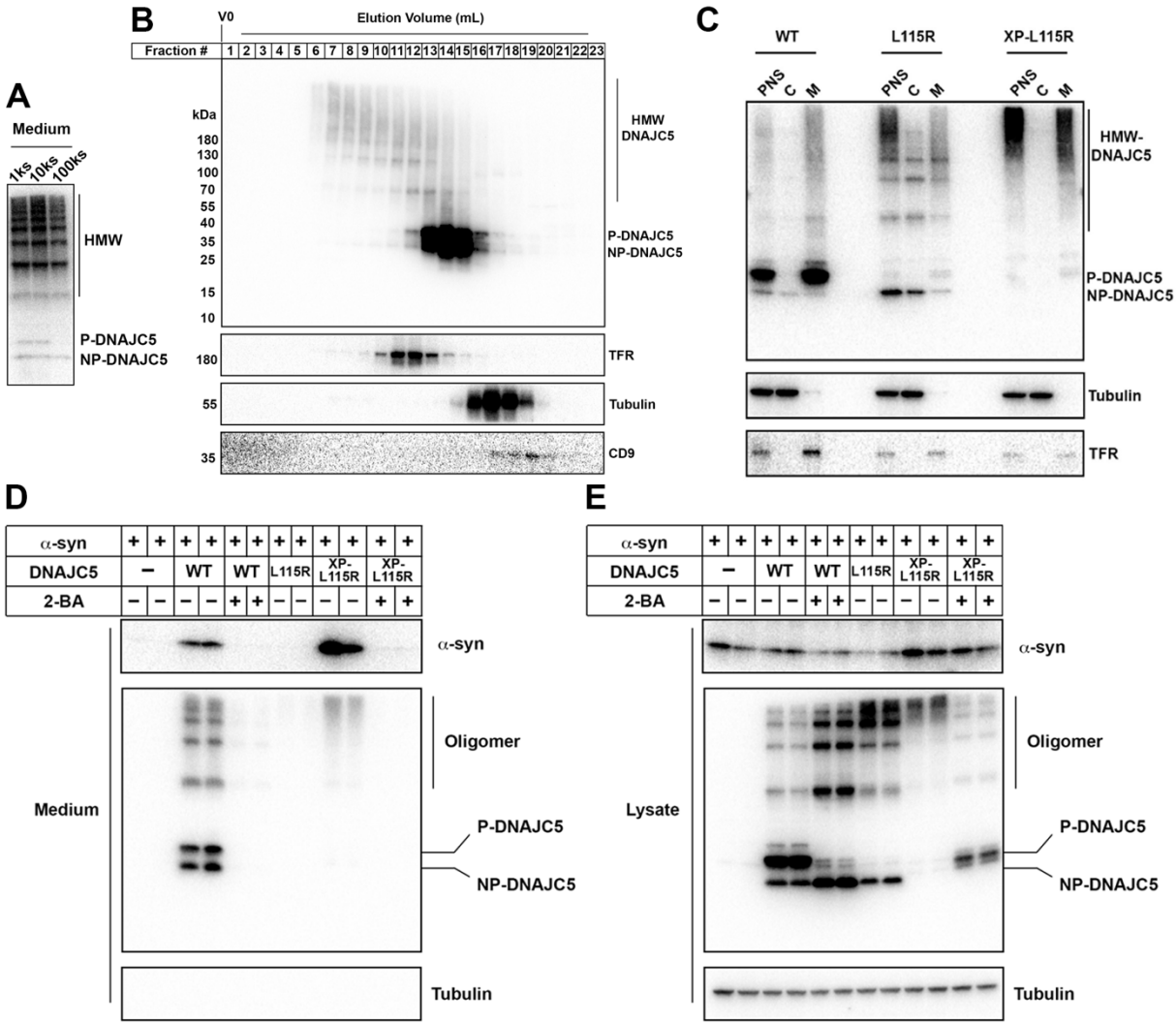

1684

1685

1686

1687 **Figure 6 – figure supplement 1**. Characterization of HMW-DNAJC5 and

1688 XPACK fusion.

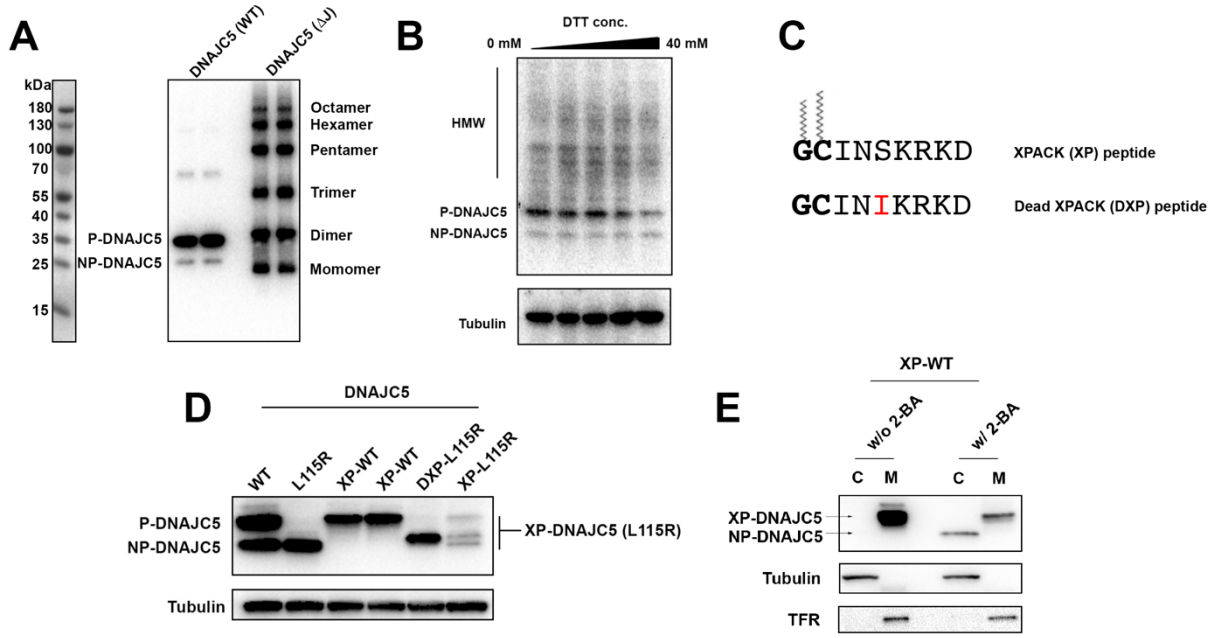

1689

1690

1691

1692

1693 **Figure 6 – figure supplement 2**. Live-cell images of XP-DNAJC5 L115R mutant

1694 and α-syn.

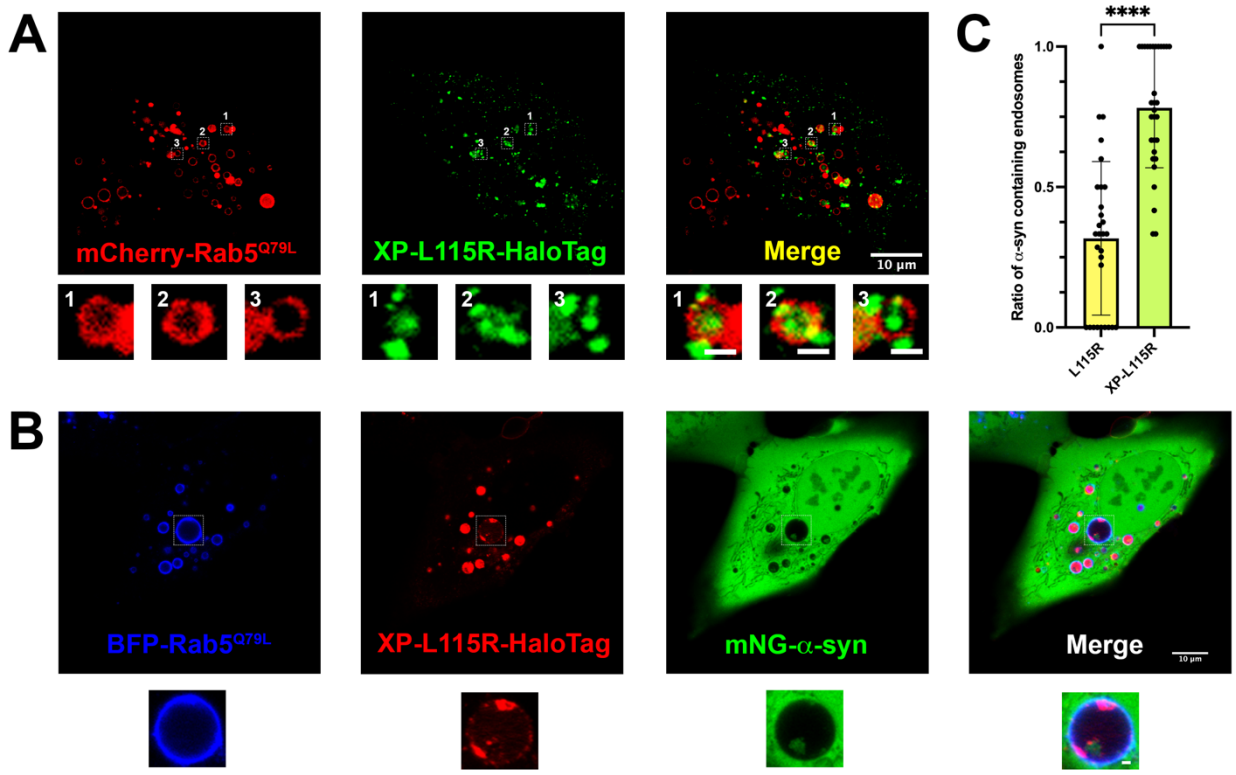

1695

1696

1697

1698 **Figure 7.** Recapitulation of endogenous DNAJC5-mediated α-syn secretion in

1699 various neuronal cell cultures.

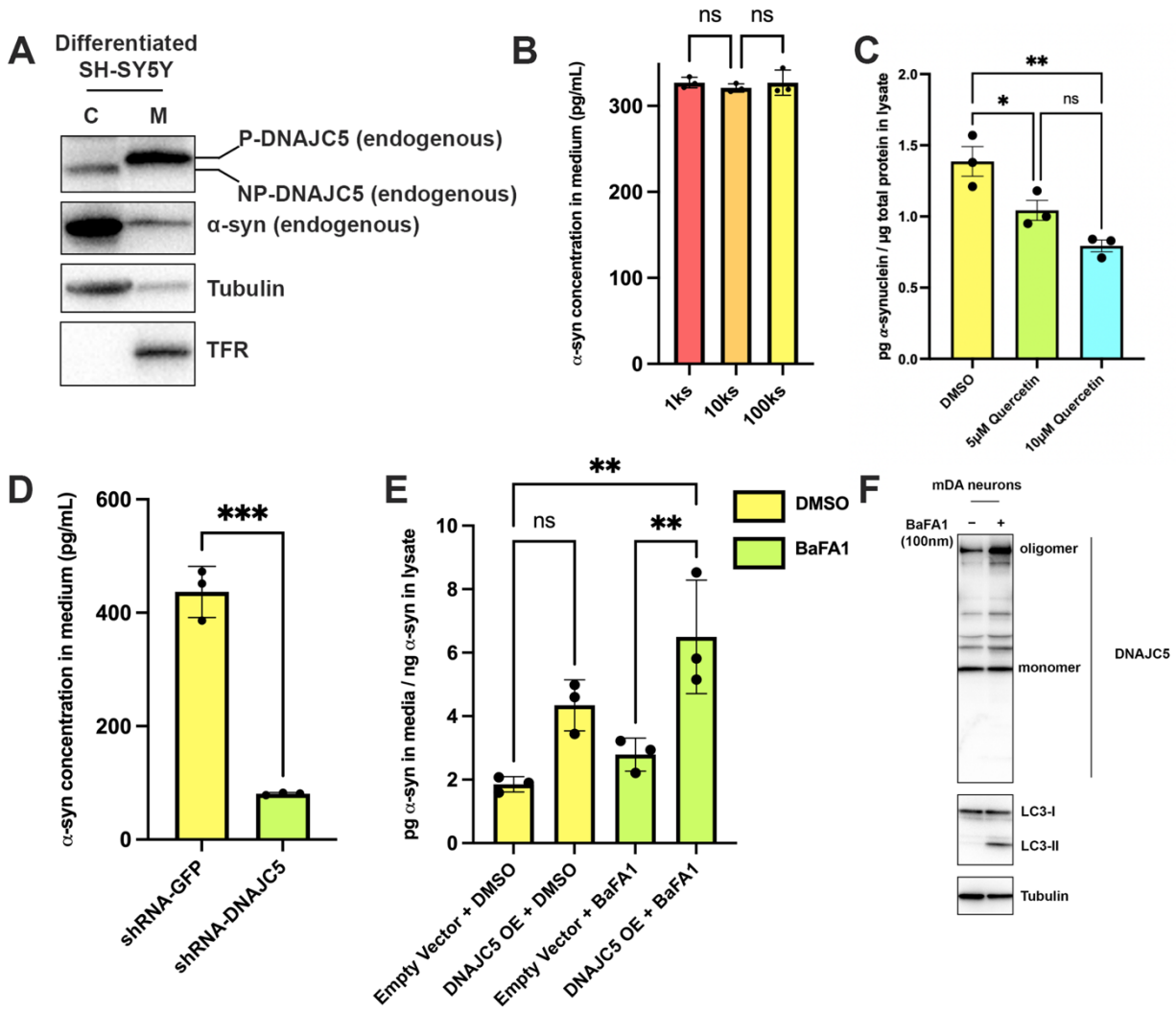

1700

1701

1702 **Figure 7 – figure supplement 1**. Basal α-syn from differentiated SH-SY5Y cells

1703 secreted in soluble form.

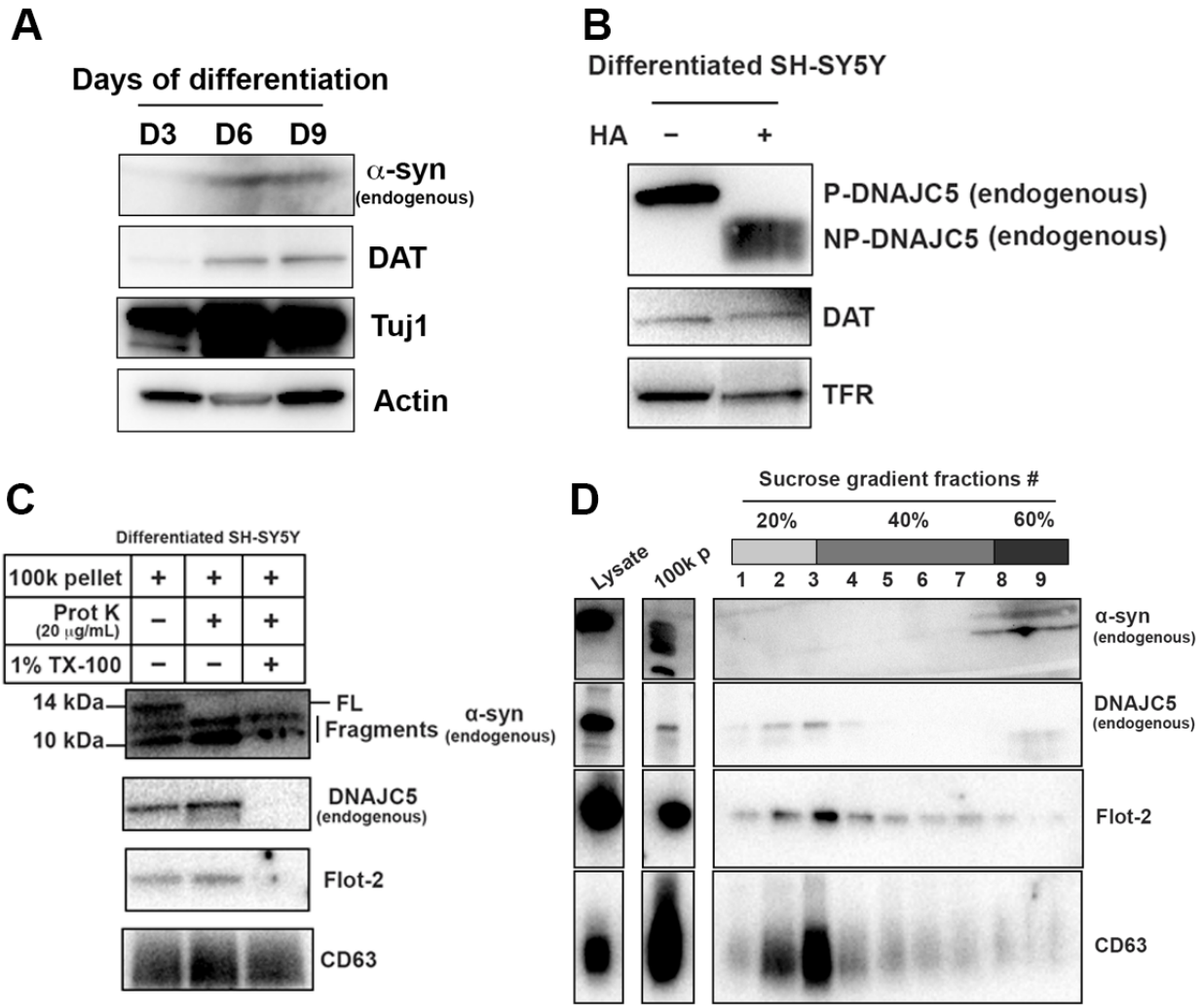

1704

1705

1706 **Figure 7 – figure supplement 2**. (A) Schematic of the differentiation protocol
1707 used to generate hiPSC-dopamine neurons. (B) DNAJC5 is palmitoylated in iPSC-
1708 dopamine neurons. (C) Partial depalmitoylation of DNAJC5 by 2-BA in iPSC-
1709 dopamine neurons does not reduce a-syn secretion.

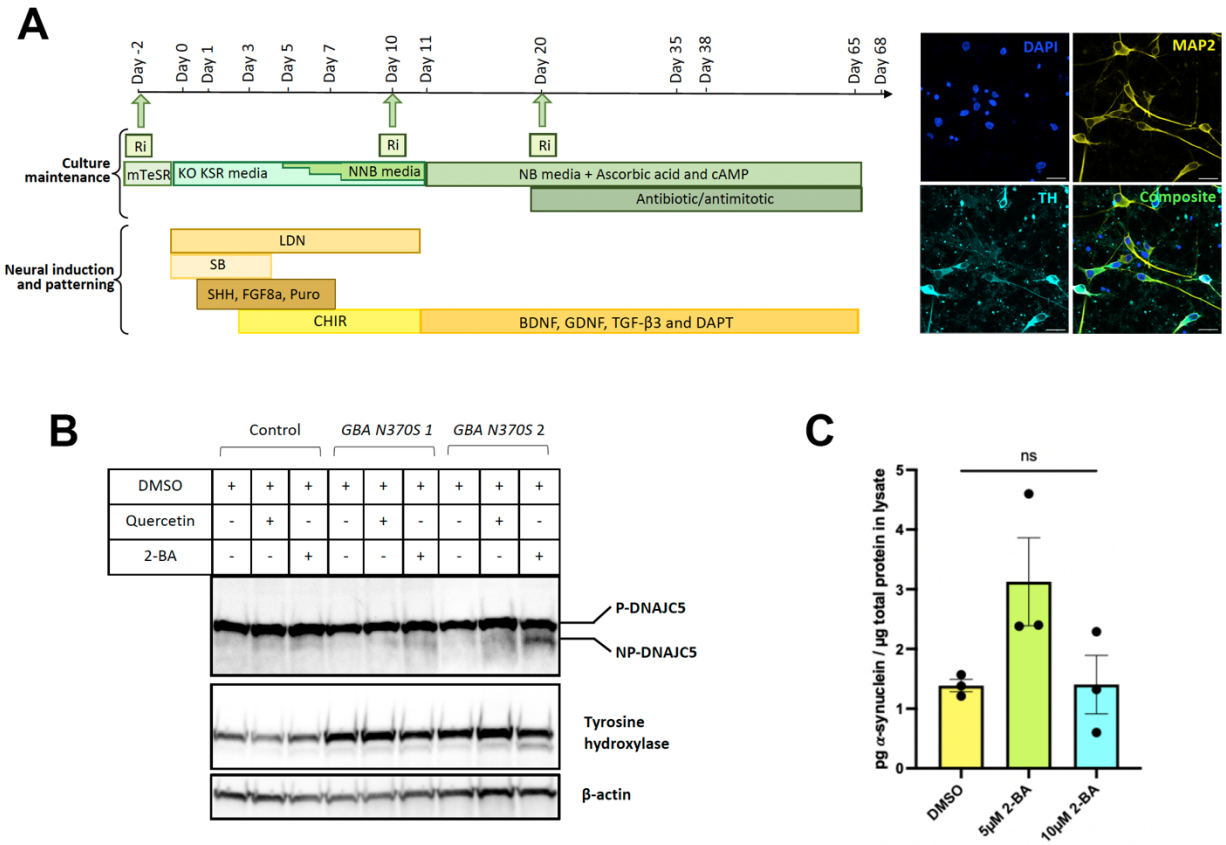

1710

1711

1712

1713

1714 **Figure 7 – figure supplement 3**. shRNA-mediated DNAJC5 knockdown in

1715 differentiated SH-SY5Y cells.

1716

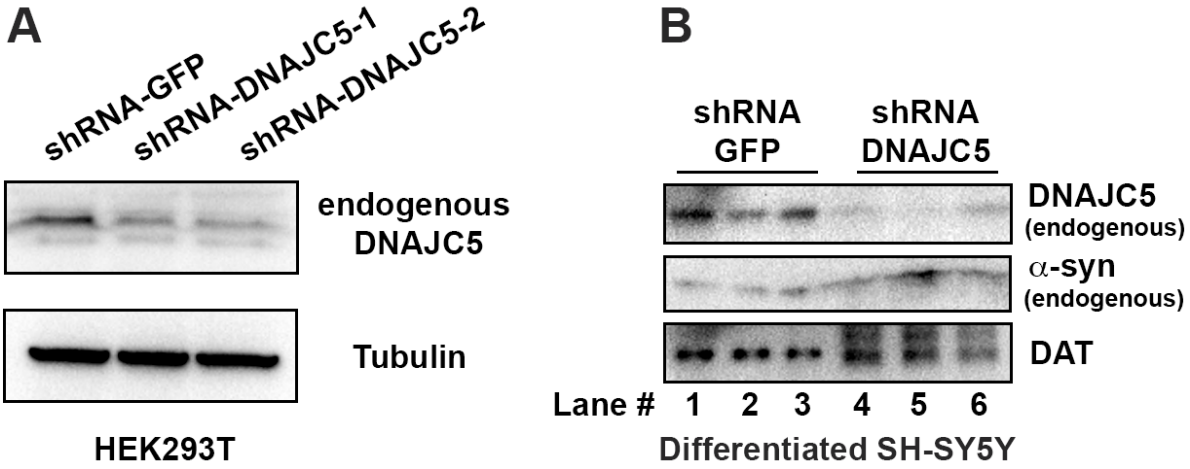

1717

1718

1719

1720 **Figure 7 – figure supplement 4**. Differentiation of mouse embryonic stem cells

1721 (mESCs) and expression of human DNAJC5.

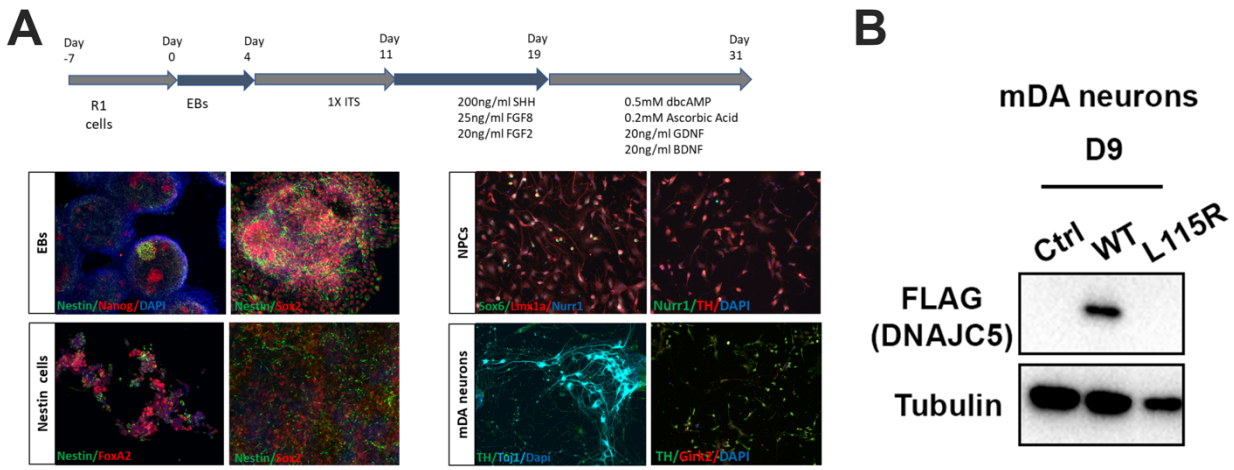

1722

1723

1724 **Figure 8**. Domain mapping of secretion-competent DNAJC5.

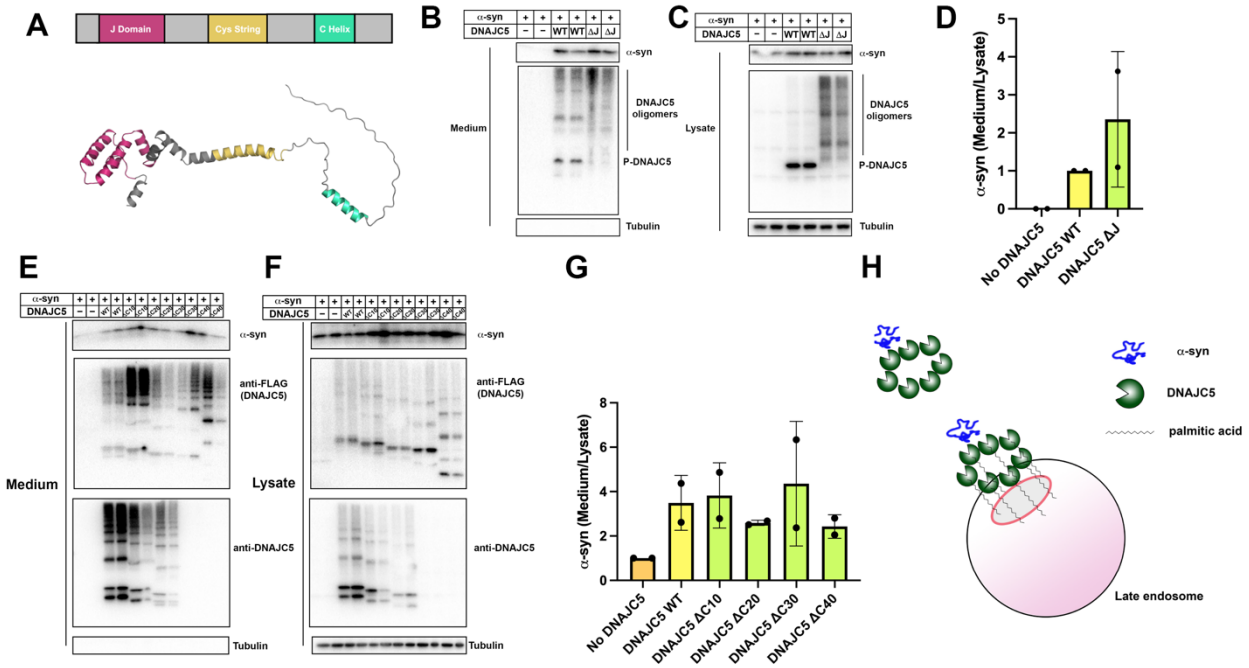

1725

1726

1727

1728

1729